

Buckling, Post-buckling and Vibrations of Composite Plates under Combined Thermomechanical Loads

Gutierrez Alvarez, J.

DOI

[10.4233/uuid:4e3e9128-8c27-41b7-8229-934e2e0834f2](https://doi.org/10.4233/uuid:4e3e9128-8c27-41b7-8229-934e2e0834f2)

Publication date

2022

Document Version

Final published version

Citation (APA)

Gutierrez Alvarez, J. (2022). *Buckling, Post-buckling and Vibrations of Composite Plates under Combined Thermomechanical Loads*. [Dissertation (TU Delft), Delft University of Technology].
<https://doi.org/10.4233/uuid:4e3e9128-8c27-41b7-8229-934e2e0834f2>

Important note

To cite this publication, please use the final published version (if applicable).
Please check the document version above.

Copyright

Other than for strictly personal use, it is not permitted to download, forward or distribute the text or part of it, without the consent of the author(s) and/or copyright holder(s), unless the work is under an open content license such as Creative Commons.

Takedown policy

Please contact us and provide details if you believe this document breaches copyrights.
We will remove access to the work immediately and investigate your claim.

**BUCKLING, POST-BUCKLING AND VIBRATIONS OF
COMPOSITE PLATES UNDER COMBINED
THERMOMECHANICAL LOADS**

BUCKLING, POST-BUCKLING AND VIBRATIONS OF COMPOSITE PLATES UNDER COMBINED THERMOMECHANICAL LOADS

Dissertation

for the purpose of obtaining the degree of doctor
at Delft University of Technology
by the authority of the Rector Magnificus Prof. dr. ir. T. H. J. van der Hagen
chair of the Board for Doctorates
to be defended publicly on Friday 14 October 2022 at 10:00 o'clock

by

Javier GUTIÉRREZ ÁLVAREZ

Master of Science in Industrial Engineering
University of León, León, Spain
born in Zaragoza, Spain

This dissertation has been approved by the promotor.

Promotor: Prof. dr. C. Bisagni

Composition of the doctoral committee:

Rector Magnificus
Prof. dr. C. Bisagni

Chairperson
Delft University of Technology, promotor

Independent members:

Prof. dr. C. Kassapoglou	Delft University of Technology
Prof. dr.-ing. R. Degenhardt	Deutsches Zentrum für Luft- und Raumfahrt e.V. (DLR)
Prof. dr. R. Butler	University of Bath
Dr. R. Vescovini	Politecnico di Milano
Prof. C. A. Dransfeld	Delft University of Technology, reserve member

Other members:

Dr. H. Abramovich	Technion - Israel Institute of Technology, retired
-------------------	--



Keywords: Thermomechanical buckling , experimental buckling, thermal testing, mechanical testing, vibration correlation technique.

Printed by: Ipskamp Printing

Front & Back: : Vibration-buckling behaviour of a heated composite plate (extracted from Ch. 5)

Copyright © 2022 by Javier Gutiérrez Álvarez

ISBN 978-94-6421-869-5

An electronic version of this dissertation is available at
<http://repository.tudelft.nl/>.

Audentes fortuna iuvat.
Fortune favors the bold.

Virgil

To my parents.

CONTENTS

List of Figures	xi
Summary	xv
Samenvatting	xvii
1 Introduction	1
1.1 Motivation	1
1.2 Thermomechanical buckling in aerospace structures	3
1.3 Analytical prediction methods in thermomechanical buckling	5
1.4 Numerical prediction methods in thermomechanical buckling	6
1.5 Experimental work in heated composite plates	7
1.5.1 Thermal buckling experiments.	7
1.5.2 Thermomechanical buckling experiments.	9
1.5.3 Vibration-buckling experiments	10
1.6 Research objectives and Thesis outline	11
2 Closed-form solutions for thermomechanical buckling of orthotropic composite plates	23
2.1 Introduction	24
2.2 Problem formulation	25
2.3 Application cases	29
2.3.1 Buckling of heated, fully restrained plates	29
2.3.2 Buckling of loaded and heated plates	34
2.4 Conclusions.	40
3 A Study on Thermal Buckling and Mode Jumping of Metallic and Composite Plates	45
3.1 Introduction	45
3.2 Mode jumping on heated composite plates	47
3.3 Analysis to identify composite plates presenting a mode jump under Heating	49
3.4 Test setup	55
3.5 Thermal tests	57
3.6 Conclusions.	63
4 Investigation on buckling and mode jumping of composite plates under thermomechanical loads	69
4.1 Introduction	70
4.2 Buckling and mode jumping on heated and mechanically loaded composite plates	72

4.3	Preliminary analysis: mode jumping in plates subjected to thermal and mechanical loads.	74
4.4	Test setup	78
4.5	Experimental results	82
4.5.1	Pure heating and pure compression load cases	82
4.5.2	Combined load cases	85
4.6	Conclusions.	94
5	Vibration-buckling tests on heated composite plates	103
5.1	Introduction	103
5.2	Vibration Correlation Technique in heated plates: buckling and mode jumping	105
5.3	Experimental setups	108
5.4	Testing methodology	111
5.5	Experimental results for test setup No. 1	112
5.5.1	Prediction of buckling using VCT	116
5.5.2	Detection of the mode jumping	117
5.6	Experimental results for test setup No. 2	118
5.6.1	Prediction of buckling using VCT	120
5.6.2	Detection of the mode jumping	122
5.7	Results summary	123
5.7.1	VCT buckling prediction	123
5.7.2	Observations about mode jumping	124
5.8	Conclusions.	125
6	Final conclusion and recommendations	131
6.1	Detailed conclusions	133
6.2	Recommendations for future research	138
	Acknowledgements	141
	Curriculum Vitæ	143
	List of Publications	145

LIST OF FIGURES

1.1 Boom supersonic's XB-1 composite + titanium fuselage [9]	2
1.2 Airbus ZEROe hydrogen aircraft, blended wing concept [12]	3
1.3 Schematic representation of a high-speed wing (a) detail view of structural panel mounted on fuselage; (b) explanatory graph.	4
1.4 A heated composite plate: (a) room temperature; (b) post-buckling regime; (c) after a mode jump.	5
1.5 Experimental deflections in thermal buckling experiment [50]	8
1.6 Test setup by Fields et al. [58] for combined loading of hypersonic panels	9
1.7 Vibration correlation experiments on compressed cylinders [59]	10
1.8 Ph.D. thesis diagram.	12
2.1 Heated plates: (a) Plate with transversal expansion restrained and prescribed length variation. (b) Plate with all expansions restrained.	25
2.2 Buckling temperatures of fully restrained, heated composite plates with different lengths. Material: <i>AS4/3502</i> ; Layup: $[45/-45/0/90]_{2s}$	32
2.3 Buckling temperatures of fully restrained, heated composite plates with different lengths. Material: <i>IM7/8552</i> ; Layup: $[45/-45/0/90]_{2s}$	33
2.4 Buckling temperatures of fully restrained, heated composite plates with different lengths. Material: <i>IM7/8552</i> ; Layup: $[20/-20]_{4s}$	34
2.5 Buckling chart for a loaded and heated composite plate. Geometry: $a = 575mm$, $b = 375mm$; Material: <i>AS4/3502</i> ; Layup: $[45/-45/0/90]_{2s}$	36
2.6 Buckling chart for a loaded and heated composite plate. Geometry: $a = 575mm$, $b = 375mm$; Material: <i>IM7/8552</i> ; Layup: $[45/-45/0/90]_{2s}$	37
2.7 Buckling chart for a loaded and heated composite plate. Geometry: $a = 575mm$, $b = 375mm$; Material: <i>IM7/8552</i> ; stacking: $[20/-20]_{4s}$	38
3.1 Plate geometry, boundary conditions and heating load.	48
3.2 Thermal equilibrium path of a post-buckled composite plate.	49
3.3 Properties of composite plates: (a) Bending stiffness for $[\theta/-\theta]_{2s}$ laminates; (b) CTE's for $[\theta/-\theta]_{2s}$ laminates.	50
3.4 Plate with frame: (a) FE model; (b) Specimen.	51
3.5 Analysis error and computational time vs. element size.	51
3.6 Linear buckling temperatures for $[\theta/-\theta]_{2s}$ laminates.	53
3.7 Mode jumping of composite plates: (a) Mode jumping temperature for $[\theta/-\theta]_{2s}$ laminates; (b) Effect of imperfections for $[30/-30]_{2s}$ laminate.	54
3.8 Mode jumping temperature for different laminates: (a) $[\theta/-\theta]_{2s}$ laminates; (b) $[\theta/-\theta/\varphi/-\varphi]_s$ laminates with $\varphi = \theta - 25$	54
3.9 Specimen inside oven.	56

3.10 Test setup.	56
3.11 Heating cycle for aluminum alloy plate.	57
3.12 Out-of-plane deformation for aluminum alloy plate: (a) FE analysis; (b) Test.	58
3.13 Temperature vs. out-of-plane deformation for the three plates.	59
3.14 Heating cycle for for $[30/ - 30/5/ - 5]_s$ plate.	59
3.15 Out-of-plane deformation for $[30/ - 30/5/ - 5]_s$ composite plate: (a) FE analysis; (b) Test.	60
3.16 Heating cycle for for $[35/ - 35/10/ - 10]_s$ plate.	61
3.17 Out-of-plane deformation for $[35/ - 35/10/ - 10]_s$ composite plate: (a) FE analysis; (b) Test.	61
4.1 Plate under thermal and mechanical loads: (a) Plate boundary conditions; (b) FE model.	72
4.2 Mode jumping under thermal and mechanical loads.	73
4.3 FE predictions: Buckling chart for combined loading.	76
4.4 FE Load vs deflection curves: (a) Heating + Compression ; (b) Compression + Heating.	77
4.5 Test setup: (a) Front view; (b) Side view.	79
4.6 Test setup: sensor distribution	80
4.7 Example of sensor measurements: (a) Strain gauges in pure compression test; (b) Thermocouples in pure heating test.	81
4.8 Test results: (a) Pure heating case ; (b) Pure compression case.	83
4.9 Experimental and numerical deflection shapes: Pure heating; (b) Pure compression.	84
4.10 Experimental buckling chart.	86
4.11 Test results for "Compression + Heating" case: (a) $\Delta_y = -0.028 \text{ mm}$; (b) $\Delta_y = -0.081 \text{ mm}$	87
4.12 Test results for "Heating + Compression" cases: $\Delta T = 14.3^\circ\text{C}$; (b) $\Delta T = 23.1^\circ\text{C}$; (c) $\Delta T = 38.5^\circ\text{C}$; (d) $\Delta T = 56.9^\circ\text{C}$	91
4.13 Experimental deflection shapes under combined loading.	92
4.14 Comparison between experimental results and numerical predictions.	93
4.15 Measurement of initial imperfections in the plate.	94
5.1 Plate reference system.	106
5.2 Behaviour of a heated composite plate: Out-of-plane deflection and squared frequency as function of the temperature variation.	108
5.3 Test setup No. 1: (a) Details of plate fixture; (b) Complete setup.	110
5.4 Test setup No. 2: (a) Front view; (b) Lateral view.	110
5.5 Thermocouple distribution: (a) Test setup No. 1; (b) Test setup No. 2	111
5.6 Out-of-plane displacements w for $[30/ - 30/5/ - 5]_s$ plate.	112
5.7 Southwell plot for $[30/ - 30/5/ - 5]_s$ plate.	113
5.8 Thermocouple measurements for $[30/ - 30/5/ - 5]_s$ plate	113
5.9 Frequency spectra for $[30/ - 30/5/ - 5]_s$ plate	115
5.10 Examples of vibration mode shapes at various temperatures for test setup No. 1.	116

5.11	Frequencies vs. temperature for $[30/-30/5/-5]_s$ plate: (a) Lowest vibration mode; (b) Three lowest vibration modes.	117
5.12	Out-of-plane displacements w for $[35/-35/10/-10]_s$ plate.. . . .	119
5.13	Temperature distributions for $[35/-35/10/-10]_s$ plate	119
5.14	Frequency spectra for $[35/-35/10/-10]_s$ plate	121
5.15	Frequencies vs. temperature for $[35/-35/10/-10]_s$ plate: (a) Lowest vibration mode; (b) Three lowest vibration modes.	122

SUMMARY

A big technological leap in Carbon Fibre Reinforced Plastics (CFRP's) has brought to the market materials that are able to operate under severe thermomechanical loading conditions and yet remain lightweight. This is of high interest for new developments in aerostructures, such as supersonic airliners or the hydrogen aircraft. A continuous need for improvement in weight efficiency motivates this research, which delves into the possibility of using thermomechanical buckling to increase structural performance in future CFRP aerostructures. In this regard, it is well understood that plates that buckle under mechanical loads can operate safely, and they can even carry a significant amount of load before they experience material failure. Since future high-speed composite aircraft will have to endure thermomechanical loads, it is fair to consider that some parts of these new vehicles could, to some degree, be capable to operate under thermomechanical post-buckling.

The goal of this PhD dissertation is to advance the knowledge on thermomechanical buckling of composite plates, by investigating diverse aspects of the behaviour of this phenomenon. In particular, special attention is given to study the occurrence of mode jumps in post-buckling. Mode jumping phenomena alter the shape of a plate and can impact certain aspects of its functionality, e.g. aerodynamics, yet they could have potentially interesting future applications if they were to be appropriately controlled. Three kinds of methodologies, analytical, numerical and experimental, have been followed during this research. However, a clear emphasis has been put in the latter, since this thesis is mostly focused in the design and execution of experiments in thermomechanical buckling of composite plates.

This dissertation is composed of four independent investigations, being the first of them an analytical study on linear thermomechanical buckling, and the other three experimental studies on deep thermomechanical post-buckling behaviour. Four independent studies are presented in Chapters 2 to 5 of this thesis. In Chapter 2, an analytical, closed-form solution for the study of linear buckling of thin, symmetric and balanced composite laminated plates subjected to thermomechanical loads was derived. The formulation is based on a Duhamel-Neumann constitutive approach, and laminate theory to derive the plate governing equations. The mechanical load was introduced in the formulation as plate size variation, and heating load was implemented as uniform temperature increment. The formulation was limited to simply supported boundary conditions. The obtained formula relates critical buckling temperatures to initially applied plate size variation. In Chapter 3, a numerical-experimental study of thermal buckling under heating is presented. A set of parametric analysis was performed to identify composite plates that present a mode jump when heated. Two composite plates were identified and were subsequently tested in a newly developed test setup for thermal buckling of composite plates. The aforementioned setup was devised around a frame with a low coefficient of thermal expansion, so that the plate could experience buckling and mode

jumping when heated, and could successfully reproduce thermal buckling and mode jumping in the tested plates. Chapter 4 reports a combined numerical-experimental study of composite plates, analysing the interaction between mechanical and thermal loads in relation to buckling and mode jumping. A novel test setup for thermomechanical testing was designed. This setup made use of the frame used in previous chapter to restrain thermal expansion, and by applying compression to the frame, mechanical shortening could be indirectly applied to the plate. In this way, it was possible to study interactions between thermal and mechanical loading states. Experimental results revealed that a linear decrease of the mode jumping temperature could be observed for increasing levels of compression, and the same was also true when the order of applications of the loads was inverted. Chapter 5 presents an experimental investigation on vibrations of heated composite plates leading to thermal buckling. The experiments were performed considering two main goals: the application of the Vibration Correlation Technique for the detection of thermal buckling in composite plates; and the exploration of the frequency variations before and after the occurrence of a mode jump in post-buckling regime. Two variations of the test setups used in previous chapters were used. The setups shared thermal expansion frame, while they differentiate on the type of heating source and mechanical boundary conditions. The plates were excited acoustically using a loudspeaker, and the vibration frequencies were monitored and acquired using a laser vibrometer. Buckling temperatures were successfully predicted using the Vibration Correlation Technique. Changes in frequency, potentially related to the occurrence of the mode jump, were also detected.

SAMENVATTING

Een grote technologische sprong voorwaarts van koolstofvezel versterkte kunststof heeft materialen op de markt gebracht die in staat zijn om onder extreme thermo-mechanische belasting te presteren en toch licht zijn. Dit is erg interessant voor nieuwe ontwikkelingen in luchtvaart-constructies, zoals supersonische vliegtuigen of vliegtuigen die op waterstof vliegen. Dit onderzoek wordt gemotiveerd door de onophoudelijke nood aan lichtere constructies, waar ook de mogelijkheid om thermo-mechanische knik te gebruiken om de structurele prestaties van koolstofvezel versterkte kunststof constructies te verbeteren. In dit opzicht is het al bekend dat platen die knikken onder mechanische belasting nog veilig gebruikt kunnen worden, en ze kunnen zelfs nog een significant deel van de kracht dragen voor het materiaal faalt. Omdat toekomstige hogesnelheid composieten vliegtuigen thermo-mechanische belasting zullen moeten doorstaan, is het aannemelijk dat bepaalde delen van deze voertuigen, tot een bepaald niveau, onder thermo-mechanische post-knik zullen opereren.

Het doel van deze PhD is om de kennis over thermo-mechanische knik van composieten panelen te verbeteren, door het onderzoeken van verschillende aspecten van het gedrag van dit fenomeen. Extra aandacht is besteed aan de studie van de sprong in knikmodus in post-knik. Door de sprong in knikmodus verandert de vorm van een plaat en dit beïnvloed bepaalde functionaliteiten, bijvoorbeeld de aerodynamica; toch kunnen ze potentieel interessante toepassingen hebben als ze goed gecontroleerd kunnen worden. Drie verschillende methodes zijn toegepast tijdens dit onderzoek: analytisch, numeriek en experimenteel. Echter is er een duidelijke nadruk gelegd op de laatste omdat dit proefschrift vooral focust op het ontwerp en uitvoering van experimenten in thermo-mechanische knik van composieten panelen.

Dit proefschrift bestaat uit vier onafhankelijke onderzoeken, waar de eerste een analytische studie over lineaire thermo-mechanische knik is, en de andere drie experimentele onderzoeken zijn over diep thermo-mechanisch post-knik gedrag. Vier onafhankelijke studies worden besproken in hoofdstukken 2 tot 5 van dit proefschrift. In hoofdstuk 2 is een analytische, gesloten-vorm formule afgeleid om de lineaire knik van dunne, symmetrische en gebalanceerde composieten laminaten onder thermo-mechanische belasting te bestuderen. De formulering is gebaseerd op Duhamel-Neumann aannames, en laminaat-theorie om de constitutieve vergelijking van de plaat te bepalen. De mechanische belasting is geformuleerd als een verandering van de grootte van de plaat, en de warmte-belasting is geïmplementeerd als een uniforme temperatuur. De formulering was enkel geldig voor eenvoudig ondersteunde randvoorwaarden. De verkregen formule linkt de kritische knik-temperaturen aan de initiële verandering in grootte van de plaat. In hoofdstuk 3 is een numeriek-experimentele studie van thermische knik door verwarming gepresenteerd. Een reeks parametrische analyses is gedaan om de laminaten te vinden die een sprong in knikmodus tonen tijdens het verwarmen. Twee composieten platen werden gevonden and vervolgens getest in een nieuwe testopstelling voor thermi-

sche knik van composieten platen. Deze opstelling was gebouwd rond een inklemming van lage thermisch expansie-coëfficiënt, zodat de plaat knik en een sprong in knikmodus kan ondergaan tijdens het verwarmen, om zo het numerieke model van thermische knik en sprongen in knikmodus te valideren. Hoofdstuk 4 beschrijft een gecombineerde numeriek-analytische studie van composieten platen, en analyseert de wisselwerking tussen mechanische en thermische belasting gerelateerd aan knik en sprong in knikmodus. Een nieuwe testopstelling voor thermo-mechanisch testen was ontworpen. Deze testopstelling gebruikt de inklemming van het vorige hoofdstuk en door druk aan te brengen op deze inklemming kan een mechanische verkleining indirect op de plaat worden aangebracht. Op deze manier was het mogelijk om de wisselwerking tussen thermische en mechanische belasting te bestuderen. Experimentele resultaten lieten zien dat er een lineaire afname was van de temperatuur waar een sprong in knikmodus ontstond als er meer mechanische druk op werd gezet, en hetzelfde werd gevonden als de volgorde van de krachten omgekeerd werd. Hoofdstuk 5 presenteert een experimentele studie over trilling van verwarmde composieten panelen die leiden tot thermische knik. De experimenten hadden twee doelen: het gebruik van de trillingen-correlatie techniek om thermische knik in composieten panelen te vinden; en het ontdekken van de variatie in trillingen voor en na een sprong in knikmodus in het post-knik regime. Twee variaties van de testopstelling van de vorige hoofdstukken zijn gebruikt. De opstellingen hadden dezelfde inklemming, maar een andere warmtebron en mechanische randvoorwaarden. De platen zijn akoestisch geëxciteerd door een luidspreker en de trillingsfrequenties werden gemeten door een laser vibrometer. Knik-temperaturen zijn goed voorspeld door het gebruik van de trillingen-correlatie techniek. Veranderingen in de frequentie, mogelijk gerelateerd aan het voorkomen van een sprong in knikmodus, zijn ook opgemerkt.

1

INTRODUCTION

*It's not about standing still and becoming safe.
If anybody wants to keep creating they have to be all about change.*

Miles Davis

You can't get to the moon by climbing successively taller trees.

Mo's Law of Evolutionary Development

1.1. MOTIVATION

CARBON FIBER REINFORCED PLASTICS (CFRP's) have greatly contributed to reshape aerospace designs due to their outstanding trade-off in structural properties. They have been present since the early ages of aircraft and spacecraft technology, contributing to countless innovative designs [1], [2]. However, it was not till recently that these materials became widely known to the common public. This was mostly caused by the appearance of large airliners such as the Airbus A350 or the Boeing 787 Dreamliner, which make extensive use of CFRP's for almost the totality of their primary structure. Previous models of commercial aircraft used these materials for critical parts in the fuselages, such as the center wingbox of the A380. These materials can deliver great performances, either as monolithic plates or shells, or assembled in sandwich compounds.

CFRP's have also gradually reached the applications in extreme environments. This is the case in vehicles such as supersonic aircraft, satellites and launcher structures. During their service lives, these vehicles must endure harsh conditions that comprise combinations of heat and mechanical loads. State-of-the-art CFRPs, such as graphite fiber/PMR-15 and graphite fiber/PMR-11-55, can reliably work thousands of hours at

temperatures between 290 and 345°C [3]; other resin materials offer cyanate esters, polyimides, and BMIs can also greatly perform at high temperatures [4], [5]. Moreover, the market is constantly evolving and producing new CFRP's suitable for high temperatures [6]. Such improvements in material properties have certainly motivated new developments in civil aircraft technology, such as the return of the supersonic airliner. Future high-speed commercial aircraft can greatly benefit from the highly efficient structural designs made possible by CFRP's. New composite high-speed aircraft could make a difference in performance and profitability with respect to previous supersonic airliners, the Tu-144 and the Concorde, built in metallic materials. Currently, the NASA's X-59 Quiet SuperSonic Technology (QueSST) is under ground testing [7], and the Boom XB-1 demonstrator aircraft, shown in Fig. 1.1, has already had its roll-out and it is undergoing ground tests, preparing for its maiden flight. The aircraft model Boom Overture, with capacity for 50 passengers, is expected to enter service in 2029 [8], [9].



Figure 1.1: Boom supersonic's XB-1 composite + titanium fuselage [9]

Looking in another direction, the urge for the reduction of CO_2 footprint due to global warming [10] is pushing the industry towards alternative energy and fuel sources. In order to satisfy such demands, Airbus has chosen to work towards the hydrogen aircraft and is currently working on the *ZEROe* hydrogen aircraft demonstrator, shown in Fig. 1.2. This concept has the potential to produce profound changes in the aircraft industry. Classic structural concepts will have to evolve to integrate the thin-walled, possibly load-bearing cryogenic LH_2 tanks [11]. Composite materials can greatly contribute to achieve the technical challenges that these developments may pose.

A constant search for increasingly performing aircraft pushes structural designers towards the adoption of increasingly smaller gauges for skin and inner structural parts in their designs. On one hand, this can produce significant weight savings; on the other hand, such reductions can greatly increase the risk of buckling, especially in scenarios where mechanical and thermal loads overlap. While mechanical buckling has been used in multiple occasions as a mechanism for weight saving, thermal buckling has classically been a banned area for stress engineers, since this phenomenon is known to have caused aeroelastic phenomena during the early ages of supersonic flight. Motivated by the evolution and improvements in new generation composite materials, this research

intends to revisit old concepts and re-evaluate the possibility of allowing aircraft areas to operate under thermomechanical buckling conditions. With such overarching goal, several aspect of buckling, post-buckling and vibration of composite plates under thermomechanical loads will be investigated in this dissertation.



Figure 1.2: Airbus ZEROe hydrogen aircraft, blended wing concept [12]

1.2. THERMOMECHANICAL BUCKLING IN AEROSPACE STRUCTURES

Flat structural panels in an aircraft structure have to carry their share of in-service loads. When a flat panel is subjected to increasingly larger compressive loads, it will remain flat up to a point in which it will start deflecting out of plane. This phenomenon is known as “buckling”, and for flat plates is considered to be a stable structural configuration. However, a plate may lose its original flat geometry and yet be able to perform its structural duty. In fact, typical aircraft structural panels are able to carry load far beyond their buckling loads before collapse [13]–[15]. Multiple aircraft have taken advantage of this feature, setting the permissible load above the buckling threshold at certain locations. In-service aircraft loads can be purely mechanical, but also thermal. Thermal buckling occurs when a heated component is not allowed to expand and buckling occurs as a result of thermal stresses. Buckling caused by the overlap of thermal and mechanical stresses is denoted as thermomechanical buckling. When thermal and mechanical loads act together, they can alter the buckling and post-buckling behavior of a flat panel. The occurrence of thermomechanical buckling in a wing panel is illustrated in Fig. 1.3, where a representation of a flat panel mounted on a portion of a high-speed wing airframe is shown. The wing, represented in Fig. 1.3 (a), is composed of stiff frame elements, represented here as axis Y , and less stiff structural ribs, laid along direction X . Under a thermal increment, light structural parts like ribs or stringers respond fast to temperature changes, allowing thermal expansion along X axis, heavy spars or frames react much slower, restricting panel dilatations along Y axis. On top of the thermal stresses generated by aerodynamic heating, the panel has to endure the bending and twisting

mechanical loads carried by the wing. Under these conditions, the panel may either remain flat or buckle, depending on the combination of mechanical load and temperature, as illustrated in Fig. 1.3 (b). A panel under thermomechanical buckling can remain perfectly functional, and CFRP's are suitable candidates to operate under thermomechanical post-buckling conditions, because they are able to maintain structural performances at high temperatures, as well as sustaining highly deformed states and return to their original configuration.

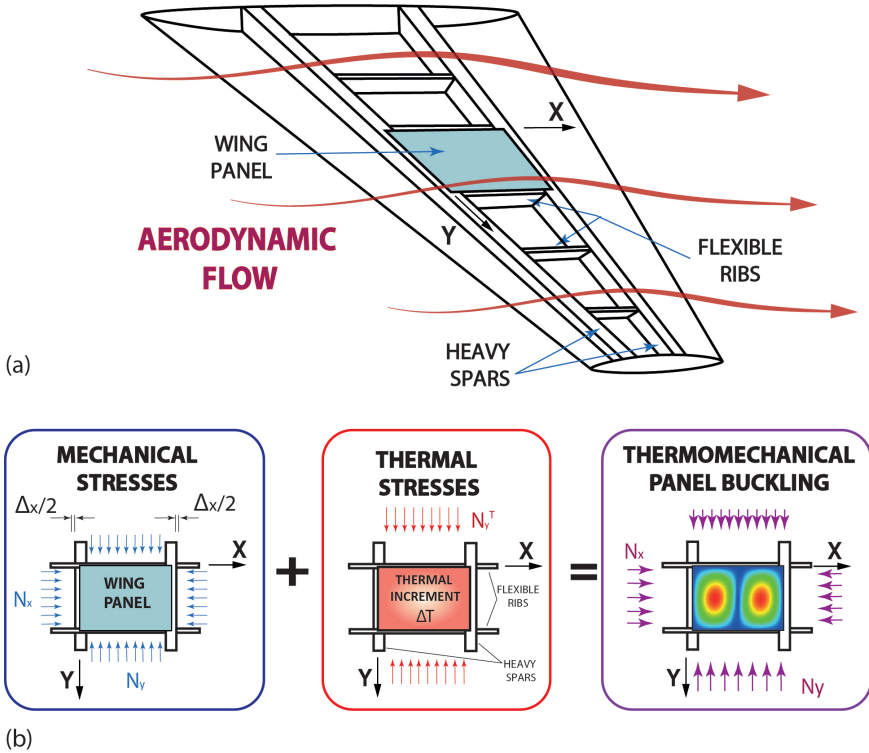


Figure 1.3: Schematic representation of a high-speed wing (a) detail view of structural panel mounted on fuselage; (b) explanatory graph.

Along their operative lives, composite plates in post-buckling can experience sudden changes in shape due to variations in the load. These shape changes are known as mode changes or mode jumps. A mode jump is a dynamic event that occurs when the current structural shape becomes unstable as a consequence of rising compressive loads. An example of this is shown in Fig. 1.4, where a heated composite plate experiences an increase from one into two half-waves when temperature is risen. The origin of these jumps may be originated by thermal loads, mechanical loads, or a combination of both. The occurrence of these jumps is a relevant event in the thermomechanical post-buckling regime of a plate, since it alters the shape of the plate and it can have an impact

on other aspects of its functionality. In this research, an emphasis has been made in understanding what characteristics make a composite flat panel prone to experience these events, and how does thermomechanical load interaction influences its occurrence.

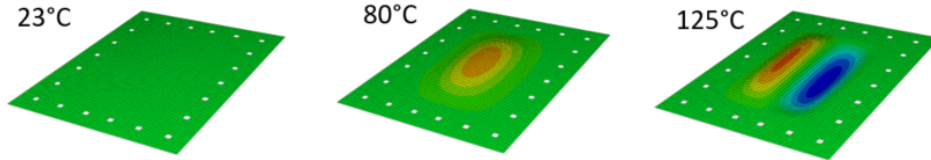


Figure 1.4: A heated composite plate: (a) room temperature; (b) post-buckling regime; (c) after a mode jump.

Thermomechanical buckling behavior can be approached from three different perspectives or methodologies: analytical, numerical and experimental. Even though these three approaches have been used in this thesis, a special emphasis has been put into the latter, mostly focusing in the design and performance of thermal and thermomechanical buckling experiments. Experimentation is an essential part in the investigation and understanding of buckling, but it is both costly and labor intensive. Numerical and analytical predictions can be an invaluable help in the design and preparation of experiments. Due to their different nature, analytical and numerical predictive methodologies have very different strengths and weaknesses. Far from being mutually exclusive, these two approaches are highly complementary, being the best results achieved when both are used in combination.

1.3. ANALYTICAL PREDICTION METHODS IN THERMOMECHANICAL BUCKLING

There are several ways to perform analytical predictions for buckling and post-buckling in thin composite plates. The most common approaches rely on the use of the Föppl-Von Kármán non-linear plate governing equations as starting point. This set of partial differential equations take account of the effect of large deflections, as well as coupling between the bending and membrane stresses in the plate [16]. In order to account for the effects of thermal expansion in composite plates, the governing equations need to be derived using Duhamel-Neumann constitutive equations for orthotropic solids [17] in combination with lamination theory. The way of dealing with linear buckling and post-buckling behavior is essentially different. The extraction of the linear buckling load in a perfect plate is typically a linear eigenvalue problem, in which the lowest eigenvalue yields the sought buckling load. Regarding initial post-buckling behavior, it can often be well captured by using asymptotic analysis around the critical buckling load [18]–[20], but this method is only valid for small plate deflections. When the load-carrying capabilities of a plate in post-buckling need to be estimated, asymptotic analysis is no longer sufficient and the nonlinear governing equations must be solved directly [13]. The best

possible outcome for any buckling or post-buckling problem is finding a closed formula. However, this is often mathematically unattainable and most of the times the solution needs to be approximated. Solution approximations can be found using different strategies, such as the Galerkin method [21], energy minimization [22], [23] or perturbation techniques [24], [25]. Diverse studies have been recently performed using these methodologies, in order to study the effect of certain parameters over the buckling temperature, such as material properties [26], [27] irregular temperature distributions [28], irregular geometry [29]. Occasionally, closed form solutions can be reached by making simplifications in the original assumptions or by neglecting terms in the governing equations. These simplifications reduce the range of validity of the solution, but they can help deliver closed formulas that are valid for many common use cases. Closed formulas also provide the engineer with a grasp of the physics of the problem. Even if they are not directly related to the work this dissertation, other analytical approaches tackle thermomechanical buckling in composite plates by using different methodologies, such as using different layer kinematics to selectively apply transverse shear sensitivity to each layer [30]. Also, work in layer-wise and zig-zag theories can be found in recent literature [31], as well as work in multi-laminate theories [30], which take into account laminates of different nature stacked together.

Analytical methodologies are a very powerful instrument to investigate linear buckling and post-buckling in composite plates. However, the solving procedure for the non-linear cases can often become strenuous due to the manipulation of large, complex algebraic expressions. Also, the obtained solutions are limited to the originally assumed boundary conditions and load distributions, which makes these rather specific and with a limited range of applicability. In the present dissertation, the use of analytical methods has been used in Chapter 2 for the study of linear buckling. The contribution of this investigation is the deduction of a closed formula for the linear buckling of an orthotropic, rectangular plate under combined thermomechanical load. This formula allows to study plates and create diagrams that relate buckling temperatures with externally applied mechanical load. Conversely, Finite Element Analysis was extensively used for the study of the post-buckling and mode jumping behavior.

1.4. NUMERICAL PREDICTION METHODS IN THERMOMECHANICAL BUCKLING

Finite Element Analysis (FEA) is an essential tool for the simulation of buckling and post-buckling in composite plates. In FEA, the studied structure is discretized into smaller parts or elements. The solutions delivered by this method are an approximation, and the accuracy of the solution will depend on the density of the mesh. Since Finite Element models can be computationally costly, appropriate mesh sizes should always be sought by performing convergence studies. For large models, the need of large processing times and robust computational power are significant drawbacks of this approach. However, FEA allows for remarkable flexibility, since there is virtually no cost in using complex geometries, unconventional stacking orientations, applying complex load distributions or unusual boundary conditions. FEA makes also easier the implementation of advanced behavior models [32]–[34]. Such advantages make FEA the optimal approach for simu-

lating thermomechanical buckling in real structural parts [35], [36]. However, despite its versatility FEA also provides little to no information about the driving parameters of the studied problem. It can, nevertheless, be a powerful tool to perform parametric analysis for thermal buckling [37]–[39].

During the present dissertation, diverse effect of thermomechanical load interaction over plate buckling were studied. When combined loads were applied, this was always done in a sequential manner, by applying sequentially “heating” and “compression” phases, or the other way around. In this context, the calculation of the linear buckling load can be done by performing two analysis steps: in the first step, the structure is preloaded with the first load type, and in the second step, an eigenvalue analysis of the pre-loaded structure is performed. Thermomechanical post-buckling can be simulated using several procedures which are substantially different in accuracy and capabilities. First, the most common way to study post-buckling numerically is the standard, geometrically nonlinear analysis. During the solution process, the load is progressively applied in discrete increments, and the values for the displacements are calculated iteratively after each load increment. Static nonlinear analysis can effectively assess initial post-buckling behavior, however, it cannot capture events such as snap-back/snap-through phenomena, due to the stiffness matrix of the structure becoming singular and the root-solving algorithm not being able to converge. Second, the arc-length method can typically follow changes in load path. The magnitude and size of the applied load increment become unknowns in the algorithm, and the stiffness matrix is modified to avoid becoming singular. However, the method has been proven unreliable in the proximity of bifurcation points [40]. At last, dynamic explicit numerical procedures take into account the inertial and damping properties of the structure, and simulate the structural behavior by numerically integrating the equations of motion. Mode jumping is a dynamic event, and these methods are the most reliable procedure to capture such events. They have consistently, successfully predicted the buckling of composite cylindrical shells [41], [42], the occurrence of mode jumping in flat, stiffened composite panels [43], [44] and the mode jumping in heated metallic plates [45]. Even though, the numerical integration process is a much more computationally costly procedure in comparison to the static nonlinear and arc-length methods, in which the load is applied quasi-statically. Dynamic explicit simulations have been extensively used during this thesis for the preparation of experiments in Chapters 3 and 4, as well as for corroboration of results in Chapter 5.

1.5. EXPERIMENTAL WORK IN HEATED COMPOSITE PLATES

1.5.1. THERMAL BUCKLING EXPERIMENTS

Typical thermal buckling test experiments performed over flat plates rely on a very similar principle. The tested plate is assembled into a frame that has a lower Coefficient of Thermal Expansion (CTE) than the tested plate. When the assembly is heated, the plate and the frame expand unequally, and the plate starts deflecting out-of-plane as a consequence of the constrained thermal expansion. Thermally buckled plates typically deflect into a deformed shape with only one half wave along both plate main axis. An example of this is shown in Fig. 1.5, where the results of a thermal buckling test on a metallic plate are shown. Most of recent experiments in thermal buckling have been performed over

metallic materials [46]–[49].

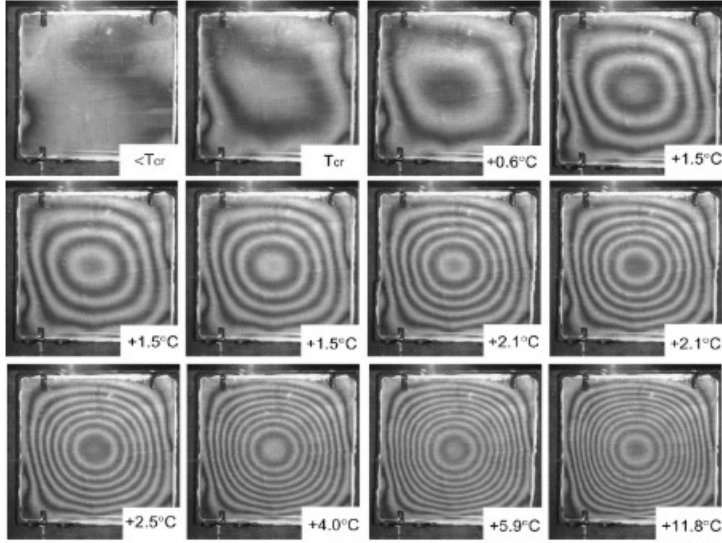


Figure 1.5: Experimental deflections in thermal buckling experiment [50]

In Chapter 3, a test setup for thermal buckling in composite plates is presented. The goals of the proposed experimental setup were to reproduce experimentally the occurrences of both thermal buckling and mode jumping in composite plates. Making CRFP plates buckle under heat is a difficult task. In CFRP's, the matrix usually has a significantly high CTE, but carbon fibers have an almost zero thermal expansion along the fiber directions. Due to this, CFRP orthotropic laminates often have two different CTE's along X and y direction. Large laminate CTE's in one direction can be achieved by using suitable stacking orientations. However, the laminate will always have a very small CTE in the remaining direction, and hence the functionality of the experiment relies on the frame not experiencing large size variations. This problem has occasionally been tackled by implementing a water-cooling to the frame [48], [51].

During this investigation, two strategies were followed. First, the use of a first a low CTE fitting made of Invar 36 material, suitable for testing a wide variety of laminates. Second, a numerical investigation was performed to identify suitable layout candidates which achieve mode jumps in their post-buckling regime, changing from the typical one-half-wave typical shape exemplified in Fig. 1.5, into a shape with two half-waves. The most innovative aspect of these experiments is the use of stacking orientations to regulate the thermal buckling and mode jumping temperatures, as well as the successful experimental reproduction of both phenomena.

1.5.2. THERMOMECHANICAL BUCKLING EXPERIMENTS

Experiments in thermomechanical buckling are much less frequent in literature than those for thermal buckling. Possible reasons for this are the difficulties in the design, implementation and execution of these experiments: when mechanical and thermal loads are simultaneously applied, numerous issues appear due to the interferences between mechanical and thermal boundary conditions [52]. During the last decades, a rather limited amount of tests have been reported. The most fundamental work was performed in the 60's -70's decades, mostly over heated metallic cylinders [53], [54]. Great experimental efforts were performed on the experimentation of hat-stiffened, titanium metal composite panels under combined loads [55], [56]. More recently, relevant experiments were also performed over shallow curved CFRP panels [57].

The most remarkable effort in reproducing combined thermomechanical buckling was reported by Fields et al. [58], who tested stiffened panels made of titanium matrix composite material under different combinations of axial load, shear and heat. The test setup, reported in Fig. 1.6, was formed by an external structural frame and a set of 8 actuators which were capable of introducing compression and shearing loads. These actuators are reported in Fig. 1.6 (a) with numbers ranging from 1 to 9, corresponding the 1 to the axial actuator for the introduction of compressive load, and numbers 3 to 9 to the actuators for shear loading. Heating loads were introduced using infrared lamps (not in the figure). The tested hat-stiffened panel is represented in in Fig. 1.6 (a) as a black rectangle, and shown in Fig. 1.6 (b), where it is attached to the triangular fittings used for axial load introduction. This kind of test setups can be an invaluable asset for experimental research in aerospace structures. Such test setups are, however, very large in size, complex and costly, and thus often unfeasible for a regular research laboratory.

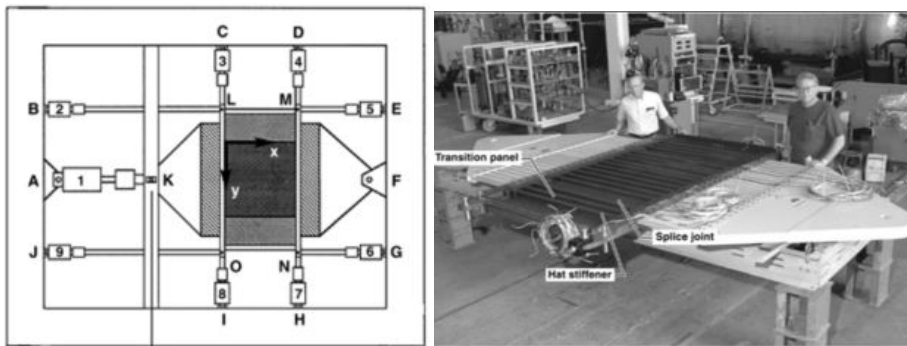


Figure 1.6: Test setup by Fields et al. [58] for combined loading of hypersonic panels

In Chapter 4 of this thesis, a second experimental campaign is presented. Two main goals were pursued: the development of an experimental setup that could test the thermomechanical buckling of composite plates, and the study of the influence of combined loading over both buckling and mode jumping phenomena in composite plates. This second test setup can be seen as an incremental step from the experiments presented in Chapter 3, since its working principle also relies on a low CTE frame fixture for the

restriction of the thermal expansions of the plate. Mechanical loads were indirectly introduced in the plate by applying a vertical displacement directly over the Invar 36 frame using a compression machine, and a IR lamp array was used for the heating of the tested plate. The most innovative contribution of this investigation is the study of the influence of combined loading over the mode jumping temperature.

1.5.3. VIBRATION-BUCKLING EXPERIMENTS

Thin-walled structures subjected to mechanical loads experience variations in their vibration frequencies. For instance, when a plate is subjected to a gradually increasing compressive load, the vibration mode with identical shape as the buckling mode experiences a decrease in frequency. Often, a linear relation can be established between the applied load and the square of the frequencies f^2 of the aforementioned vibration mode. In a perfectly flat plate, vibration frequencies become zero at the buckling load; in a real plate, however, the frequency never reaches zero due to the presence of geometrical imperfections. Nevertheless, the in f^2 vs load linear relation holds for most of the loading process, and reliable estimations of the buckling load can be performed by mapping the decrease in f^2 for increasing values of the load.

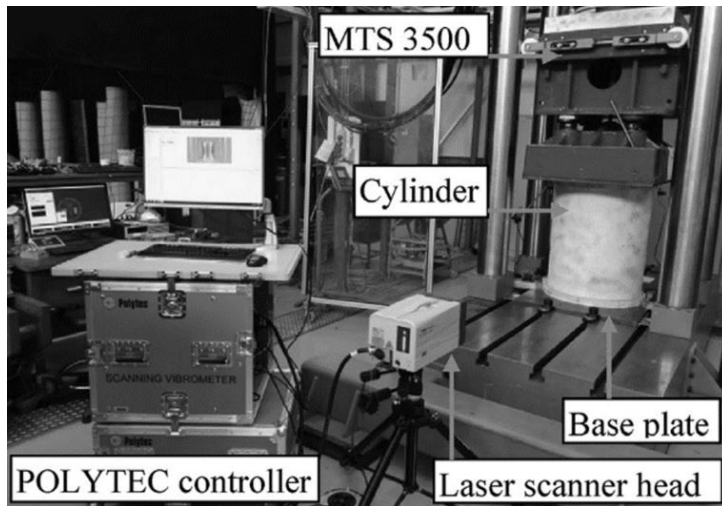


Figure 1.7: Vibration correlation experiments on compressed cylinders [59]

Frequencies at different load levels can be measured experimentally via hammer impact or laser vibrometry tests. The buckling load can be then estimated by performing a linear extrapolation on the measured data points. This procedure is known as Vibration Correlation Technique (VCT), and is a well-established experimental method for the in-situ determination of the buckling load, applicable to a large range of structural types [60]. Very often, good estimations of the buckling load can be done with data extracted

at load levels below 60% of the estimated buckling load, which makes VCT a reliable non-destructive method. Latest research on this topic concerns the study of metallic plates [61], fixed and steered fiber composite cylinders [61]–[63], or grid-stiffened shells [64]. An example of this kind of experiment, recently performed by Labans et al. [59], is reported in Fig. 1.7.

Since thermal buckling experiments are not numerous, the scarcity of experimental data regarding the VCT applied to heated composite plates is even more pronounced. Additionally, while vibration changes can be used to predict buckling using VCT, it is not known whether the occurrence of a mode jump is registered in the frequency signature of the plate. In Chapter 5, a third experimental study was conducted with two goals: exploring the applicability of VCT for buckling prediction on heated composite plates and exploring changes in frequency patterns at load levels close to the occurrence of the mode jumps. For this, two plates were tested in two different test setups. These setups were modified versions of the experimental setups reported in Chapter 3 and Chapter 4. The most relevant contributions of this investigation are the reported experimental data for the application of VCT to heated composite plates, as well as observations of vibration behavior of plates after the occurrence of a mode jump. A good understanding of VCT for the prediction of buckling of heated composite structures could be a highly valuable asset for experimentation on future aerospace vehicles.

1.6. RESEARCH OBJECTIVES AND THESIS OUTLINE

The main goal of this thesis is gaining understanding on buckling and post-buckling states in composite plates subjected to thermomechanical loads, putting an emphasis in the interaction between these two load types and their influence over buckling and post-buckling phenomena.

It is desired to obtain a grasp on the real potential of post-buckling states for common aerospace applications, as well as contributing to develop methodologies and approaches for the design of aerospace structures that can operate on those states. For this Ph.D. research study, the design space has been limited to rectangular flat plates with symmetric and balanced stacking orientations. These research objectives have been articulated into four research questions:

1. What is the relation between thermal and external mechanical loads in the onset of thermomechanical buckling on flat composite plates?
2. Is it possible to predict whether or not a composite plate will experience mode jumps during a thermal buckling experiment? If yes, can the mode jumping temperature be predicted accurately?
3. During an experiment in thermal buckling, would the occurrence of an hypothetical mode jump be in any way affected by the introduction of additional, external mechanical load? If yes, are there any relation between these two factors?
4. Can the Vibration Correlation Technique (VCT) be successfully applied to heated composite plates to determine thermal buckling? And also, does the occurrence of a mode jump during a thermal buckling experiment leave identifiable traces in the frequency signature of the tested plate?

In order to answer these questions, the thesis in hand is structured as a compendium of four independent investigations, corresponding to four different journal articles that have been reproduced in chapters 2 to 5 of this thesis. This layout allows each chapter to be read individually, since they are self-contained entities. Due to this, eventual repetitions on certain aspects on the content can eventually be found along this thesis. The author apologizes for the inconveniences that such redundancies may cause. The layout of the thesis has been illustrated in Fig. 1.8, in the form of a flow chart that represents the path followed during the present research. In the figure, the studied topics are represented inside white boxes, labelled with black balloons that indicate the corresponding thesis chapter.

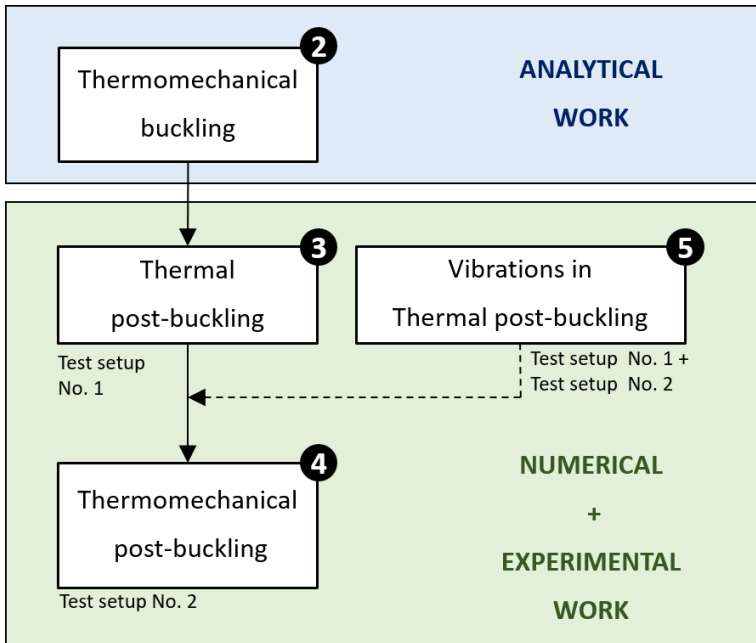


Figure 1.8: Ph.D. thesis diagram.

In Fig. 1.8 it can be seen how a clear division exists between Chapter 2 and Chapters 3 to 5, from the standpoints of both topic and research approach. While Chapter 2 is an analytical study on linear buckling, Chapters 3 to 5 combine numerical and experimental techniques to study post-buckling. Chapter 2 consists on a study over the onset of buckling on plates subjected to combined thermal and mechanical loads, which provided valuable information on the most relevant parameters and trends in the onset of thermomechanical buckling. Through the deduction of a closed-form equation, the relation between external mechanical load and temperature could be elucidated, helping to set the path to the investigations performed in posterior chapters. Chapter 3 is an investigation of thermal post-buckling. First, a set of parametric studies were performed to identify plates showing mode jumps in their thermal post-buckling regime. These analysis were also critical for identifying plate dimensions and layouts suitable for fur-

ther experimentation. Based on the information gained during the parametric studies, a novel test setup, labelled in the figure as Test Setup No. 1, was designed and built. This test setup had the capability of inducing thermal buckling to plates by restraining their in-plane thermal expansion. The combination of the preliminary numerical studies and the performed experiments provided important hints towards the understanding of mode jumping behavior on heated composite plates. The designed test setup was also an important stepping stone towards a more sophisticated test setup in the subsequent step of this research, presented in next chapter. Chapter 4 dealt with the effect of combined thermal and mechanical loads over the post-buckling regime. A set of numerical analysis studying the effect of different combinations of thermomechanical loads were performed over plates obtained in Chapter 3. The results of these analysis revealed relevant trends and helped in the design of a new experimental setup. This setup, named Test Setup No. 2, was capable to apply both compression and heating loads simultaneously. Chapter 5 consisted on an experimental study of plate vibration of thermally buckled composite plates. This study was performed using modifications of the test setups used in previous chapters. The Vibration Correlation Technique was used to predict the onset of buckling, and changes in vibration modes in the proximity of the mode jumps were investigated, in order to look for changes in the frequencies that could be related to the mode jump. For this, variations of previously designed Test Setup No.1 and Test Setup No. 2 were used. In Chapter 6, the main conclusions reached during this Ph.D. Thesis are presented, lays out the final conclusions, as well as discusses future work.

BIBLIOGRAPHY

- [1] C. Kassapoglou, *Design and Analysis of Composite Structures*. Oxford, UK: John Wiley & Sons Ltd, May 2013, ISBN: 9781118536933. DOI: 10.1002/9781118536933. [Online]. Available: <http://doi.wiley.com/10.1002/9781118536933>.
- [2] R. Jones, *Mechanics of Composite Materials*, English, 2nd ed. Taylor & Francis, 1983, vol. 18, pp. 434–439. [Online]. Available: <http://catdir.loc.gov/catdir/enhancements/fy0647/98018290-d.html%20http://link.springer.com/10.1007/BF00611782>.
- [3] Z. Huda and P. Edi, “Materials selection in design of structures and engines of supersonic aircrafts: A review”, *Materials and Design*, vol. 46, pp. 552–560, 2013, ISSN: 02641275. DOI: 10.1016/j.matdes.2012.10.001. [Online]. Available: <http://dx.doi.org/10.1016/j.matdes.2012.10.001>.
- [4] Toray, *Toray's ultra-high temperature composites*. [Online]. Available: <https://www.toraytac.com/products/thermoset/high-temperature-polyimides> (visited on 03/23/2022).
- [5] Hexcel Corporation, *M65 - Toughened bismaleimide resin for advanced composites*. [Online]. Available: <https://www.hexcel.com/Resources/DataSheets/Prepreg> (visited on 03/23/2022).
- [6] V. McConnell, *Resins for the hot zone, part II: BMIs, CEs, benzoxazines and phthalonitriles*. [Online]. Available: <https://www.compositesworld.com/articles/resins-for-the-hot-zone-part-ii-bmis-ces-benzoxazines-and-phthalonitriles> (visited on 03/23/2022).
- [7] G. Nehls, *Lockheed Martin prepares X-59 for quiet supersonic flight testing*, 2021. [Online]. Available: <https://www.compositesworld.com/news/lockheed-martin-prepares-x-59-for-quiet-supersonic-flight-testing> (visited on 03/23/2022).
- [8] B. Supersonic, *Boom Overture*. [Online]. Available: <https://boomsupersonic.com/overture>.
- [9] T. Pallini and D. Slotnick, *The startup that wants to bring back ultra-fast supersonic travel just unveiled the prototype for its Overture passenger plan*, 2020. [Online]. Available: <https://www.businessinsider.com/supersonic-startup-boom-unveils-xb-1-prototype-begins-flight-testing-2020-10>.
- [10] European Commission, “Flightpath 2050 : Europe's vision for aviation : maintaining global leadership and serving society's needs”, 2011. DOI: 10.2777/50266. [Online]. Available: <https://op.europa.eu/en/publication-detail/-/publication/296a9bd7-fef9-4ae8-82c4-a21ff48be673/language-en>.

- [11] G. D. Brewer, *Hydrogen Aircraft Technology*, CRC, Ed. Boca Raton: Routledge, Nov. 2017, ISBN: 9780203751480. DOI: [10.1201/9780203751480](https://doi.org/10.1201/9780203751480). [Online]. Available: <https://www.taylorfrancis.com/books/9781351439794>.
- [12] G. Norris, *Airbus reveals refined ZEROe blended wing body concept*, 2022. [Online]. Available: <https://aviationweek.com/shownews/singapore-airshow/airbus-reveals-refined-zeroe-blended-wing-body-concept> (visited on 04/13/2022).
- [13] J. Singer, J. Arbocz, and T. Weller, *Buckling Experiments: Experimental Methods in Buckling of Thin-Walled Structures*. Hoboken, NJ, USA: John Wiley & Sons, Inc., 2002, vol. 2, ISBN: 9780470172995. DOI: [10.1002/9780470172995](https://doi.org/10.1002/9780470172995). [Online]. Available: <http://doi.wiley.com/10.1002/9780470172995>.
- [14] C. Bisagni, R. Vescovini, and C. G. Dávila, “Single-stringer compression specimen for the assessment of damage tolerance of postbuckled structures”, *Journal of Aircraft*, vol. 48, no. 2, pp. 495–502, 2011, ISSN: 0021-8669. DOI: [10.2514/1.C031106](https://doi.org/10.2514/1.C031106). [Online]. Available: <http://arc.aiaa.org/doi/10.2514/1.C031106>.
- [15] R. Vescovini and C. G. Dávila, “Simplified models for the study of postbuckled hat-stiffened composite panels”, *Nasa Technical Memorandum*, vol. NASA/TM–20, no. February, 2012. [Online]. Available: <https://ntrs.nasa.gov/citations/20120002670>.
- [16] E. A. Thornton, *Thermal Structures for Aerospace Applications* (AIAA Education Series). American Institute of Aeronautics and Astronautics, Jan. 1996, pp. 397–441, ISBN: 978-1-56347-190-2. DOI: [10.2514/4.862540](https://doi.org/10.2514/4.862540). arXiv: [arXiv:1011.1669v3](https://arxiv.org/abs/1011.1669v3). [Online]. Available: <https://arc.aiaa.org/doi/book/10.2514/4.862540>.
- [17] M. P. Nemeth, “An in-depth tutorial on constitutive equations for elastic anisotropic materials (NASA/TM–2011-217314)”, *National Aeronautics and Space Administration*, no. December, p. 588, 2011. [Online]. Available: <http://ntrs.nasa.gov/search.jsp?R=20110023650>.
- [18] W. Koiter, *The Stability of Elastic Equilibrium*. (Ph.D Thesis) Department of Mechanics, Shipbuilding, and Airplane Building, Technische Hooge School Delft, 1945, ISBN: 0000000000.
- [19] H. Chen and L. Virgin, “Finite element analysis of post-buckling dynamics in plates-Part I: An asymptotic approach”, *International Journal of Solids and Structures*, vol. 43, no. 13, pp. 3983–4007, 2006, ISSN: 00207683. DOI: [10.1016/j.ijsoistr.2005.04.036](https://doi.org/10.1016/j.ijsoistr.2005.04.036).
- [20] H. S. Shen, “Thermomechanical postbuckling of imperfect shear deformable laminated plates on elastic foundations”, *Computer Methods in Applied Mechanics and Engineering*, vol. 189, no. 3, pp. 761–784, 2000, ISSN: 00457825. DOI: [10.1016/S0045-7825\(99\)00328-X](https://doi.org/10.1016/S0045-7825(99)00328-X).
- [21] C. L. Dym and I. H. Shames, *Solid Mechanics*. New York, NY: Springer New York, 2013, ISBN: 978-1-4614-6033-6. DOI: [10.1007/978-1-4614-6034-3](https://doi.org/10.1007/978-1-4614-6034-3). [Online]. Available: <http://link.springer.com/10.1007/978-1-4614-6034-3>.

- [22] M. P. Nemeth, "Buckling behavior of long anisotropic plates subjected to fully restrained thermal expansion", *TP-2003-212131, National Aeronautics and Space Administration*, no. November, 2003, ISSN: 02734508. [Online]. Available: <http://hdl.handle.net/2060/19970004648>.
- [23] M. P. Nemeth, "Buckling behavior of long anisotropic plates subjected to restrained thermal expansion and mechanical loads", *Journal of Thermal Stresses*, vol. 23, no. 9, pp. 873–916, Dec. 2000, ISSN: 1521074X. DOI: [10.1080/014957300750040122](https://doi.org/10.1080/014957300750040122). [Online]. Available: <http://www.tandfonline.com/doi/abs/10.1080/014957300750040122>.
- [24] C. A. Meyers and M. W. Hyer, "Thermal buckling and postbuckling of symmetrically laminated composite plates", *Journal of Thermal Stresses*, vol. 14, no. 4, pp. 519–540, 1991, ISSN: 1521074X. DOI: [10.1080/01495739108927083](https://doi.org/10.1080/01495739108927083).
- [25] T. R. Tauchert, "Temperature and absorbed moisture", in *Buckling and Postbuckling of Composite Plates*, G. J. Turvey and I. H. Marshall, Eds. Dordrecht: Springer Netherlands, 1995, pp. 190–226, ISBN: 978-94-011-1228-4. DOI: [10.1007/978-94-011-1228-4_6](https://doi.org/10.1007/978-94-011-1228-4_6). [Online]. Available: https://doi.org/10.1007/978-94-011-1228-4_6.
- [26] J. Li, X. Tian, Z. Han, and Y. Narita, "Stochastic thermal buckling analysis of laminated plates using perturbation technique", *Composite Structures*, vol. 139, pp. 1–12, 2016, ISSN: 02638223. DOI: [10.1016/j.compstruct.2015.11.076](https://doi.org/10.1016/j.compstruct.2015.11.076). [Online]. Available: <http://dx.doi.org/10.1016/j.compstruct.2015.11.076>.
- [27] N. Sharma, M. Nishad, D. K. Maiti, M. R. Sunny, and B. N. Singh, "Uncertainty quantification in buckling strength of variable stiffness laminated composite plate under thermal loading", *Composite Structures*, vol. 275, no. February, p. 114486, 2021, ISSN: 02638223. DOI: [10.1016/j.compstruct.2021.114486](https://doi.org/10.1016/j.compstruct.2021.114486). [Online]. Available: <https://doi.org/10.1016/j.compstruct.2021.114486>.
- [28] R. Kumar, L. S. Ramachandra, and B. Banerjee, "Semi-analytical approach for thermal buckling and postbuckling response of rectangular composite plates subjected to localized thermal heating", *Acta Mechanica*, vol. 228, no. 5, pp. 1767–1791, 2017, ISSN: 00015970. DOI: [10.1007/s00707-016-1797-9](https://doi.org/10.1007/s00707-016-1797-9).
- [29] S. Xu and W. J. Bottega, "Thermo-Mechanical Buckling of Stepped Circular Bi-Laminates", *International Journal of Mechanical Sciences*, vol. 198, no. February, p. 106344, 2021, ISSN: 00207403. DOI: [10.1016/j.ijmecsci.2021.106344](https://doi.org/10.1016/j.ijmecsci.2021.106344).
- [30] R. Vescovini, M. D'Ottavio, L. Dozio, and O. Polit, "Thermal buckling response of laminated and sandwich plates using refined 2-D models", *Composite Structures*, vol. 176, pp. 313–328, 2017, ISSN: 02638223. DOI: [10.1016/j.compstruct.2017.05.021](https://doi.org/10.1016/j.compstruct.2017.05.021). [Online]. Available: <http://dx.doi.org/10.1016/j.compstruct.2017.05.021>.
- [31] F. A. Fazzolari and E. Carrera, "Thermo-mechanical buckling analysis of anisotropic multilayered composite and sandwich plates by using refined variable-kinematics theories", *Journal of Thermal Stresses*, vol. 36, no. 4, pp. 321–350, 2013, ISSN: 01495739. DOI: [10.1080/01495739.2013.770642](https://doi.org/10.1080/01495739.2013.770642).

- [32] E. Carrera, F. A. Fazzolari, and M. Cinefra, *Thermal Stress Analysis of Composite Beams, Plates and Shells*. London: Elsevier Inc., 2017, ISBN: 9780124200937.
- [33] M. Cetkovic, "Thermo-mechanical bending of laminated composite and sandwich plates using layerwise displacement model", *Composite Structures*, vol. 125, pp. 388–399, 2015, ISSN: 02638223. DOI: [10.1016/j.compstruct.2015.01.051](https://doi.org/10.1016/j.compstruct.2015.01.051). [Online]. Available: <http://dx.doi.org/10.1016/j.compstruct.2016.01.082%20http://dx.doi.org/10.1016/j.compstruct.2015.01.051>.
- [34] A. K. Noor and J. M. Peterst, "Postbuckling of multilayered composite plates subjected to combined axial and thermal loads",
- [35] W. Ko, "Thermal analysis stiffened and mechanical buckling of hypersonic aircraft panels with varying hat-face sheet geometry and fiber orientation", *NASA Technical Memorandum 4770*, 1996. [Online]. Available: <https://ntrs.nasa.gov/citations/19970005336>.
- [36] J. Lee and M. Bhatia, "Impact of corrugations on bifurcation and thermoelastic responses of hat-stiffened panels", *Thin-Walled Structures*, vol. 140, no. October 2018, pp. 209–221, Jul. 2019, ISSN: 02638231. DOI: [10.1016/j.tws.2019.03.027](https://doi.org/10.1016/j.tws.2019.03.027). [Online]. Available: <https://linkinghub.elsevier.com/retrieve/pii/S0263823118311273%20https://doi.org/10.1016/j.tws.2019.03.027>.
- [37] K. R. Thangaratnam, Palaninathan, and J. Ramachandran, "Thermal buckling of composite laminated plates", *Computers and Structures*, vol. 32, no. 5, pp. 1117–1124, 1989, ISSN: 00457949. DOI: [10.1016/0045-7949\(89\)90413-6](https://doi.org/10.1016/0045-7949(89)90413-6).
- [38] L. C. Shiau, S. Y. Kuo, and C. Y. Chen, "Thermal buckling behavior of composite laminated plates", *Composite Structures*, vol. 92, no. 2, pp. 508–514, 2010, ISSN: 02638223. DOI: [10.1016/j.compstruct.2009.08.035](https://doi.org/10.1016/j.compstruct.2009.08.035). [Online]. Available: <http://www.sciencedirect.com/science/article/pii/S0045794989904136>.
- [39] V. K. Verma and B. N. Singh, "Thermal buckling of laminated composite plates with random geometric and material properties", *International Journal of Structural Stability and Dynamics*, vol. 9, no. 2, pp. 187–211, 2009, ISSN: 02194554. DOI: [10.1142/S0219455409002990](https://doi.org/10.1142/S0219455409002990).
- [40] M. Cerini and B. Falzon, "Use of the arc-length method for capturing mode jumping in postbuckling aerostructures", *AIAA Journal*, vol. 43, no. 3, pp. 681–689, 2008, ISSN: 0001-1452. DOI: [10.2514/1.7914](https://doi.org/10.2514/1.7914).
- [41] C. Bisagni, "Numerical analysis and experimental correlation of composite shell buckling and post-buckling", *Composites Part B: Engineering*, vol. 31, no. 8, pp. 655–667, 2000, ISSN: 13598368. DOI: [10.1016/S1359-8368\(00\)00031-7](https://doi.org/10.1016/S1359-8368(00)00031-7).
- [42] I. Uriol Balbin and C. Bisagni, "Buckling of sandwich cylindrical shells with shear deformable core through nondimensional parameters", *Thin-Walled Structures*, vol. 161, p. 107393, 2021, ISSN: 02638231. DOI: [10.1016/j.tws.2020.107393](https://doi.org/10.1016/j.tws.2020.107393). [Online]. Available: <https://doi.org/10.1016/j.tws.2020.107393>.
- [43] B. Falzon and D. Hitchings, "Capturing mode-switching in postbuckling composite panels using a modified explicit procedure", *Composite Structures*, vol. 60, pp. 447–453, 2003, ISSN: 02638223. DOI: [10.1016/S0263-8223\(03\)00019-9](https://doi.org/10.1016/S0263-8223(03)00019-9).

- [44] L. Lanzi, "A numerical and experimental investigation on composite stiffened panels into post-buckling", *Thin-Walled Structures*, vol. 42, no. 12, pp. 1645–1664, 2004, ISSN: 0263-8231. DOI: <https://doi.org/10.1016/j.tws.2004.06.001>. [Online]. Available: <https://www.sciencedirect.com/science/article/pii/S0263823104001272>.
- [45] H. Chen and L. Virgin, "Dynamic analysis of modal shifting and mode jumping in thermally buckled plates", *Journal of Sound and Vibration*, vol. 278, no. 1-2, pp. 233–256, 2004, ISSN: 0022460X. DOI: [10.1016/j.jsv.2003.10.054](https://doi.org/10.1016/j.jsv.2003.10.054).
- [46] V. Bhagat, J. P., and P. Jeyaraj, "Experimental investigation on buckling strength of cylindrical panel: Effect of non-uniform temperature field", *International Journal of Non-Linear Mechanics*, vol. 99, no. December 2017, pp. 247–257, Mar. 2018, ISSN: 00207462. DOI: [10.1016/j.ijnonlinmec.2017.12.005](https://doi.org/10.1016/j.ijnonlinmec.2017.12.005). [Online]. Available: <https://doi.org/10.1016/j.ijnonlinmec.2017.12.005>.
- [47] E. A. Thornton, M. F. Coyle, and R. N. McLeod, "Experimental study of plate buckling induced by spatial temperature gradients", *Journal of Thermal Stresses*, vol. 17, no. 2, pp. 191–212, Apr. 1994, ISSN: 0149-5739. DOI: [10.1080/01495739408946255](https://doi.org/10.1080/01495739408946255). [Online]. Available: <http://www.tandfonline.com/doi/full/10.1080/01495739408946255>.
- [48] K. D. Murphy and D. Ferreira, "Thermal buckling of rectangular plates", *International Journal of Solids and Structures*, vol. 38, no. 22-23, pp. 3979–3994, May 2001, ISSN: 00207683. DOI: [10.1016/S0020-7683\(00\)00240-7](https://doi.org/10.1016/S0020-7683(00)00240-7). [Online]. Available: <https://linkinghub.elsevier.com/retrieve/pii/S0020768300002407>.
- [49] D. A. Ehrhardt and L. N. Virgin, "Experiments on the thermal post-buckling of panels, including localized heating", *Journal of Sound and Vibration*, vol. 439, pp. 300–309, Jan. 2019, ISSN: 0022460X. DOI: [10.1016/j.jsv.2018.08.043](https://doi.org/10.1016/j.jsv.2018.08.043).
- [50] J. F. Rakow and A. M. Waas, "Thermal buckling of metal foam sandwich panels for convective thermal protection systems", *Journal of Spacecraft and Rockets*, vol. 42, no. 5, pp. 832–844, Sep. 2005, ISSN: 0022-4650. DOI: [10.2514/1.9741](https://doi.org/10.2514/1.9741). [Online]. Available: <http://arc.aiaa.org/doi/abs/10.2514/1.9741%20https://arc.aiaa.org/doi/10.2514/1.9741>.
- [51] Y. Xu, S. Ren, W. Zhang, Z. Wu, W. Gong, and H. Li, "Study of thermal buckling behavior of plain woven C/SiC composite plate using digital image correlation technique and finite element simulation", *Thin-Walled Structures*, vol. 131, no. October 2017, pp. 385–392, Oct. 2018, ISSN: 02638231. DOI: [10.1016/j.tws.2018.07.023](https://doi.org/10.1016/j.tws.2018.07.023). [Online]. Available: <https://doi.org/10.1016/j.tws.2018.07.023%20https://linkinghub.elsevier.com/retrieve/pii/S0263823117312788>.
- [52] M. Blosser, "Boundary Conditions for Aerospace Thermal-Structural Tests", in : *Aerospace Thermal Structures and Materials for a New Era*, vol. 168, Washington DC: American Institute of Aeronautics and Astronautics, Jan. 1995, pp. 119–144. DOI: [10.2514/5.9781600866364.0119.0144](https://doi.org/10.2514/5.9781600866364.0119.0144). [Online]. Available: <http://arc.aiaa.org/doi/10.2514/5.9781600866364.0119.0144%20https://arc.aiaa.org/doi/10.2514/5.9781600866364.0119.0144>.

- [53] M. Anderson and M. Card, “Buckling of ring-stiffened cylinders under a pure bending moment and a nonuniform temperature distribution”, Tech. Rep. November, Nov. 1962. [Online]. Available: <https://ntrs.nasa.gov/citations/19630000305>.
- [54] D. Bushnell and S. Smith, “Stress and buckling of nonuniformly heated cylindrical and conical shells”, *AIAA Journal*, vol. 9, no. 12, pp. 2314–2321, Dec. 1971, ISSN: 0001-1452. DOI: [10.2514/3.6515](https://doi.org/10.2514/3.6515). [Online]. Available: <https://arc.aiaa.org/doi/10.2514/3.6515>.
- [55] W. Percy and R. Fields, “Buckling analysis and test correlation of hat stiffened panels for hypersonic vehicles”, in *2nd International Aerospace Planes Conference*, Reston, Virginia: American Institute of Aeronautics and Astronautics, Oct. 1990. DOI: [10.2514/6.1990-5219](https://doi.org/10.2514/6.1990-5219). [Online]. Available: <http://arc.aiaa.org/doi/10.2514/6.1990-5219%20https://arc.aiaa.org/doi/10.2514/6.1990-5219>.
- [56] R. C. Thompson and W. L. Richards, “Thermal-structural panel buckling tests”, *NASA Technical Memorandum 104243*, no. December 1991, 1991. [Online]. Available: <https://ntrs.nasa.gov/citations/19920006186>.
- [57] N. Breivik, M. Nyer, J. Starnes, Jr., N. Breivik, M. Nyer, and J. Starnes, Jr., “Thermal and mechanical buckling and postbuckling responses of selected curved composite panels”, in *38th Structures, Structural Dynamics, and Materials Conference*, Reston, Virginia: American Institute of Aeronautics and Astronautics, Apr. 1997, pp. 2471–2480. DOI: [10.2514/6.1997-1247](https://doi.org/10.2514/6.1997-1247). [Online]. Available: <http://arc.aiaa.org/doi/10.2514/6.1997-1247%20https://arc.aiaa.org/doi/10.2514/6.1997-1247>.
- [58] R. A. Fields, W. L. Richards, and M. V. DeAngelis, “Combined loads test fixture for thermal-structural testing of aerospace vehicle panel concepts”, *NASA Technical Memorandum TM-2004-212039*, no. February, 2004. [Online]. Available: <https://ntrs.nasa.gov/citations/20040031531>.
- [59] E. Labans, H. Abramovich, and C. Bisagni, “An experimental vibration-buckling investigation on classical and variable angle tow composite shells under axial compression”, *Journal of Sound and Vibration*, vol. 449, pp. 315–329, 2019, ISSN: 10958568. DOI: [10.1016/j.jsv.2019.02.034](https://doi.org/10.1016/j.jsv.2019.02.034). [Online]. Available: <https://doi.org/10.1016/j.jsv.2019.02.034>.
- [60] H. Abramovich, “The Vibration Correlation Technique – A reliable nondestructive method to predict buckling loads of thin walled structures”, *Thin-Walled Structures*, vol. 159, no. May 2020, p. 107308, 2021, ISSN: 02638231. DOI: [10.1016/j.tws.2020.107308](https://doi.org/10.1016/j.tws.2020.107308). [Online]. Available: <https://doi.org/10.1016/j.tws.2020.107308>.
- [61] M. A. Arbelo, S. F. M. De Almeida, M. V. Donadon, *et al.*, “Vibration correlation technique for the estimation of real boundary conditions and buckling load of unstiffened plates and cylindrical shells”, *Thin-Walled Structures*, vol. 79, pp. 119–128, 2014, ISSN: 02638231. DOI: [10.1016/j.tws.2014.02.006](https://doi.org/10.1016/j.tws.2014.02.006).
- [62] E. Labans and C. Bisagni, “Buckling and free vibration study of variable and constant-stiffness cylindrical shells”, *Composite Structures*, vol. 210, pp. 446–457, 2019, ISSN: 02638223. DOI: [10.1016/j.compstruct.2018.11.061](https://doi.org/10.1016/j.compstruct.2018.11.061).

- [63] M. A. Arbelo, K. Kalnins, O. Ozolins, E. Skukis, S. G. Castro, and R. Degenhardt, “Experimental and numerical estimation of buckling load on unstiffened cylindrical shells using a vibration correlation technique”, *Thin-Walled Structures*, vol. 94, pp. 273–279, 2015, ISSN: 02638231. DOI: [10.1016/j.tws.2015.04.024](https://doi.org/10.1016/j.tws.2015.04.024).
- [64] D. Shahgholian-Ghahfarokhi and G. Rahimi, “Buckling load prediction of grid-stiffened composite cylindrical shells using the vibration correlation technique”, *Composites Science and Technology*, vol. 167, no. September, pp. 470–481, 2018, ISSN: 02663538. DOI: [10.1016/j.compscitech.2018.08.046](https://doi.org/10.1016/j.compscitech.2018.08.046). [Online]. Available: <https://doi.org/10.1016/j.compscitech.2018.08.046>.

2

CLOSED-FORM SOLUTIONS FOR THERMOMECHANICAL BUCKLING OF ORTHOTROPIC COMPOSITE PLATES

*Yo soy yo y mi circunstancia.
I am I plus my circumstances.*

José Ortega y Gasset

A closed-form solution is derived for the buckling of orthotropic composite plates under the effect of thermal and mechanical loads. The plates are subjected to constant temperature increment and length variation while the width expansion is constrained. The problem is formulated in terms of displacement components, studied using classical plate theory in combination with classical lamination theory. An analytical formula that relates critical temperatures to applied plate displacements is obtained. The buckling of heated, fully restrained plates is also derived as a particular case. Examples of plates made of different materials and lay-ups are presented in graphical form, and are verified by finite element analysis. The obtained formula can be used during initial design, for sensitivity analysis and also for obtaining desired buckling shapes.

This chapter has been adapted from: J. Gutiérrez Álvarez and C. Bisagni, "Closed-form solutions for thermo-mechanical buckling of orthotropic composite plates", *Composite Structures*, vol. 233, no. May 2019, p. 111 622, Feb. 2020, ISSN: 02638223. DOI: 10.1016/j.compstruct.2019.111622.

2.1. INTRODUCTION

THERMOMECHANICAL loads are present in many applications, and often represent a challenge for structures working in extreme environments. For example, this is the case of supersonic aircraft, which, in addition to mechanical loads, must endure the thermal loads inherent to high speed flight. Under such demanding conditions their lightweight design makes them highly susceptible to buckling. In order to preserve safety, efficiency and structural performance, understanding thermomechanical buckling becomes a key task.

Thermal buckling has been a topic of research since the early stages of supersonic flight, when the focus was on structures made of metallic materials. In the following decades, several research activities were conducted to investigate the thermal buckling of laminate composite materials. Whitney and Ashton [1] studied the effect of temperature and moisture in composite plates incorporating a generalized Duhamel-Neumann formulation, and assessed the buckling behaviour of generic, unsymmetric plates with all normal expansions restricted. Tauchert and Huang [2] extended this formulation for the study of thick antisymmetric laminate plates, incorporating Mindlin plate theory, solving the problem via the Galerkin method and assessing the effect of fixed and sliding boundary conditions. In later studies, Tauchert [3] particularized these studies into symmetric laminates using Rayleigh-Ritz method, while Sun and Hsu [4] developed a formula for thick, cross-ply, symmetric and balanced laminates using the Galerkin method. Meyers and Hyer [5] studied buckling and postbuckling of symmetric laminates, investigating the influence of the deviation of the load direction with respect to the material axis, using the Rayleigh-Ritz method. Abramovich [6] studied the buckling of cross-ply laminates under uniform thermal increment, considering a first-order shear deformation theory. Jones [7] investigated both unidirectional and cross-ply laminates under uniform heating and restricted normal expansions. Specially remarkable is the effort of Nemeth [8], who derived the buckling temperatures for an extensive range of long, fully restrained laminated plates. Wittrick and Williams studied the buckling of anisotropic plates under combined loading [9]. Matsunaga [10] developed 2D global higher-order deformation theory for thermal buckling of cross-ply laminated composite and sandwich plates. More recently, Vescovini et al. [11] developed a refined 2D model for generic panels (both sandwich and monolithic), able to selectively account for higher order theories in specific regions of interest. Li et al. conducted research on the effect of scatter in material properties [12] and on the effect of thermal gradients over the buckling temperature [13].

Thermal buckling has also been approached using finite element analysis: Shi et al. [14] studied thermal buckling and postbuckling of composite plates using the finite element modal coordinate method; Shiau et al. [15] assessed the influence of the lamina stiffness ratio E_L/E_T and lamina thermal expansion ratio α_2/α_1 in the buckling pattern formation of heated laminated plates using the finite element method. Ounis et al. [16] proposed a new type of finite element using a combination of linear isoparametric membrane element and a high precision rectangular Hermitian element.

However, most of mentioned analytical and numerical studies consider only thermal buckling, i.e. buckling caused merely by constrained thermal expansions, plate edges are

kept straight and constant in length and the original dimensions of the panel remain unchanged. The influence of external mechanical loads in the buckling temperature and shape cannot be assessed unless plate size variation is incorporated in the formulation. Although in the last decade extensive analytical research has been done in the field of pure mechanical buckling [17]–[23], only few studies explore the buckling of mechanically and thermally loaded panels, like the one of Jones [24] for metallic materials, or Nemeth [25] for infinite laminate plates. Some authors like Noor et al. [26], or more recently Nali and Carrera [27], studied thermomechanical buckling using finite element models based on multilayered panel formulations.

This paper presents an analytical formulation for the calculation of buckling temperatures under the effect of external mechanical load and restrained transversal expansion. The analysis of symmetric and balanced composite laminated plates is presented, where temperature increment is applied and mechanical load is introduced in the form of shortening. Examples of plates made of different composite materials and different lay-ups are analysed and compared. The obtained formula can be used during initial design, for sensitivity analysis and also for deriving specific buckling shapes.

2.2. PROBLEM FORMULATION

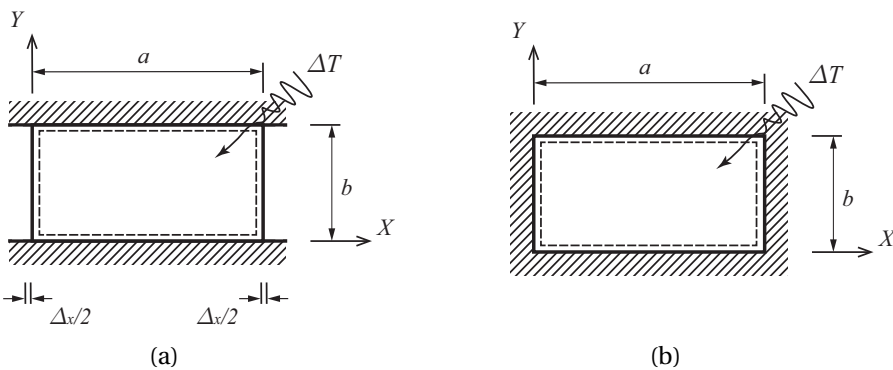


Figure 2.1: Heated plates: (a) Plate with transversal expansion restrained and prescribed length variation. (b) Plate with all expansions restrained.

A rectangular plate of length a and width b is considered. The plate is placed in a XYZ coordinate system, being the plane XY coincident with the mid-plane of the plate, and the Z axis perpendicular to this plane. In the present study two different types of boundary conditions are considered. The first type consists of plates that can experiment variations in length while their width remains unchanged. Plate edges are not allowed to displace out-of-plane. A graphical representation of the described constraints can be found in Fig. 2.1 (a), while the corresponding equations are presented below:

$$\begin{aligned} \text{at } X = 0, a: \quad u^0 = \pm \Delta_x / 2 \quad \text{at } Y = 0, b: \quad u^0 = \text{free} \\ v^0 = \text{free} \quad v^0 = 0 \\ w^0 = 0 \quad w^0 = 0 \end{aligned}$$

2

where u^0 , v^0 , w^0 are the displacements of the plate mid-plane in the respective X , Y and Z directions. The plate is subjected to total length variations Δ_x along X axis. Positive values of Δ_x are taken for plate stretching, while plate shortening is assumed negative. The plate experiments an uniform temperature increment ΔT respect from a stress-free state. The order of load application is indifferent: ΔT can be applied before Δ_x , and also the other way around.

The second type of boundary conditions can be understood as a particular case of the first type. For this case, both plate length and width remain unchanged. The equations describing this new set of constraints can be easily achieved enforcing $\Delta_x = 0$ in the equations for the first type. The corresponding graphical representation is reported in Fig. 2.1 (b).

A plate under the first type of boundary conditions will now be considered. The plate is analysed by means of classical plate theory plate theory in combination with classical lamination theory (CLT). Each ply is oriented at a generic angle θ , which is defined with respect to the X reference axis and is assumed to be counter-clockwise positive. The laminate layup is assumed to be orthotropic and material properties are considered to remain constant within the analysed range of temperatures.

The in-plane behaviour of the laminate is governed by the membrane constitutive equations (Eq. 5.2):

$$\begin{Bmatrix} N_x \\ N_y \\ N_{xy} \end{Bmatrix} = \begin{bmatrix} A_{11} & A_{12} & 0 \\ A_{12} & A_{22} & 0 \\ 0 & 0 & A_{66} \end{bmatrix} \begin{Bmatrix} \varepsilon_{xx}^0 \\ \varepsilon_{yy}^0 \\ \gamma_{xy}^0 \end{Bmatrix} - \begin{Bmatrix} N_x^T \\ N_y^T \\ N_{xy}^T \end{Bmatrix} \quad (2.1)$$

where N_x , N_y , N_{xy} are the force resultants at the plate edges, the terms A_{ij} ($i, j = 1, 2, 6$) are the membrane stiffness terms from CLT, ε_{xx}^0 , ε_{yy}^0 , γ_{xy}^0 are the engineering strains of the mid-plane of the plate, and N_x^T , N_y^T , N_{xy}^T are the thermal force resultants. The in-plane displacements can be described as linear functions of the total plate length variations Δ_x . The thermal force resultants are expressed as showed in Eq. 2.2:

$$\begin{Bmatrix} N_x^T \\ N_y^T \\ N_{xy}^T \end{Bmatrix} = \sum_{k=1}^N \int_{z_{k-1}}^{z_k} \begin{bmatrix} Q_{xx} & Q_{xy} & Q_{xs} \\ Q_{xy} & Q_{yy} & Q_{ys} \\ Q_{xs} & Q_{ys} & Q_{ss} \end{bmatrix} \begin{Bmatrix} \alpha_x^{(k)} \\ \alpha_y^{(k)} \\ \alpha_{xy}^{(k)} \end{Bmatrix} \Delta T dz \quad (2.2)$$

where Q_{ij} ($i, j = x, y, s$) are the in-plane stiffnesses of a single lamina projected into XYZ coordinate system, k is a generic lamina number and N the total amount of laminae, and $\alpha_x^{(k)}$, $\alpha_y^{(k)}$, $\alpha_{xy}^{(k)}$ are the coefficients of thermal expansion (CTE) for a single lamina in the same coordinate system. Considering the temperature distribution homoge-

neous, the thermal force resultants are linear functions of ΔT , and can be expressed as in Eqs. 2.3:

$$N_x^T = \hat{N}_x^T \Delta T \quad N_y^T = \hat{N}_y^T \Delta T \quad N_{xy}^T = \hat{N}_{xy}^T \Delta T \quad (2.3)$$

where \hat{N}_x^T , \hat{N}_y^T , \hat{N}_{xy}^T are the thermal force resultants per unit thermal change. These quantities are function of lamina properties and stacking orientation. For symmetric and balanced laminates, \hat{N}_{xy}^T vanishes.

The membrane state is analysed considering linear displacements along the length and zero across the width, yielding Eqs. 2.4, which are solution to the pre-buckling problem:

$$N_x = A_{11} \frac{\Delta x}{a} - \hat{N}_x^T \Delta T$$

$$N_y = A_{12} \frac{\Delta x}{a} - \hat{N}_y^T \Delta T \quad (2.4)$$

being $N_{xy} = 0$. Eqs. 2.4 represent the force resultants at the plate edges and constitute the membrane state of the loaded plate. They are functions of both Δx and ΔT .

The buckling equation is expressed by Eq. 2.5:

$$D_{11} w_{,xxxx} + 2(D_{12} + 2D_{66}) w_{,xxyy} + D_{22} w_{,yyyy} - N_x w_{,xx} - N_y w_{,yy} = 0 \quad (2.5)$$

being the D_{ij} ($i, j = 1, 2, 6$) the laminate bending stiffnesses, and meaning the comma in the subindex partial differentiation with respect to the indicated variable. A solution for Eq. 2.5 is now assumed. This solution has the form of double Fourier series, as presented in Eq. 2.6:

$$w = \sum_{m=1}^{\infty} \sum_{n=1}^{\infty} W_{mn} \sin\left(\frac{m\pi x}{a}\right) \sin\left(\frac{n\pi y}{b}\right) \quad (2.6)$$

where W_{mn} ($m, n = 1, 2, 3, \dots$) are the amplitudes of the Fourier series terms, and m and n represent the number of half-waves in X and Y directions. After substituting Eq. 2.6 for the out-of-plane displacements and Eqs. 2.4 for the in-plane force resultants into Eq. 2.5, Eq. 2.7 appears:

$$\begin{aligned}
& \sum_{m=1}^{\infty} \sum_{n=1}^{\infty} \left(\frac{\pi^4 (a^4 n^4 D_{22} + 2 a^2 b^2 m^2 n^2 (D_{12} + 2 D_{66}))}{a^4 b^4} + \right. \\
& + \frac{\pi^4 b^4 m^4 D_{11}}{a^4 b^4} - \frac{\pi^2 (\hat{N}_x^T a b^2 m^2 \Delta T + \hat{N}_y^T a^3 n^2 \Delta T)}{a^3 b^2} + \\
& \left. - \frac{\pi^2 (-(a^2 n^2 A_{12} - b^2 m^2 A_{11}) \Delta_x)}{a^3 b^2} \right) \cdot W_{mn} \sin\left(\frac{m\pi x}{a}\right) \sin\left(\frac{n\pi y}{b}\right) = 0
\end{aligned} \tag{2.7}$$

After proper evaluation, the expression in Eq. 2.8 is obtained:

$$\begin{aligned}
\Delta T = & \frac{a^2 n^2 A_{12} + b^2 m^2 A_{11}}{b^2 m^2 \hat{N}_x^T + a^2 n^2 \hat{N}_y^T} \left(\frac{\Delta_x}{a} \right) + \\
& + \frac{\pi^2 (b^4 m^4 D_{11} + 2 a^2 b^2 m^2 n^2 (D_{12} + 2 D_{66}) + a^4 n^4 D_{22})}{a^2 b^2 (b^2 m^2 \hat{N}_x^T + a^2 n^2 \hat{N}_y^T)}
\end{aligned} \tag{2.8}$$

Eq. 2.8 represents the states of equilibrium for which the out-of-plane deflections are nonzero. For each state of equilibrium given by the number of half-waves m and n , the obtained Eq. 2.8 relates plate length variations Δ_x with thermal increments ΔT . For a certain value of Δ_x , the buckling temperature ΔT_{cr} is given by the buckling configuration (i.e. number of half-waves m and n) that delivers the lowest absolute value of ΔT . The presented deduction has been done using Δ_x as loading condition. A deduction using force resultants is also possible. However, it would introduce complexity as two types of force resultants, one mechanical and another thermal, would be necessary.

Eq. 2.8 has been deduced using simply supported boundary conditions. These are a simplification of reality and may not always capture the behaviour of the actual boundary conditions in a real structure.

2.3. APPLICATION CASES

A few examples of heated composite plates are here presented. The plates are subjected to the two types of boundary conditions described in section 2.2. The first set examples, reported in section 2.3.1, deal with the case of fully restrained thermal expansions. Results in this section are given in the form of buckling charts, illustrating the change of ΔT_{cr} versus varying aspect ratio a/b . The second set of examples, presented in section 2.3.2 correspond to the first type of boundary conditions, and cope with the case of simultaneous heating and external mechanical load. For this section, results are given in the form of buckling charts representing the variation of ΔT_{cr} versus applied Δ_x .

For all presented buckling charts, a few finite element analyses are performed in Abaqus for verification. In all diagrams, the results of the corresponding eigenvalue analyses are reported with the symbol of a circle. Buckling shapes obtained using Abaqus are also reported next to the corresponding buckling curve in the diagrams.

2.3.1. BUCKLING OF HEATED, FULLY RESTRAINED PLATES

An orthotropic composite laminate plate is now considered. The plate has in-plane expansions along X and Y axis restrained, while it experiments a uniform temperature increment ΔT . The plate can buckle when a ΔT is applied. The equation for thermal buckling can be obtained from previously deduced Eq. 2.8. Considering that the plate does not experiment any length variation, $\Delta_x = 0$. Thus, Eq. 2.9 unfolds:

$$\Delta T = \frac{\pi^2 (b^4 m^4 D_{11} + 2a^2 b^2 m^2 n^2 (D_{12} + 2D_{66}) + a^4 n^4 D_{22})}{a^2 b^2 (b^2 m^2 \hat{N}_x^T + a^2 n^2 \hat{N}_y^T)} \quad (2.9)$$

Eq. 2.9 gives the thermal buckling of thin, orthotropic, fully restrained composite laminated plates. For a certain plate geometry, material and stacking orientation, ΔT_{cr} is given by the buckling shape, i.e. values of m and n , delivering the minimal absolute value of ΔT . This equation has been already obtained in previous studies [2], [4].

Some important features can be inferred from Eq. 2.9. For instance, the sign of the critical buckling temperature ΔT_{cr} can often be predicted by looking at the signs of \hat{N}_x^T and \hat{N}_y^T . If both quantities are positive, plates buckle when heated; if both quantities are negative, plates buckle when cooled down. However, when quantities \hat{N}_x^T and \hat{N}_y^T have opposite sign, plates may buckle either when heated, cooled down, or under both conditions simultaneously. This particular phenomenon can be easily clarified: for a given plate geometry, layup and material, the numerator in Eq. 2.9 is always positive, because it merely depends on plate geometry and bending stiffness; however, the denominator may have positive and negative values due to \hat{N}_x^T and \hat{N}_y^T , ultimately affecting to the sign of ΔT_{cr} .

Eq. 2.9 can also be easily related to an equivalent formula for metallic materials. In terms of material behaviour, isotropy could be seen as a particular case of orthotropy. In order to perform such conversion, the following equivalences have to be considered:

$D_{11} = D_{22} = D_{12} + 2D_{66} = D$, $A_{12}/A_{11} = \nu$, $\hat{N}_x^T = \hat{N}_y^T = \hat{N}^T = Eh\alpha\Delta T/(1 - \nu)$. Plugging these in Eq. 2.9, Eq. 2.10 unfolds:

$$\Delta T = \frac{\pi^2(1 - \nu)D}{Eh\alpha} \left(\frac{m^2}{a^2} + \frac{n^2}{b^2} \right) \tag{2.10}$$

where ν is the isotropic Poisson ratio, α the CTE for isotropic materials, and D the plate bending stiffness from classical plate theory. It is possible to note that isotropic materials, ΔT_{cr} is always reached for $m = n = 1$ configurations. Thus, Eq. 2.10 is the formula for thermal buckling of thin, fully restrained isotropic plates. Eq. 2.10 has been previously documented in literature [28], [29]. Eq. 2.9 is at first verified against results extracted from literature ([14]–[16]). The aim of this verification is establishing the range of applicability of Eq. 2.9. The three chosen bibliographic sources analyse the same benchmark case, consisting in simply supported, fully restrained composite laminated plates of dimensions $381 \times 304 \times 1.22 \text{ mm}^3$, made of composite material with following ply properties: $E_1 = 155 \text{ GPa}$, $E_2 = 8.07 \text{ GPa}$, $G_{LT} = 4.55 \text{ GPa}$, $\nu_{LT} = 0.22$, $\alpha_1 = -0.07 \cdot 10^{-6}/^\circ\text{C}$, $\alpha_2 = 30.1 \cdot 10^{-6}/^\circ\text{C}$, and stacking sequences $[0/90/90/0]_s$ and $[0/45/-45/90]_s$. These plates are also analysed applying Eq. 2.9 and performing finite element analysis using Abaqus. For the Abaqus numerical analysis, plates were modelled as rectangular geometries, meshed with rectangular S4R shell elements, with an element size of approximately 25 mm . The S4R element type is a 4-node, quadrilateral, stress/displacement shell element with reduced integration and a large-strain formulation. It takes transverse shear in account in their formulation by making use of Reissner-Mindlin Hypothesis. The results of these verifications are presented in Table 2.1. The first row of Table 2.1 corresponds to a $[0/90/90/0]_s$ layup. It is a specially orthotropic laminate. The value delivered by Eq. 2.9 is in very good agreement with the values extracted from literature, while the result delivered by Abaqus is slightly larger, approaching to the exact value delivered by Eq. 2.9 from the stiffer side, showing a difference of 0.7%. The results in the second row of Table 2.1 correspond to the $[45/-45/0/90]_s$ quasi-isotropic stacking sequence. In this case, the terms D_{16} and D_{26} are nonzero, so using Eq. 2.9 can be considered as an approximation. The value delivered by Eq. 2.9 is a bit higher than both Abaqus and literature values. This is due to the non-negligible contribution of the bending anisotropy terms.

Stacking	Eq. 2.9 [$^\circ\text{C}$]	Abaqus [$^\circ\text{C}$]	Shi [14] [$^\circ\text{C}$]	Shiau [15] [$^\circ\text{C}$]	Ounis [16] [$^\circ\text{C}$]
$[0/90/90/0]_s$	6.81	6.86	6.81	6.81	6.81
$[0/45/-45/90]_s$	7.86	7.67	7.62	7.65	7.63

Table 2.1: Verification of buckling temperatures with different composite plates

Three examples of composite laminate plates are now analysed and discussed. The first example studies plates of variable length and constant plate width $b = 375 \text{ mm}$. The plates have quasi-isotropic stacking sequence $[45/-45/0/90]_{2s}$, and are made of AS4/3502 composite material. Material properties are reported in Table 2.2. For this

combination of layup and material, both laminate CTE's α_x and α_y , as well as quantities N_x^T and N_y^T are positive. The bending-twisting coupling terms D_{16} and D_{26} are non-zero.

The buckling temperature delivered by Eq. 2.9 for the $[0/45/-45/90]_s$ laminate is up to 3.1% larger than the analytical values from literature. This finding is in line with previous studies performed by Nemeth [30], which show that, for 8-ply quasi-isotropic laminates containing ± 45 plies, neglecting the bending twisting terms in the analytical buckling solution causes the buckling load to be overestimated in around a 3%. The buckling temperature predicted by Abaqus for this plate is a 0.65% larger than analytical values from literature. This value is consistent with the difference found for the previously analyzed $[0/90/90/0]_s$ plate. These quantities are reported in Table 2.3. The output of Eq. 2.9 are plotted in Fig. 2.2, in the form of a chart representing applied ΔT versus varying aspect ratio a/b . For instance, takings $n = 1$ and $m = 1, 2, 3, \dots$, a set of dashed lines are generated, each one of them corresponding to buckling shapes of increasing number of half-waves along X direction; by repeating this operation with $m = 1, n = 1, 2, 3$, curves related to shapes with multiple half-waves in Y direction are obtained. For a certain value of the aspect ratio, ΔT_{cr} is given by the dashed curve delivering the minimal absolute value of ΔT . The buckling curve is obtained by gathering together all values of ΔT_{cr} , and is represented as bold in Fig. 2.2. A characteristic feature of quasi-isotropic laminated plates can be noted: under the case of pure thermal buckling, quasi-isotropic plates tend to buckle in a single half-wave shape in both X and Y directions, independent of plate geometry. For increasing values of the aspect ratio, ΔT_{cr} rapidly decreases and tends asymptotically to a stable value.

Material	E_{11} [GPa]	E_{22} [GPa]	G_{12} [GPa]	ν_{12}	$\alpha_1 \cdot 10^6$ [1/°C]	$\alpha_2 \cdot 10^6$ [1/°C]	t_{ply} [mm]
AS4/3502	127.6	11.3	6.0	0.3	0.45	29.6	0.127
IM7/8552	150	9.08	5.29	0.32	-5.5	25.8	0.127

Table 2.2: Material properties [25], [31].

Material	Stacking	$\alpha_x \cdot 10^6$ [1/°C]	$\alpha_y \cdot 10^6$ [1/°C]	\hat{N}_x^T [N/mm°C]	\hat{N}_y^T [N/mm°C]
AS4/3502	$[45/-45/0/90]_{2s}$	3.35	3.35	0.49	0.49
IM7/8552	$[45/-45/0/90]_{2s}$	-3.23	-3.23	-0.54	-0.54
IM7/8552	$[20/-20]_{4s}$	-8.09	20.07	-1.30	0.21

Table 2.3: Laminate CTE α_x and α_y , and thermal forces \hat{N}_x^T and \hat{N}_y^T , for different materials and layups.

For very large values of a/b , the critical temperature ΔT_{cr} tends to $\Delta T_{cr,\infty}$, which is the critical buckling temperature for simply supported, fully restrained, heated infinite plates, reported also in literature [8]. Such temperature has been reported as dash-dotted line in Fig 2.2. This trend is also observed in heated, simple supported, fully restrained metallic plates.

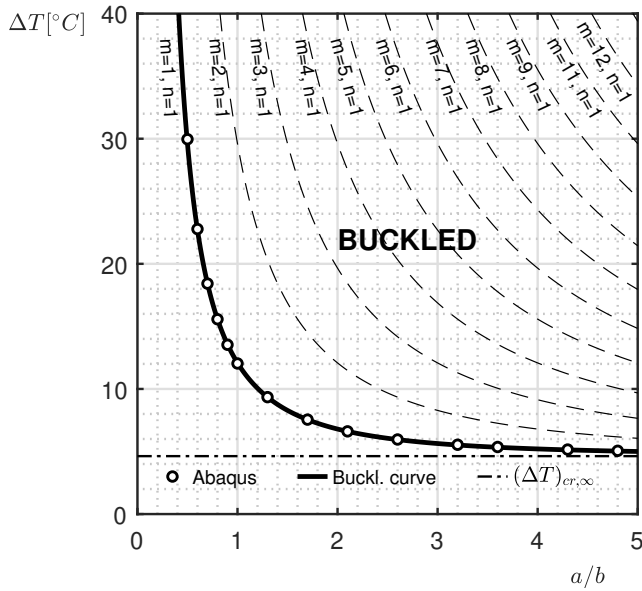


Figure 2.2: Buckling temperatures of fully restrained, heated composite plates with different lengths. Material: AS4/3502; Layup: $[45/ - 45/0/90]_{2s}$

The second example presents buckling temperatures for plates having identical geometry and stacking orientation as in previous example. However, plates are now made of *IM7/8552* composite material. For this new combination of layup and material, parameters α_x , α_y , N_x^T and N_y^T are negative, as reported in Table 2.3; as a direct consequence ΔT_{cr} will also be negative. As for previous example, the bending-twisting coupling terms are small in comparison with the rest of their bending stiffness terms, with a maximal ratio of 7%, the influence of bending anisotropy over the solution is negligible. The results delivered by Eq. 2.9 for this second example are presented in Fig. 2.3, in the form of a chart representing the change of ΔT versus a/b .

The curve of ΔT_{cr} for the current set of analysed plates shows similarities with the first analysed set of plates. Plates still buckle under a unique half-wave. However, laminate CTE's are negative due to the change of plate material, so plates now buckle under cooling and the resulting buckling chart appears as mirrored with respect from its AS4/3502 counterpart. Quasi-isotropic laminates with negative thermal expansion keep similar mechanical properties to isotropic materials, while their thermal buckling behaviour is reversed. For very long values of a/b , the critical temperature tends to $\Delta T_{cr,\infty}$, which is the critical temperature for simply supported, fully restrained, heated infinite plates reported in literature [8]. Composite laminate plates with negative thermal expansion are a consequence of either $\alpha_1^{(k)}$ and $\alpha_2^{(k)}$ lamina CTE's being negative, but also due to Poisson effect due to high fibre stiffness [1]. Such lamina properties can be used for tailoring stacking sequences with negligible or even zero thermal expansion.

The third example corresponds to plates sharing geometries with the two previous

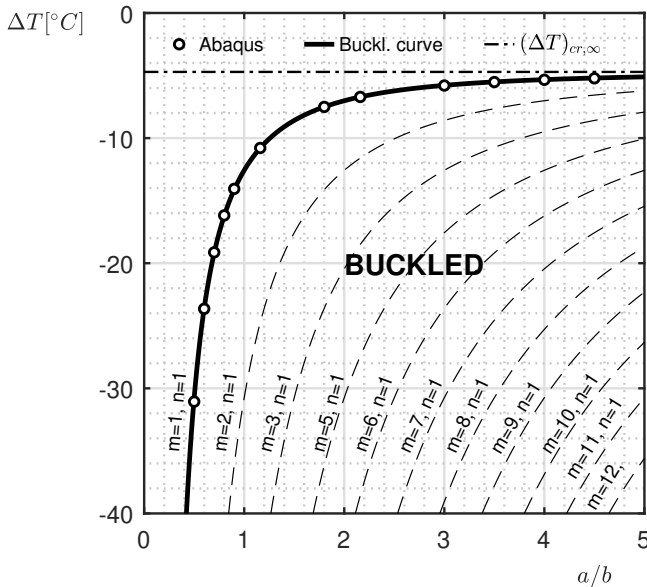


Figure 2.3: Buckling temperatures of fully restrained, heated composite plates with different lengths. Material: *IM7/8552*; Layup: $[45/-45/0/90]_{2s}$.

examples. Material remains *IM7/8552* while the layup is now $[20/-20]_{4s}$. Contrary to previously analysed quasi-isotropic laminates, this stacking sequence shows higher membrane and bending stiffness along one prevalent direction. Additionally, the present combination of material and layup shows opposite signs for \hat{N}_x^T and \hat{N}_y^T , as reported in Table 2.3. Layup is now angle-ply, so the bending-twisting coupling terms become proportionally larger. However, as shown in Ref. [30], the influence of bending anisotropy becomes smaller when the amount of layers increases. Thus, the formula can still be used for pre-sizing. As a consequence of this, plates may buckle either under heating, cooling, or both. The outcome of Eq. 2.9 is plotted in Fig. 2.4, following the same procedure used for Figs. 2.2 and 2.3. Two buckling curves appear, corresponding to both positive and negative ranges of ΔT . Thus, a certain plate can have two buckling temperatures. For instance, a plate with aspect ratio $a/b = 2.2$ will buckle under $\Delta T = 23.93^\circ\text{C}$ with shape (1,2), but also under $\Delta T = -10.47^\circ\text{C}$ with shape (2,1). The two buckling curves show opposing trends regarding the buckling shapes: for the positive range of ΔT , increasing values of a/b cause the number of half-waves along Y axis to decrease. Conversely, for negative range of ΔT , the number of half-waves increases along X axis. It is possible to note that half waves along a certain plate axis are a clear indicator of main compressive direction.

Angle-ply laminates showing high stiffness along one predominant direction can be useful when the loads are highly directional. These stacking orientations are often the output of optimization processes, where the fibres align to respond to critical loading directions. However, the direction perpendicular to the main fibre orientation is less

stiff due to the lack of fibres, and it also sees much higher thermal expansion due to the larger contribution of the matrix material. This makes them prone to buckling when expansions along this direction are somewhat restrained. Potential applications in thermal environments should be considered carefully, especially if negative laminate CTE's are present as behaviour becomes more counter intuitive.

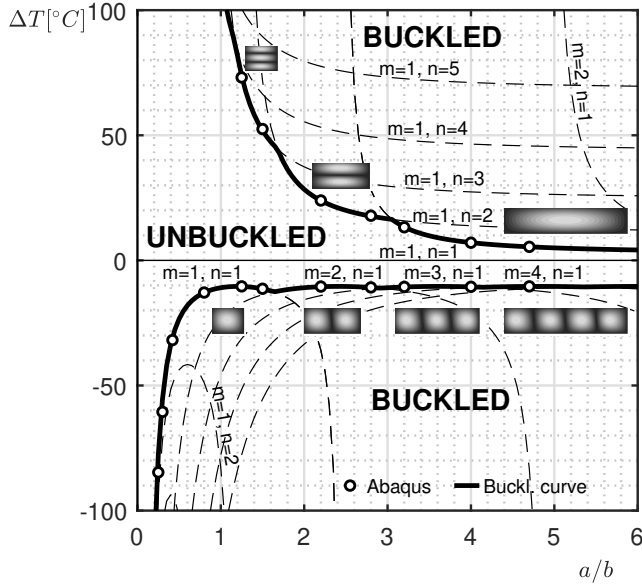


Figure 2.4: Buckling temperatures of fully restrained, heated composite plates with different lengths. Material: IM7/8552; Layup: $[20/-20]_{4s}$.

2.3.2. BUCKLING OF LOADED AND HEATED PLATES

An orthotropic composite laminate plate is now considered. Its edges are simply supported, and the plate experiences a uniform length variation Δ_x along the X axis, while the width remains constant. The plate is also subjected to a spatially uniform temperature increment ΔT . Under such situation, the plate can buckle either when a ΔT is applied, a Δ_x is applied, or both take place simultaneously. The described situation corresponds to the first type of boundary conditions specified in section 2.2. For these plate and loading conditions, Eq. 2.8 holds.

There are some substantial differences between Eq. 2.8 and Eq. 2.9. For instance, when the plate is subjected to a prescribed Δ_x , the temperature is a linear function of mechanical loading condition Δ_x . As a consequence, the load proportionality ratio $k = N_x/N_y$ no more remains constant, and the sign of ΔT_{cr} does not depend only on plate properties anymore. Eq. 2.8 can be related to a formula for isotropic materials, as done

previously with Eq. 2.9. Thus, after introducing in Eq. 2.8 the equivalences for isotropic material and doing proper rearrangements, Eq. 2.11 unfolds:

$$\frac{E\alpha hb^2}{\pi^2 D} \Delta T = \frac{a^2 b^2 n^2 \nu + b^4 m^2}{a^2 n^2 \pi^2 D} N_x + \frac{(a^2 n^2 + b^2 m^2)^2}{a^4 n^2} \quad (2.11)$$

Eq. 2.11 is the equation for thermomechanical buckling in isotropic materials, reported in literature [7].

Three examples are then presented and discussed, analysing three different thermo-mechanically loaded composite laminate plates. The three analysed plates present the same plate width b , layup and material of the three set of plates analysed in section 2.3.1, so examples in both sections can easily be related to each other. In all cases, plates are very thin in comparison to their length and width, which is unrealistic in real applications. Such choice of dimensions has been made so that obtained buckling temperatures are small, and can be applied easily during tests.

The first analysed plate is made of AS4/3502 material, with a quasi-isotropic stacking sequence $[45/-45/0/90]_{2s}$, width $b = 375 \text{ mm}$ and length $a = 575 \text{ mm}$. As stated in previous section 2.3.1, for this combination of stacking and material, the quantities α_x , α_y , N_x^T and N_y^T are positive. Results from Eq. 2.8, are plotted in a buckling chart representing ΔT versus Δ_x . Starting from a buckling shape with $m = 1$, $n = 1$ a line is obtained by plotting the resulting expression and is represented as dashed in Fig. 2.5.

By leaving now $n=1$ fixed, and assuming $m = 1, 2, 3, \dots$, analogue dashed lines can be generated, being these lines related to buckling shapes with multiple half-waves in X direction. By taking $m = 1$, $n = 1, 2, 3, \dots$ similar dashed lines related to buckling shapes with multiple half-waves in Y direction are reported.

For a certain length variation Δ_x , the critical buckling temperature ΔT_{cr} is determined by the dashed line delivering the lowest absolute value of ΔT . These lines intersect each other so the buckling shape defining the lowest ΔT will change depending on the mechanical loading condition Δ_x . The result of collecting all values of ΔT_{cr} for any given Δ_x is the buckling curve, represented as bold in Fig. 2.5, and is constituted by different segments of several intersecting dashed lines.

The buckling curve divides the loading plane $(\Delta_x, \Delta T)$ into two subspaces, corresponding to buckled and unbuckled states. The intersection of the buckling curve with the horizontal axis corresponds to the loading situation in which the plate buckles under pure mechanical loading ($\Delta T = 0^\circ \text{C}$); for this case, the length variation has a value of $\Delta_x = -0.04 \text{ mm}$ and the plate buckles under the shape of one half-wave in both X and Y directions. Conversely, the intersection with the vertical axis represents the case in which $\Delta_x = 0 \text{ mm}$ and buckles under pure heating. For this case, the plate buckles under $\Delta T_{cr} = 8.14^\circ \text{C}$, and this value can be found also in Fig. 2.2. The buckling shape has only one half-wave in both X and Y directions.

In the case that the plate experiments a stretch of $\Delta_x = 0.3 \text{ mm}$, ΔT_{cr} increases significantly, rising up to 66.62°C and the buckling presents a mode with two half waves in Y direction. It is possible to note that under heating conditions, plate stretching has stabilizing effect against buckling. States of stretching and cooling induce biaxial tension

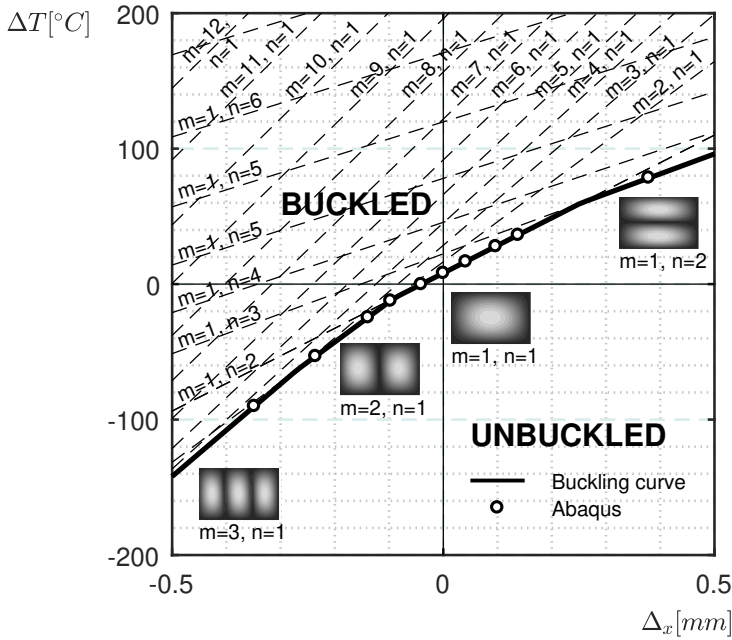


Figure 2.5: Buckling chart for a loaded and heated composite plate. Geometry: $a = 575\text{mm}$, $b = 375\text{mm}$; Material: AS4/3502; Layup: $[45/-45/0/90]_{2s}$.

states in the plate so buckling under this loading condition is not possible. Conversely, if the plate experiments a shortening of $\Delta_x = -0.02\text{ mm}$, ΔT_{cr} descends to 3.06°C . Under states of shortening and heating, the plate experiments a state of biaxial compression that noticeably reduces ΔT_{cr} . Considering now a shortening of $\Delta_x = -0.3\text{mm}$, that is larger than the critical shortening for pure mechanical loading. In order to prevent buckling, the plate should be cooled down to temperatures lower than $\Delta T_{cr} = -73.74^\circ\text{C}$. In this case, the buckling pattern corresponds to three half-waves in the axial direction.

It can be stated that the increase of mechanical condition Δ_x induces a change in the buckling temperature ΔT_{cr} , as well as variations in the direction and number of half waves. The buckling behaviour of quasi-isotropic plates under thermomechanical loads is, therefore, comparable to that one shown by metallic plates [7].

The second analysed plate shares dimensions and quasi-isotropic layup with the previously analysed plate; the only difference between the two plates is the material, which is now *IM7/8552*. The resulting buckling chart is presented in Fig. 2.6, and is generated with the same procedure used for Fig. 2.5. The new buckling chart appears as mirrored with respect to the horizontal axis when compared to its AS4/3502 counterpart. This is a consequence of the variation in sign of quantities α_x , α_y , N_x^T , N_y^T , caused by the material *IM7/8552*. The consequences of such inversion is that plate stretching has now a

stabilizing effect against cooling, and under plate compression, a positive ΔT is required in order to prevent buckling.

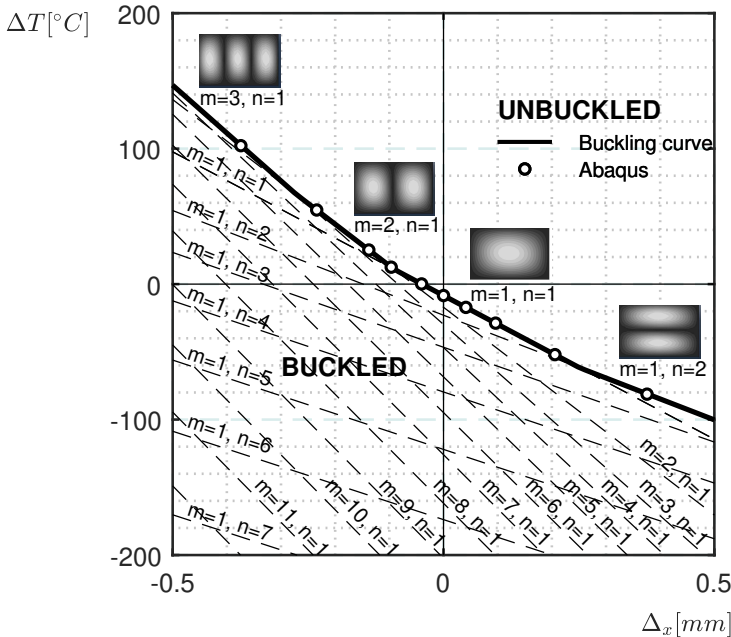


Figure 2.6: Buckling chart for a loaded and heated composite plate. Geometry: $a = 575mm, b = 375mm$; Material: $IM7/8552$; Layup: $[45/-45/0/90]_{2s}$.

The mechanical condition Δ_x induces a change in the buckling temperature ΔT_{cr} , as well as variations in the direction and number of half waves. Laminates with negative CTE's show a counter-intuitive behaviour when external mechanical load is present. This should be taken into account when considering them for any application involving notable changes in temperature.

The third analysed plate is made of $IM7/8552$ and the stacking is $[20/-20]_{4s}$. A new buckling chart, Fig. 2.7, is generated. For this combination of material and laminate stacking, N_x^T and N_y^T have opposite sign. In this case, with a stretching equal to $\Delta_x = 0.1mm$, the plate buckles under $\Delta T_{cr} = 101.8^\circ C$, with a (1,3) buckling shape, but also under $\Delta T_{cr} = -52.62^\circ C$. It is also possible to note that the graph is not symmetric with respect to X axis. For heating, the plate buckles in a pattern of increasing half-waves in transversal direction Y , while for cooling in increasing number of half-waves along X direction. It is also remarkable to see how the area for negative Δ_x area experiments a substantial reduction, and neither heating nor cooling have a proper stabilizing effect against buckling when mechanical load is compressive. This kind of information can be

valuable when considering the suitability of highly directional laminates for thermomechanically loaded environments.

2

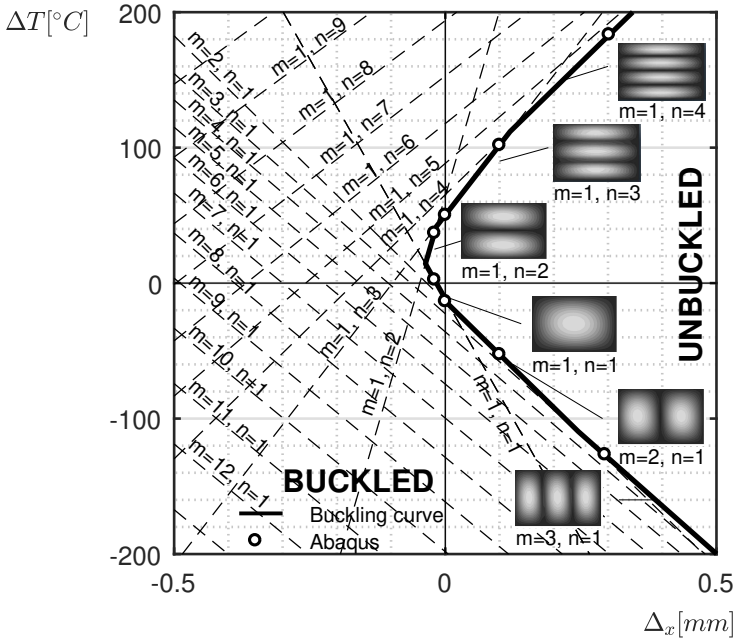


Figure 2.7: Buckling chart for a loaded and heated composite plate. Geometry: $a = 575\text{mm}$, $b = 375\text{mm}$; Material: $IM7/8552$; stacking: $[20/-20]_{4s}$.

Throughout the last three examples, it has been shown how the introduction of heat and external load, combined with restrained transversal expansions affects the buckling behaviour of some frequently used families of composite laminated plates. For structural applications in extreme environments, buckling loads experience dramatic changes when thermal increments are present. Such interaction effects should be properly contemplated early on in the sizing phases, and can be also used for obtaining desired buckling shapes.

There are other factors related to materials or manufacturing, which have not been addressed and are well worth considering. One of them is the potential effect of thermal pre-stress due to curing on buckling loads. The main drivers of residual stresses are the differences in temperature, differences in CTE between matrix and fibres, matrix shrinkage, and difference in stiffness between fibre and matrix. During the curing process, the laminate is heated beyond the glass transition temperature and then cooled down to room temperature. In this process, residual stresses arise at three levels: intralaminar, interlaminar and laminate level [32], [33]. Intralaminar stresses concern the pre-stress

arisen in the lamina due to matrix shrinkage after curing, as well as the large difference in CTE's between matrix and fibres; interlaminar stresses refer to stresses arisen between neighboring layers due to anisotropic properties, and laminate residual stresses concern the stresses by thermal gradients arisen during the curing process. When large enough, laminate residual stresses can cause warpage in a given part, since it would reach different degree of curing at different locations. However, for thin plates, through-thickness and in-plane thermal gradients during manufacturing can be easily prevented. Interlaminar residual stresses may also cause warpage of the laminate as a response to a ΔT . Nevertheless, as long as the laminate is symmetric, these stresses balance out and the laminate remains flat, only experiencing in-plane expansion or contraction [34]. In this case, and leaving aside possible material non-linearity, the laminate is expected to keep the originally predicted stiffness and mechanical behaviour throughout the whole range of temperatures, and the buckling temperatures calculated are not expected to change. However, since each lamina within the laminate is pre-stressed, the strength of the compound can be affected. This research deals with loaded under both mechanical and thermal loads, so special care needs to be taken with load cases that involve plate tension, since these loads will overlap to the preexisting residual stresses. Nevertheless, heating loads can also help alleviate the intra- and interlaminar shear stresses present at room temperature, so to ensure the integrity of a given laminated plate, a case-to-case study is required. Also, residual stresses can affect the buckling temperatures within a given assembly, such as stiffened panels: often plates and longitudinal stiffeners have different CTE's, creating in this way residual stresses that can have an impact on the buckling load[35]. Another factor that needs to be addressed is the effect of moisture in a laminated plate. Any thermoset laminate plate subjected to sustained exposure to combinations of humidity and high temperature may experience a certain degree of moisture absorption. This effect will have an impact on its material properties, as well as induce a volumetric expansion in the matrix. In the same way as thermal expansions, such expansions will generate in-plane stresses if they happened to be constrained. Previously derived equations 2.8 and 2.9 can be expanded by including the moisture expansion effect in the formulation [36]. The presented formulation assumes that the studied composite laminated plates are comparatively thin. For increasing values of the thickness, the presented formulae 2.8 and 2.9 gradually lose their validity due to transverse shear effects becoming more relevant. Another relevant factor is the temperature dependence on material characteristics: Temperature variation may induce changes on properties, making buckling temperatures differ from those predicted using material values at room temperature. Such variations are strongly dependent on the material of choice. It remains the task of the design engineer to perform a thorough research on the behaviour of any potential material within the desired range of temperatures. For example, some carbon/epoxy composite materials show an increase on longitudinal lamina stiffness within -50°C and -200°C range, as documented in Ref. [37]; Nonlinear dependence of thermal expansion on temperature have been registered in various materials, as reported in Ref. [38].

2.4. CONCLUSIONS

The buckling of orthotropic laminated plates under heating, restrained transversal expansion and external mechanical load in axial direction was investigated.

A closed formula was deduced and compared against the classical thermal buckling problem with no plate size variation. Different sets of results in graphical form for both mentioned loading cases were presented and compared. Resulting buckling charts show buckling curves that divide the displacement-temperature loading space into two subspaces, corresponding to buckled and unbuckled states. The influence of external mechanical load over the plate buckling temperature (and vice versa) was assessed. It was shown that mechanically loaded laminated plates can be either stabilized or destabilized by either cooling or heating. Besides, it was also shown how the combination of heating and mechanical load have an impact on the buckling shape, so under specific loading conditions desired plate shapes can be targeted. The proposed formula, due to its simplicity, can readily be used for initial design, sensitivity analysis or optimization.

BIBLIOGRAPHY

- [1] J. Whitney and J. Ashton, "Effect of environment on the elastic response of layered composite plates", *AIAA Journal*, vol. 9, no. 9, pp. 1708–1713, 1971, ISSN: 0001-1452. DOI: [10.2514/3.49976](https://doi.org/10.2514/3.49976).
- [2] T. R. Tauchert, "Thermal buckling of thick antisymmetric angle-ply laminates", *Journal of Thermal Stresses*, vol. 10, no. 2, pp. 113–124, 1987, ISSN: 1521074X. DOI: [10.1080/01495738708927000](https://doi.org/10.1080/01495738708927000).
- [3] T. R. Tauchert and N. N. Huang, "Thermal buckling of symmetric angle-ply laminated plates", *Composite Structures* 4, pp. 424–435, 1987. [Online]. Available: http://link.springer.com/chapter/10.1007/978-94-009-3455-9%7B%5C_%7D33.
- [4] L. X. Sun and T. R. Hsu, "Thermal buckling of laminated composite plates with transverse shear deformation", *Computers and Structures*, vol. 36, no. 5, pp. 883–889, 1990, ISSN: 00457949. DOI: [10.1016/0045-7949\(90\)90159-Y](https://doi.org/10.1016/0045-7949(90)90159-Y). [Online]. Available: <http://www.sciencedirect.com/science/article/pii/004579499090159Y>.
- [5] C. A. Meyers and M. W. Hyer, "Thermal buckling and postbuckling of symmetrically laminated composite plates", *Journal of Thermal Stresses*, vol. 14, no. 4, pp. 519–540, 1991, ISSN: 1521074X. DOI: [10.1080/01495739108927083](https://doi.org/10.1080/01495739108927083).
- [6] H. Abramovich, "Thermal buckling of cross-ply composite laminates using a first-order shear deformation theory", *Composite Structures*, vol. 28, pp. 201–213, 1994. [Online]. Available: <http://www.sciencedirect.com/science/article/pii/0263822394900493>.
- [7] R. M. Jones, "Thermal buckling of uniformly heated unidirectional and symmetric cross-ply laminated fiber-reinforced composite uniaxial in-plane restrained simply supported rectangular plates", *Composites Part A: Applied Science and Manufacturing*, vol. 36, no. 10 SPEC. ISS. Pp. 1355–1367, 2005, ISSN: 1359835X. DOI: [10.1016/j.compositesa.2005.01.028](https://doi.org/10.1016/j.compositesa.2005.01.028).
- [8] M. P. Nemeth, "Buckling behavior of long anisotropic plates subjected to fully restrained thermal expansion", *TP-2003-212131, National Aeronautics and Space Administration*, no. November, 2003, ISSN: 02734508. [Online]. Available: <http://hdl.handle.net/2060/19970004648>.
- [9] W. Wittrick and F. Williams, "Buckling and vibration of anisotropic or isotropic plate assemblies under combined loadings", *International Journal of Mechanical Sciences*, vol. 16, no. 4, pp. 209–239, 1974, ISSN: 0020-7403. DOI: [https://doi.org/10.1016/0020-7403\(74\)90069-1](https://doi.org/10.1016/0020-7403(74)90069-1). [Online]. Available: <https://www.sciencedirect.com/science/article/pii/0020740374900691>.

- [10] H. Matsunaga, “Thermal buckling of cross-ply laminated composite and sandwich plates according to a global higher-order deformation theory”, *Composite Structures*, vol. 68, no. 4, pp. 439–454, 2005, ISSN: 02638223. DOI: [10.1016/j.compstruct.2004.04.010](https://doi.org/10.1016/j.compstruct.2004.04.010).
- [11] R. Vescovini, M. D’Ottavio, L. Dozio, and O. Polit, “Thermal buckling response of laminated and sandwich plates using refined 2-D models”, *Composite Structures*, vol. 176, pp. 313–328, 2017, ISSN: 02638223. DOI: [10.1016/j.compstruct.2017.05.021](https://doi.org/10.1016/j.compstruct.2017.05.021). [Online]. Available: <http://dx.doi.org/10.1016/j.compstruct.2017.05.021>.
- [12] J. Li, X. Tian, Z. Han, and Y. Narita, “Stochastic thermal buckling analysis of laminated plates using perturbation technique”, *Composite Structures*, vol. 139, pp. 1–12, 2016, ISSN: 02638223. DOI: [10.1016/j.compstruct.2015.11.076](https://doi.org/10.1016/j.compstruct.2015.11.076). [Online]. Available: <http://dx.doi.org/10.1016/j.compstruct.2015.11.076>.
- [13] J. Li, Y. Narita, and Z. Wang, “The effects of non-uniform temperature distribution and locally distributed anisotropic properties on thermal buckling of laminated panels”, *Composite Structures*, vol. 119, pp. 610–619, 2015, ISSN: 02638223. DOI: [10.1016/j.compstruct.2014.09.011](https://doi.org/10.1016/j.compstruct.2014.09.011). [Online]. Available: <http://dx.doi.org/10.1016/j.compstruct.2014.09.011>.
- [14] Y. Shi, R. Y. Lee, and C. Mei, “Thermal postbuckling of composite plates using the finite element modal coordinate method”, *Journal of Thermal Stresses*, vol. 22, no. 6, pp. 595–614, 1999, ISSN: 1521074X. DOI: [10.1080/014957399280779](https://doi.org/10.1080/014957399280779).
- [15] L. C. Shiau, S. Y. Kuo, and C. Y. Chen, “Thermal buckling behavior of composite laminated plates”, *Composite Structures*, vol. 92, no. 2, pp. 508–514, 2010, ISSN: 02638223. DOI: [10.1016/j.compstruct.2009.08.035](https://doi.org/10.1016/j.compstruct.2009.08.035). [Online]. Available: <http://www.sciencedirect.com/science/article/pii/S0263822309004136>.
- [16] H. Ounis, A. Tati, and A. Benchabane, “Thermal buckling behavior of laminated composite plates: A finite-element study”, *Frontiers of Mechanical Engineering*, vol. 9, no. 1, pp. 41–49, 2014, ISSN: 20950241. DOI: [10.1007/s11465-014-0284-z](https://doi.org/10.1007/s11465-014-0284-z).
- [17] C. Bisagni and R. Vescovini, “Fast tool for buckling analysis and optimization of stiffened panels”, *Journal of Aircraft*, vol. 46, no. 6, pp. 2041–2053, 2009, ISSN: 0021-8669. DOI: [10.2514/1.43396](https://doi.org/10.2514/1.43396). [Online]. Available: <http://arc.aiaa.org/doi/10.2514/1.43396>.
- [18] C. Bisagni and R. Vescovini, “Analytical formulation for local buckling and post-buckling analysis of stiffened laminated panels”, *Thin-Walled Structures*, vol. 47, no. 3, pp. 318–334, 2009, ISSN: 02638231. DOI: [10.1016/j.tws.2008.07.006](https://doi.org/10.1016/j.tws.2008.07.006).
- [19] C. Bisagni, R. Vescovini, and C. Davila, “Assessment of the damage tolerance of post-buckled hat-stiffened panels using single stringer specimens”, *51st AIAA/ASME/ASCE/AHS / ASC Structures, Structural Dynamics, and Materials Conference 18th AIAA/ASME/AHS Adaptive Structures Conference 12th*, 2010, ISSN: 02734508. DOI: [10.2514/6.2010-2696](https://doi.org/10.2514/6.2010-2696). [Online]. Available: <http://arc.aiaa.org/doi/abs/10.2514/6.2010-2696>.

- [20] P. M. Weaver and M. P. Nemeth, "Improved Design Formulae for Buckling of Orthotropic Plates Under Combined Loading", *49th AIAA/ASME/ASCE/AHS/ASC Structures, Structural Dynamics, and Materials Conference
 16th AIAA/ASME/AHS Adaptive Structures Conference
 10t*, vol. 46, no. 9, pp. 1–10, 2008, ISSN: 0001-1452. DOI: [10.2514/6.2008-2273](https://doi.org/10.2514/6.2008-2273). [Online]. Available: <http://arc.aiaa.org/doi/abs/10.2514/6.2008-2273><http://arc.aiaa.org/doi/10.2514/1.37892>.
- [21] R. Vescovini and C. Bisagni, "Two-step procedure for fast post-buckling analysis of composite stiffened panels", *Computers and Structures*, vol. 128, pp. 38–47, 2013, ISSN: 00457949. DOI: [10.1016/j.compstruc.2013.06.002](https://doi.org/10.1016/j.compstruc.2013.06.002). [Online]. Available: <http://dx.doi.org/10.1016/j.compstruc.2013.06.002>.
- [22] R. Vescovini and C. Bisagni, "A fast procedure for the design of composite stiffened panels", *Aeronautical Journal*, vol. 119, no. 1212, pp. 185–201, 2015, ISSN: 00019240.
- [23] H. Abramovich and C. Bisagni, "Behavior of curved laminated composite panels and shells under axial compression", *Progress in Aerospace Sciences*, vol. 78, pp. 74–106, 2015, ISSN: 03760421. DOI: [10.1016/j.paerosci.2015.05.008](https://doi.org/10.1016/j.paerosci.2015.05.008). [Online]. Available: <http://dx.doi.org/10.1016/j.paerosci.2015.05.008>.
- [24] R. Jones, *Buckling of bars, plates, and shells*, English. Bull Ridge Corporation, 2006, ISBN: 9780978722302.
- [25] M. P. Nemeth, "Buckling behavior of long anisotropic plates subjected to restrained thermal expansion and mechanical loads", *Journal of Thermal Stresses*, vol. 23, no. 9, pp. 873–916, Dec. 2000, ISSN: 1521074X. DOI: [10.1080/014957300750040122](https://doi.org/10.1080/014957300750040122). [Online]. Available: <http://www.tandfonline.com/doi/abs/10.1080/014957300750040122>.
- [26] A. K. Noor, J. H. Starnes, and J. M. Peters, "Thermomechanical buckling and post-buckling of multilayered composite panels", *Composite Structures*, vol. 23, no. 3, pp. 233–251, 1993, ISSN: 02638223. DOI: [10.1016/0263-8223\(93\)90225-F](https://doi.org/10.1016/0263-8223(93)90225-F).
- [27] P. Nali and E. Carrera, "Accurate buckling analysis of composite layered plates with combined thermal and mechanical loadings", *Journal of Thermal Stresses*, vol. 36, no. 1, pp. 1–18, 2013, ISSN: 01495739. DOI: [10.1080/01495739.2012.663679](https://doi.org/10.1080/01495739.2012.663679). [Online]. Available: <http://www.tandfonline.com/doi/abs/10.1080/01495739.2012.663679>.
- [28] B. Boley and J. Weiner, *Theory of Thermal Stresses*. New York: Wiley, 1960, pp. 445–450.
- [29] E. A. Thornton, *Thermal Structures for Aerospace Applications* (AIAA Education Series). American Institute of Aeronautics and Astronautics, Jan. 1996, pp. 397–441, ISBN: 978-1-56347-190-2. DOI: [10.2514/4.862540](https://doi.org/10.2514/4.862540). arXiv: [arXiv:1011.1669v3](https://arxiv.org/abs/1011.1669v3). [Online]. Available: <https://arc.aiaa.org/doi/book/10.2514/4.862540>.
- [30] M. P. Nemeth, "Importance of anisotropy on buckling of compression-loaded symmetric composite plates", vol. 24, no. 11, pp. 1831–1835, 1986, ISSN: 00011452. DOI: [10.2514/3.9531](https://doi.org/10.2514/3.9531).

- [31] P. P. Camanho, P. Maimi, and C. G. Dávila, “Prediction of size effects in notched laminates using continuum damage mechanics”, *Composites Science and Technology*, vol. 67, no. 13, pp. 2715–2727, 2007, ISSN: 02663538. DOI: [10.1016/j.compscitech.2007.02.005](https://doi.org/10.1016/j.compscitech.2007.02.005).
- [32] P. P. Parlevliet, H. E. Bersee, and A. Beukers, “Residual stresses in thermoplastic composites—a study of the literature—part i: Formation of residual stresses”, *Composites Part A: Applied Science and Manufacturing*, vol. 37, no. 11, pp. 1847–1857, 2006, ISSN: 1359-835X. DOI: <https://doi.org/10.1016/j.compositesa.2005.12.025>. [Online]. Available: <https://www.sciencedirect.com/science/article/pii/S1359835X06000145>.
- [33] B. Seers, R. Tomlinson, and P. Fairclough, “Residual stress in fiber reinforced thermosetting composites: A review of measurement techniques”, *Polymer Composites*, vol. 42, no. 4, pp. 1631–1647, 2021. DOI: <https://doi.org/10.1002/pc.25934>. eprint: <https://onlinelibrary.wiley.com/doi/pdf/10.1002/pc.25934>. [Online]. Available: <https://onlinelibrary.wiley.com/doi/abs/10.1002/pc.25934>.
- [34] S. F. M. de Almeida and J. S. Hansen, “Buckling of composite plates with local damage and thermal residual stresses”, *AIAA Journal*, vol. 40, no. 2, pp. 340–345, 2012, ISSN: 0001-1452. DOI: [10.2514/3.15067](https://doi.org/10.2514/3.15067).
- [35] S. F. Müller de Almeida and J. S. Hansen, “Enhanced elastic buckling loads of composite plates with tailored thermal residual stresses”, *Journal of Applied Mechanics*, vol. 64, no. 4, p. 772, 1997, ISSN: 00218936. DOI: [10.1115/1.2788981](https://doi.org/10.1115/1.2788981).
- [36] T. R. Tauchert, “Temperature and absorbed moisture”, in *Buckling and Postbuckling of Composite Plates*, G. J. Turvey and I. H. Marshall, Eds. Dordrecht: Springer Netherlands, 1995, pp. 190–226, ISBN: 978-94-011-1228-4. DOI: [10.1007/978-94-011-1228-4_6](https://doi.org/10.1007/978-94-011-1228-4_6). [Online]. Available: https://doi.org/10.1007/978-94-011-1228-4_6.
- [37] M. G. Kim, S. G. Kang, C. G. Kim, and C. W. Kong, “Tensile response of graphite/epoxy composites at low temperatures”, *Composite Structures*, vol. 79, no. 1, pp. 84–89, 2007, ISSN: 02638223. DOI: [10.1016/j.compstruct.2005.11.031](https://doi.org/10.1016/j.compstruct.2005.11.031).
- [38] R. P. Reed and M. Golda, “Cryogenic properties of unidirectional composites”, *Cryogenics*, vol. 34, no. 11, pp. 909–928, 1994, ISSN: 00112275. DOI: [10.1016/0011-2275\(94\)90077-9](https://doi.org/10.1016/0011-2275(94)90077-9).

3

A STUDY ON THERMAL BUCKLING AND MODE JUMPING OF METALLIC AND COMPOSITE PLATES

*La experiencia es una llama que no alumbra sino quemando.
Experience is a flame that only illuminates by burning.*

Benito Pérez Galdós

Composite plates in post-buckling regime can experience mode jumping in their buckling shape, suddenly increasing the number of half-waves. This phenomenon can be advantageous, because the shape change could be used for local morphing or structural adaptability in future aerospace structures. A study of this phenomenon under heating is here presented, combining numerical and experimental techniques. At first, a set of parametric analysis was conducted to identify composite panels that present a mode jump when heated. Three plates were selected, one in aluminum alloy 2024T3, and two in AS4/8552 composite material, with layup $[30/-30/5/-5]_s$ and $[35/-35/10/-10]_s$. The plates were tested in a new test setup for thermal buckling based on low thermal expansion fixtures. The mode jumping was successfully obtained experimentally for both composite plates. Numerical simulations predicted the general trends for all plates, and the mode jumps for the composite plates.

3.1. INTRODUCTION

THIN-WALLED composite structures are present in a wide range of aerospace applications, where they are required to operate under extreme conditions. Good examples

This chapter has been adapted from: J. Gutiérrez Álvarez and C. Bisagni, "A Study on Thermal Buckling and Mode Jumping of Metallic and Composite Plates," *Aerospace*, vol. 8, no. 2, p. 56, Feb. 2021, doi: 10.3390/aerospace8020056.

are high-speed aircraft, which must cope with combinations of thermal and mechanical loads, and satellites, which endure large cyclic temperature oscillations. Such loading conditions make these structures susceptible to buckling. This phenomenon has been largely considered as an undesirable event, due to the significant impact it has over the stiffness and the ability of a structure to carry load. The use of post-buckled states in structural design has been mainly limited, if used at all, as a contribution to increase the mass efficiency of a vehicle. In this respect, plate elements are perfect candidates for this use due to their well-known stable nonlinear behavior. Composite materials add versatility and expand the design space for the structural designer, because plate buckling and post-buckling behavior can be tailored by varying the laminate stacking orientation [1], [2]. Also, their elastic behavior allows the structure to return unscathed to the original state once the load decreases.

New research tendencies are observing buckling from a different standpoint: buckled states are no longer ‘forbidden’, but rather an additional structural state that has properties on its own and can offer additional functionalities [3]. A new research direction uses buckling as a mechanism for shape adaptability or morphing: the load triggers a shape change without the need of any additional actuator. For instance, several authors explore the shape change through mechanically induced buckling: Vos et al. studied control actuation through post-buckled precompressed structural elements [4], and Runkel et al. [5] explored the change in torsional stiffness in a wingbox allowing buckling in one of its plate side elements. Changing the shape through heat has also been investigated: Eckstein et al. investigated the multi-stability in shell structures using temperature increments [6], and the use of thermal gradients in hybrid laminates [7].

In some situations buckled plates may experience a sudden change in buckling shape, also known as a mode jump. The topic of mode jumping or mode change has been approached in limited occasions: While the contributions to the field of simulation of composite materials are numerous, [8]–[10], the amount of papers tackling the subject are more scarce [11]. The phenomenon has been thoroughly investigated numerically and experimentally by Falzon and Hitchings [12] and Falzon and Cerini [13], who proved the suitability of nonlinear dynamic explicit procedures for the prediction of this phenomenon in uniaxially compressed composite panels, and proved the large energy release after a mode jump. In a similar fashion, even though significant contributions have been made in the experimentation of buckling in the last decade (Arbelo et al. [14], [15], Bisagni et al. [16], [17], or Labans et al. [18]), to the best knowledge of the authors there are no experimental studies in the field of mode jumping of heated composite plates. There is, however, an experimental study done by Ehrhardt [19] in heated metallic plates, who showed that alternative equilibrium paths were reached when an external perturbation was present.

In order to demonstrate the feasibility of mode jumping under heating as a means to obtain shape change, experimental studies become an essential milestone. A large part of available bibliography on tests in thermal buckling of plates and shells refer to high-speed applications. This is the case of Percy and Fields [20] and Thompson and Richards [21], who tested two identical hat stiffened flat plates made in titanium and titanium matrix composite under diverse combinations of heating and mechanical loads,

contributing in this way to new design concepts in heated structures; Rakow and Waas [22] tested metallic foam sandwich plates using an oven, taking advantage of the differences in thermal expansion between fixture and specimen; and other authors such as Murphy et al. [23], Amabili et al. [24] or Thornton [25] performed experimental studies on buckling of heated metallic plates using diverse approaches and heating source types. Most of these tests address thermal buckling on metallic materials, and only just a few tests of carbon composite plates and shells are available in literature: Breivik and Hyer [26] tested curved composite panels under both mechanical and thermal loads, showing that temperature gradients found had a relatively small effect over the considered specimens, Fields et al. [27] performed a thermostructural tests on a titanium matrix composite panel presenting a novel experimental setup for combined loading, and Wu and Gürdal [28] performed heating tests on carbon composite, fiber steered panels, as a first step towards the application of fiber tailoring in heated aerospace structures. More recently, Xu et al. [29] tested the thermal buckling of a flat panel of carbon fiber-reinforced, silicon carbide ceramic matrix composite.

The goal of this research is to study the feasibility of a new morphing possibility in which shape changes are induced into structural composite plates by heating and without the contribution of any external actuator. This phenomenon can take advantage of post-buckling regime and the mode jumps at higher load levels. This could offer advantages and complement existent or future designs of high-speed aircraft, or also deployable structures in which low weight and multi-functionality are desirable.

A methodology for selecting laminates that present mode jumping in their nonlinear post-buckling regime is described and applied. As a result, two composite plates are selected and subsequently tested in a novel experimental setup. Prior to that, a preliminary test of an aluminum alloy plate is also performed. Results are presented in the form of deflection curves and out-of-plane deformation plots.

In particular in Section 3.2 the mode jumping phenomenon is explained in detail; while in Section 3.3 a methodology for selecting laminates that present mode jumping in their nonlinear post-buckling regime is described and applied, leading to the selection of two AS4/8552 composite plates for experimentation. In Section 3.4 a novel experimental setup for thermal buckling of plates is presented; and in Section 3.5 the results of a preliminary test on a plate made in 2024T3 aluminum alloy and of the tests on both composite plates are reported in the form of deflection curves and out-of-plane deformation plots. Finally, all findings of this investigation are summarized in the conclusions in Section 3.6.

3.2. MODE JUMPING ON HEATED COMPOSITE PLATES

Mode jumping, also called mode switch or mode change, can be defined as a sudden variation in the post-buckled shape of a loaded panel, characterized by a fast switch from one buckling mode into another one [15]. In this study, mode changes caused by temperature increments are investigated. The studied phenomenon can be qualitatively described with the help of a generic flat plate, shown in Fig. 3.1. The plate has length a , width b and thickness h , and is located in a Cartesian system XYZ , with XY coordinates

in plane with the mid-plane of the plate. In-plane size variations along X , Y axis are constrained and rotations around plate edges are also constrained. The plate is subjected to a homogeneous temperature increment ΔT that is applied in a quasi-static manner.

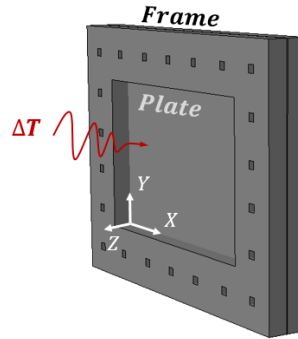


Figure 3.1: Plate geometry, boundary conditions and heating load.

The response of the plate can be represented in a graph as reported in Fig. 3.2, with temperature variation ΔT versus out-of-plane position Z of the point at the middle of the plate. Initially, the plate is considered to be at a stress-free state. Applying temperature increments ΔT , in-plane stresses arise as a consequence of restrained thermal expansion, and the plate starts to follow the equilibrium path reported as a bold black line. The plate, however, remains flat up until when its equilibrium path finds a bifurcation point. Temperature at this location is represented as ΔT_{b1} , and is known as the first bifurcation temperature or also buckling temperature. For temperatures beyond this value the plate starts deforming out of plane, typically in a half-wave buckling shape. The plate is now in post-buckling state and therefore under non-linear behavior. If temperature keeps increasing, plates with some particular stacking orientation may experience a sudden change into a different, stable buckling shape. This event is commonly known as mode jumping. The temperature indicated as ΔT_{b2} in the graph is known as mode jumping temperature, and the plate changes usually from a half-wave buckling configuration to two half-waves.

The described equilibrium path corresponds to a plate without imperfections. This is, however, an ideal case and in reality geometrical imperfections are always present. Due to this, the post-buckling behavior may differ from the ideal case. An example of a plate with initial geometric imperfections is also illustrated in Fig. 3.2 reported as a blue dashed line. Depending on imperfection shape and amplitude, equilibrium path will vary, altering not only the nonlinear deflection path but also the mode jumping temperature $(\Delta T)_{b2}$. Additionally, other factors such as size variation due to expansion of the boundary conditions may have a significant impact in the nonlinear behaviour of the plate.

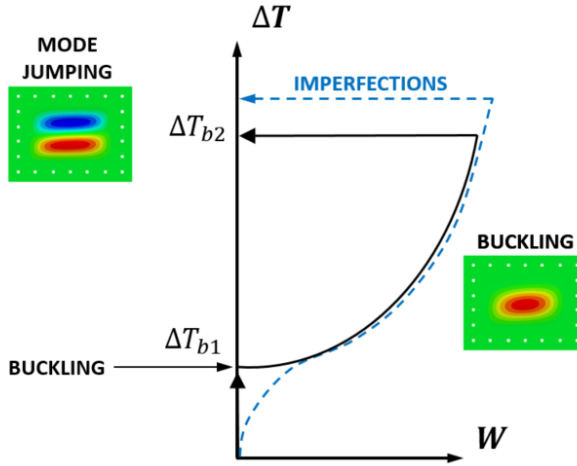


Figure 3.2: Thermal equilibrium path of a post-buckled composite plate.

3.3. ANALYSIS TO IDENTIFY COMPOSITE PLATES PRESENTING A MODE JUMP UNDER HEATING

To select configurations of composite plates that achieve a mode jump under heating, three steps were conducted. First, a set of design requirements was established. Second, the design space was inspected for the existence of plates showing mode jumping through a parametric analysis in which both linear buckling and post-buckling behavior were examined. Third, the stacking orientations were improved by fine-tuning the layups.

In the first step, the design space was established by imposing geometry and layup constraints. A fixed plate size of 300 mm x 200 mm compatible with the available oven was imposed. The plate was also required to have symmetric and balanced stacking orientation with a total number of 8 plies. The material AS4/8552 [30], with properties reported in Table 3.1, was used for all analyses. This is a common carbon composite material which is not suitable for high temperatures, so a temperature limit of $\Delta T = 120^\circ\text{C}$ was imposed for the tests. As a consequence mode jumping temperature can never exceed this value.

Assuming that in-plane plate size variations are perfectly constrained, the thermal buckling of a given composite laminated plate is governed by the laminate coefficients of thermal expansion (CTE) as well by the bending and membrane stiffness. Taking a generic angle-ply laminate $[\theta / -\theta]_{2s}$, and using laminate theory, the variation of the bending stiffness components D_{11} and D_{22} , and the CTE α_x and α_y can be plotted versus the generic angle θ , which is defined with respect to the X reference axis and is counter-clockwise positive. These are reported in Figs. 3.3 (a) and (b), respectively.

Material	E_{11} [GPa]	E_{22} [GPa]	G_{12} [GPa]	ν_{12}	α_1 [$\frac{\mu m}{m^{\circ}C}$]	α_2 [$\frac{\mu m}{m^{\circ}C}$]	t_{ply} [mm]	ρ [kg/m ³]
AS4/8552	135	9.68	5.6	0.30	0.28	28.0	0.181	1.58
Invar 36		140		0.33		1.5		8.05
2024T3		72.3		0.33		24		2.73

Table 3.1: Material properties.

It is possible to note that for small values of angle θ , the bending stiffness along X axis D_{11} is large, with its maximum at zero degrees, while CTE along X direction α_x is very low. Conversely, D_{11} is minimized at 90° , while α_x is maximized. Thus, bending stiffness and thermal expansion show opposite trends, and a balance between these two factors must be achieved. In reality, boundary conditions will expand, stretching the plate and changing the buckling temperature. Due to this, the effect of boundary conditions was considered for the next steps in the laminate selection process taking into account the plate frame in the analyses.

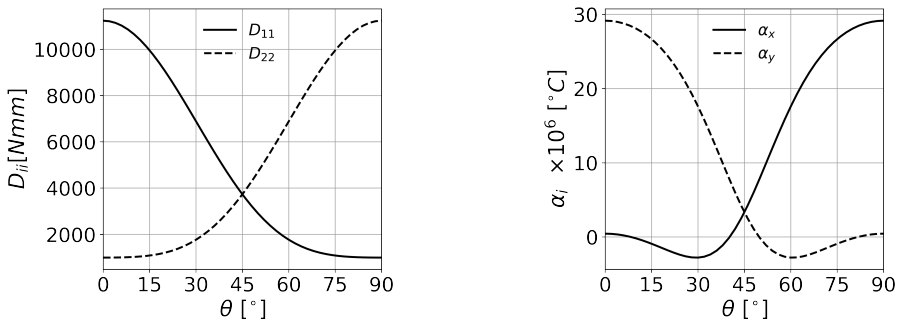


Figure 3.3: Properties of composite plates: (a) Bending stiffness for $[\theta / -\theta]_{2s}$ laminates; (b) CTE's for $[\theta / -\theta]_{2s}$ laminates.

In the second step, the defined design space was examined for plates presenting mode jumping in their post-buckling range. At the beginning, a generic symmetric and balanced $[\theta / -\theta]_{2s}$ stacking orientation was chosen. The laminates were studied using two finite element (FE) analyses: the buckling temperatures were calculated through a linear buckling analysis, while the simulations for plate nonlinear behavior were performed using a dynamic explicit procedure. All simulations were performed with the FE model reported in Fig. 3.4 (a) and using the software Abaqus (Dassault Systemes, Paris, FR).

The models present dimensions of $440 \text{ mm} \times 340 \text{ mm}$. Boundary conditions were introduced considering the surrounding structural frame to which the plate is attached. The frame overlaps with the outer area of the plate and has a cross section with width

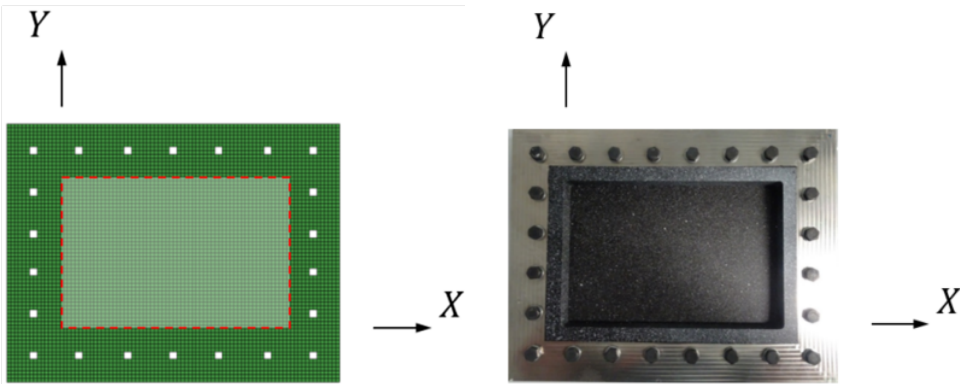


Figure 3.4: Plate with frame: (a) FE model; (b) Specimen.

of 70 mm, so that the plate free area is 300 mm × 200 mm. The frame was made from *Invar* 36 material, which material properties are reported in Table 3.1. Plate and frame were meshed using S4R element. As the overlapping meshed areas corresponding to the plate and the frame have equal element size and nodes at identical positions, they were connected by means of a simple nodal merging operation. The influence of element size over the linear buckling temperature is reported in Fig. 3.5, where both error and normalized computational time are plotted versus element size.

Adopting a 5 mm element length, an error of 0.2% can be achieved with relatively small computing times. As the overlapping meshed areas corresponding to the plate and the frame have equal element size and nodes at identical positions, they were connected by means of a simple nodal merging operation. Due to this modelling simplification, no friction or slipping effects between plate and frame are considered. During the loading, the plate expansions are constrained by the much stiffer frame, that is, in any case, allowed to expand freely. For all the analysis it was assumed that both plate and boundary conditions are always at the same temperature.

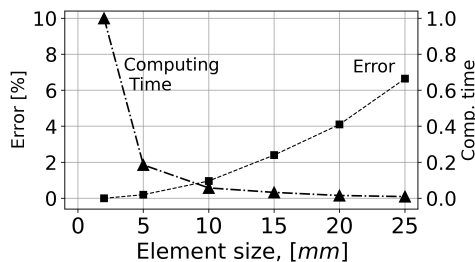


Figure 3.5: Analysis error and computational time vs. element size.

A set of linear buckling analysis for laminates with stacking $[\theta / -\theta]_{2s}$ is displayed in Fig. 3.6, ranging the value of θ from 0° to 90° in 5° increments. A total of five curves, each one collecting the eigenvalues from a particular mode shape, are reported. For each value of θ , at least two eigenvalues are reported: the lowest eigenvalue defines the buckling temperature ΔT_{b1} , as well as its corresponding buckling shape; conversely, higher eigenvalues indicate that the plate has alternative states of equilibrium at a temperature higher than ΔT_{b1} . For a plate to naturally jump into another mode shape, the final-state mode shape must be captured as a higher eigenvalue in the linear buckling analysis. For instance, for $\theta = 30^\circ C$, the plate reaches buckling at a $\Delta T_{b1} = 57.62^\circ C$ under mode (1, 1), and a second eigenvalue for mode shape (1, 2) at $\Delta T = 68.12^\circ C$.

The results for buckling temperatures obtained in Fig. 3.6 can be divided in intervals: for values of θ within the range $[0^\circ, 20^\circ]$ plates buckle under a (1, 2) mode; eigenvalues for modes (1, 1) and (1, 2) are however very close. Within the range $\theta = [25^\circ C, 40^\circ C]$ plates buckle under a (1, 1) mode shape, and the distance between the curves corresponding to shapes (1, 1) and (1, 2) increases with angle θ . In this range, mode jumps from a (1, 1) to a (1, 2) buckling shape are possible. For range $\theta = [45^\circ, 90^\circ]$, mode (1, 2) is no longer present. The range of interest for $[\theta / -\theta]_{2s}$ laminates, valid for the selected plate geometry and boundary conditions, is defined by $\theta = [25^\circ C, 40^\circ C]$.

After having found a range of interest, numerical predictions for the post-buckling behavior of three composite plates with $\theta = 25^\circ C$, $30^\circ C$ and $35^\circ C$ are presented in Fig. 3.7. For these analyses, an initial imperfection with the shape of the 1st buckling mode and amplitude of 0.5% of plate thickness was assumed. Being the imperfection amplitude small, the nonlinear behavior comes to resemble the ideal plate nonlinear behavior. For the three plates, once ΔT_{b1} is trespassed, out-of-plane deflections start increasing, assuming a (1, 1) buckling shape. For $\theta = 25^\circ C$ the mode jump is reached at $\Delta T_{b2} = 52.8^\circ C$, for $\theta = 30^\circ C$ this happens at $\Delta T_{b2} = 91.2^\circ C$, and for $\theta = 35^\circ C$ the mode jump occurs at $\Delta T_{b2} = 192.8^\circ C$ that is beyond the maximal temperature of $120^\circ C$.

It can be observed that for the studied range of θ , mode jumping temperature ΔT_{b2} and maximal plate deflections tend to increase with angle θ . This trend is also observed for linear buckling temperature ΔT_{b1} , reported in Fig. 3.6. The reasons are the decrease of α_y and the increase of bending stiffness D_{22} along Y direction for growing values of θ , as reported in Figs. 3.3 (a,b). It must also be noted that for the analyzed range of θ , the laminate CTE α_x has a negative value, stretching the plate when it is heated and therefore stabilizing the plate against buckling.

The effect of plate imperfections is illustrated in Fig. 3.7 b, where the post-buckling behavior of the composite plate with $[30 / -30]_{2s}$ laminate and different imperfections is reported. Three analyses were conducted with an initial imperfection with the shape of a (1, 1) buckling mode and amplitudes of 1%, 5% and 10% of plate thickness, plus an analysis with a (1, 2) buckling mode imperfection and amplitude of 5% of plate thickness. In particular, ΔT is plotted versus the out-of-plane deflections W , measured in the center of the plate. The plate with the 1% imperfection amplitude, represented as a continuous line, starts deflecting out of plane at a temperature close to the linear eigenvalue buckling temperature reported in Fig. 3.6. Then, the deflection W keeps growing till an abrupt mode change happens at $\Delta T_{b2} = 91.2^\circ C$. An analogue behavior can be observed in the curves for 5% and 10% imperfection amplitude, reported in Fig. 3.7 (b) as dashed

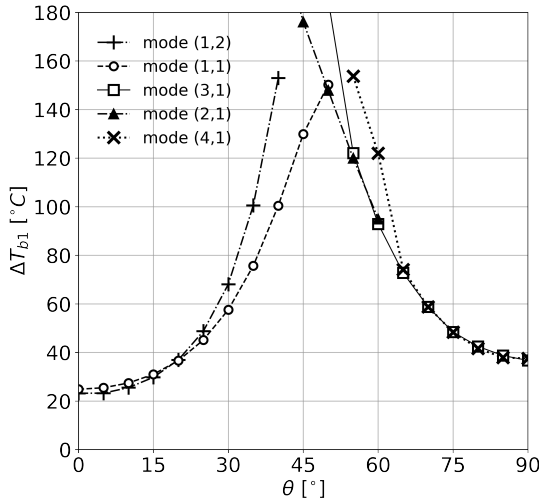


Figure 3.6: Linear buckling temperatures for $[\theta / -\theta]_{2s}$ laminates.

and dot-dashed lines, where ΔT_{b2} tends to increase with imperfection amplitude up to 96.0°C and 100.8°C respectively. However, if an initial imperfection with the shape of the 2^{nd} mode is assumed instead, the mode jump temperature decreases, and with a sufficiently large imperfection amplitude, the plate buckles directly under a (1, 2) mode, skipping the (1, 1) lowest eigenvalue shape.

A parametric study is so conducted for $[\theta / -\theta]_{2s}$ laminates within the range of interest $\theta = [25^\circ, 40^\circ]$ and the results are presented in Fig. 3.8 (a), where both linear and nonlinear plate behavior are reported. The black bold line collects the 1^{st} eigenvalues or buckling temperatures obtained in the linear buckling analysis, while the black thin line reports the 2^{nd} linear eigenvalue: for instance, considering $\theta = 30^\circ$, the figure shows that the plate has the first eigenvalue at $\Delta T_{b1} = 57.62^\circ$, and has a second eigenvalue at $\Delta T = 68.12^\circ$ with a mode shape (1, 2). The blue curves report the mode jumping temperatures for different imperfection shapes and amplitudes: the blue bold line collects values of ΔT_{b2} for plates with 0.5% 1^{st} mode imperfection amplitude, the blue dot-dashed and dotted lines report values of ΔT_{b2} for 5% and 10% imperfection amplitude, and at last, a blue dashed line captures values of ΔT_{b2} for a 5% imperfection shape with a 2^{nd} mode shape. Considering a plate with $\theta = 30^\circ$ and 0.5%, 5% and 10% of 1^{st} mode imperfection amplitudes, the plate would find a mode jump at $\Delta T_{b2} = 91.2^\circ$, 96.0° and 100.8° respectively, matching values previously reported in Fig. 3.7 (b). It can be observed how for all analyzed values of θ , increasing amplitudes of 1^{st} mode shape imperfection tend to rise ΔT_{b2} . Conversely, 2^{nd} mode imperfections tend to decrease ΔT_{b2} . Within the range $\theta = [25^\circ, 30^\circ]$, the lines for ΔT_{b1} and ΔT_{b2} overlap, meaning that the plate buck-

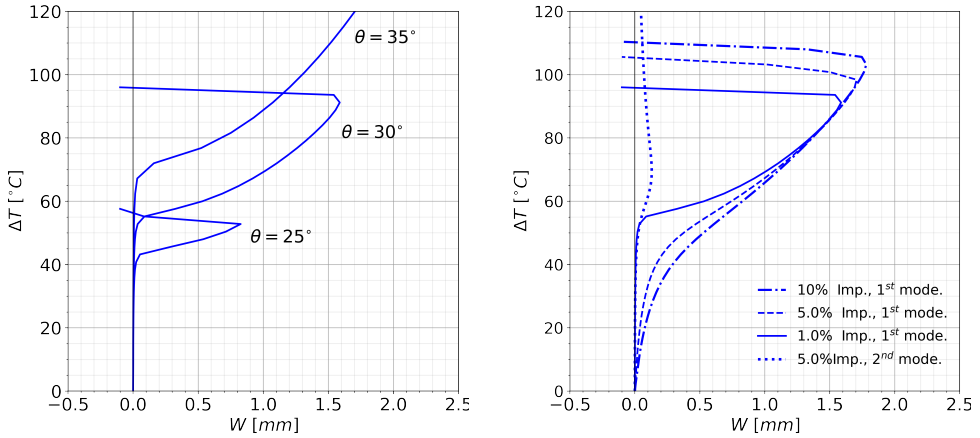


Figure 3.7: Mode jumping of composite plates: (a) Mode jumping temperature for $[\theta/ - \theta]_{2s}$ laminates; (b) Effect of imperfections for $[30/ - 30]_{2s}$ laminate.

les directly under a (1,2) shape. $[35/ - 35]_{2s}$ layup shows a ΔT_{b2} beyond $120^\circ C$, so the remaining candidate layups are $[25/ - 25]_{2s}$ and $[30/ - 30]_{2s}$.

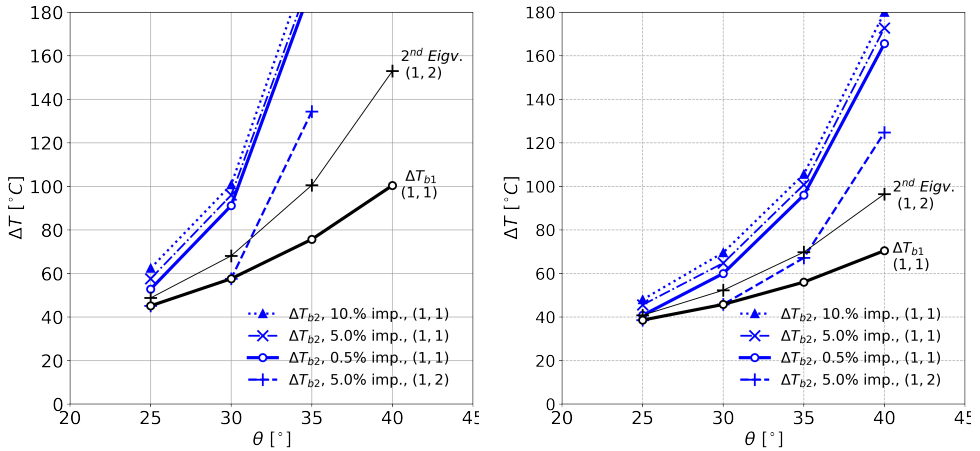


Figure 3.8: Mode jumping temperature for different laminates: (a) $[\theta/ - \theta]_{2s}$ laminates; (b) $[\theta/ - \theta/\phi - \phi]_s$ laminates with $\phi = \theta - 25$.

In the third and last step, the stacking orientations were improved by fine-tuning the layups. The objective was to make them more suitable for experimentation by decreasing both ΔT_{b1} and ΔT_{b2} . This can be achieved by using a generic angle-ply laminate in the form $[\theta/ - \theta/\phi - \phi]_s$, where both angles are smaller than 45° and the outer layer angle θ is significantly larger than ϕ . Taking for example $\phi = \theta - 25^\circ$, the bending stiff-

ness along Y axis D_{22} does not decrease substantially, as D_{22} is mainly formed by the contributions of the outer plies and angle θ remains constant. On the other hand, α_y increases significantly, and also α_x increases, changes its sign and becomes positive. Results for $\varphi = \theta - 25^\circ$ are reported in Fig. 3.8 (b) for the range $\theta = [25^\circ, 40^\circ]$. For the considered values of θ , it can be appreciated a decrease of both ΔT_{b1} and ΔT_{b2} . As a consequence, laminates with $\theta = 35^\circ$ show a mode jump within 120°C range, even if a moderate 2^{nd} mode imperfection is present. Consequently, two stacking orientations of the type $[\theta / -\theta / \varphi / -\varphi]_s$ are selected for experimentation: $[30 / -30 / 5 / -5]_s$ and $[35 / -35 / 10 / -10]_s$.

3.4. TEST SETUP

Three specimens were manufactured and tested. The first plate was made in aluminum alloy 2024T3 [31] with a thickness of 1 mm. The aim of this first test was assessing the functionality of the test setup and providing a benchmark using an isotropic material with well-defined properties. The second and third specimens were made of AS4/8552 composite material, with stacking orientations $[30 / -30 / 5 / -5]_s$ and $[35 / -35 / 10 / -10]_s$. For the manufacturing of the plates, each individual layer was cut in an automated cutting table in order to ensure the accuracy in the ply orientation. After that, the layers were stacked by hand and ultimately cured in an autoclave. For the tests, the plate is fixed in the frame, which has the function of providing support to the plate as well as restraining its thermal expansion during the test, as shown in Fig. 3.9. The frame is composed of two symmetric parts between which the plate is placed and then assembled together with steel bolts. The frame is made of *Invar* 36 material, which has a very low *CTE*.

Before a test starts, the plate and the frame have to be bolted together. The frame relies on the bolted joint to restrain the thermal expansion in the plate. The selected steel bolts have a *CTE* of $12.2 \mu\text{m}/\text{m}^\circ\text{C}$, which is much higher than the *CTE* of *Invar* 36 material. The assembly torque needs to be high enough to ensure that not too much bolt pretension is lost through heating due to the difference in *CTE* between frame and bolts. A total assembly torque of 60 Nm is gradually brought to the fixture in three levels, following a crossed path to ensure uniform compression throughout the frame. To induce the temperature increment, a Vötsch brand oven was used (Vötsch Industrietechnik GmbH, Reiskirchen, DE). It had a volume capacity of $600 \text{ mm} \times 600 \text{ mm} \times 600 \text{ mm}$. A metallic steel support, reported in Fig. 3.9, was used to keep the frame in a vertical position.

The test setup is presented in Fig. 3.10. For the test, the original door of the oven is removed and substituted by a replacement wooden hatch with an inner ceramic lining. This hatch has a rectangular hole that allows direct visual contact with the plate for measurement acquisition. A rectangular, metallic adaptor with the same cross section as the hole is used for sealing gap between frame and hatch.

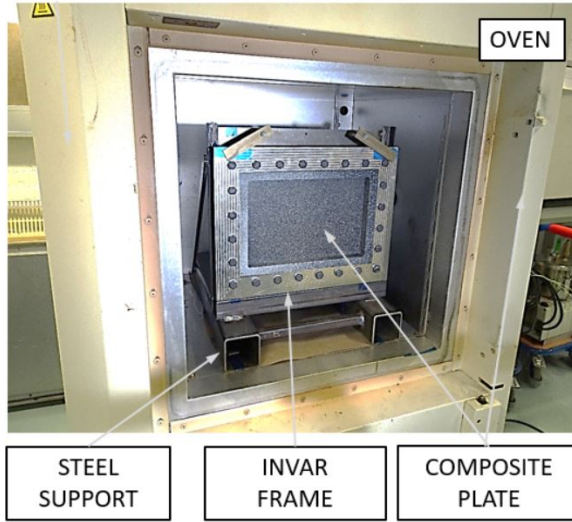


Figure 3.9: Specimen inside oven.

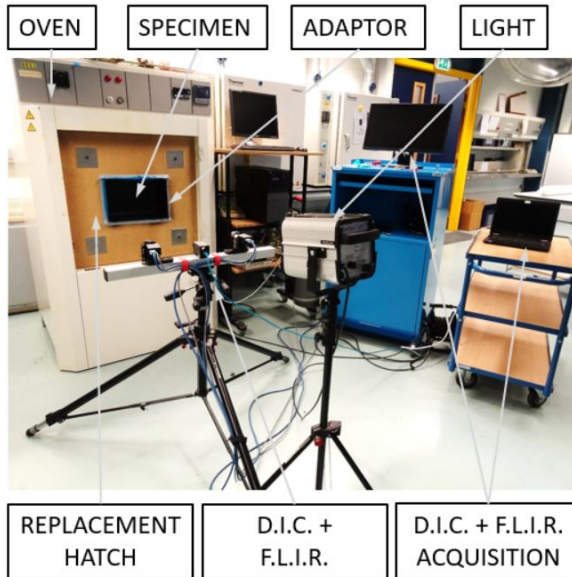


Figure 3.10: Test setup.

The acquisition systems collect measurements for both displacement and temperature of the plate during the complete duration of the experiment. The measurement of the out-of-plane displacement is performed with a Vic3D Digital Image Correlation (DIC) system (Correlated Solutions, Irmo, SC, USA), equipped with two cameras. The plate has to be painted with a white speckle pattern over black background. During the tests, the temperature is monitored using a thermocouple sensor placed at the center of the plate and using an A65 thermocamera (FLIR Systems, Arlington, VA, USA) placed on the outside of the oven.

In the FE analysis the plate is loaded by applying temperature increments with respect to the initial reference temperature. In order to being able to compare experimental results with numerical analysis, a reference temperature T_{ref} must be added to applied ΔT in the analysis. Indeed it is considered that at T_{ref} the plate is in an in-plane stress free state. T_{ref} was calculated here as the average temperature before and after bolting operation, measured in the fixture. Thus, the equation $T_{analysis} = T_{ref} + \Delta T$ holds.

The tests consist in the gradual, monotonic heating of the plate and frame. Thermocouples start recording 10 minutes before test start. Once the test initiates, *DIC* and *FLIR* thermocamera system start recording data. For all measurement system, an acquisition rate of 1 measurement every 10 s was used.

3.5. THERMAL TESTS

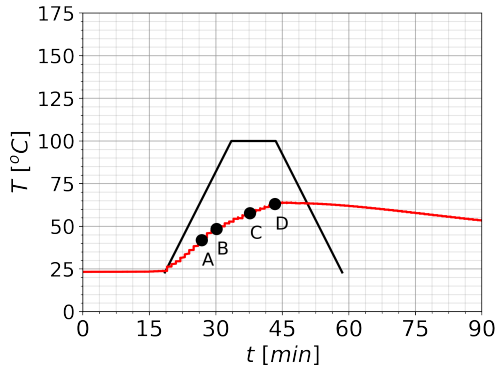


Figure 3.11: Heating cycle for aluminum alloy plate.

The first test was performed with the plate made in aluminum alloy 2024T3 of 1 mm thickness. The temperature path measured by the thermocouple is displayed in Fig. 3.11. The goal temperature path into the oven is represented as a black bold line, while temperature measured in the thermocouple is represented as a red bold line. A large difference between the two curves can be appreciated. It is believed this difference was caused by air convection on the external face of the plate.

The contour plots for numerical and experimental deflections are presented in Fig. 3.12. For all numerical analyses, a 1st mode shape imperfection with a 10% amplitude was considered. The obtained experimental plots show reasonably good correlation with the numerical results: predicted and obtained buckling shapes are matching in shape, even if the experimental values are larger than the predictions. This becomes evident in the curves plotted in Fig. 3.13 where Z -coordinate was plotted versus the temperature for the three plates. For the aluminum alloy plate the Z -coordinate was measured at plate position $(a/2, b/2)$. Two curves are plotted, one blue dotted and a black curve with round markers representing the FE and experimental results, respectively. Even if the experimental deflections result to be noticeably larger, the numerical prediction captures the essence of the plate nonlinear behavior. The metallic plate shows no mode jumping.

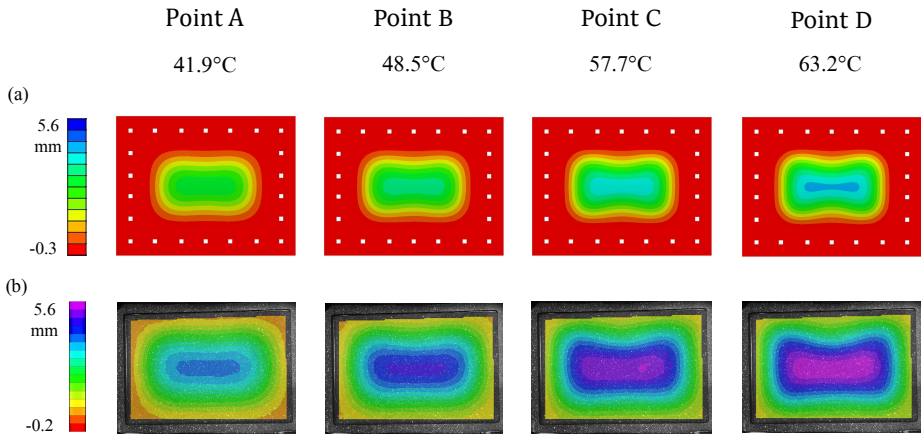


Figure 3.12: Out-of-plane deformation for aluminum alloy plate: (a) FE analysis; (b) Test.

The second test was performed on the composite plate with $[30/-30/5/-5]_s$ layup. A graph of temperature as a function of time is reported in Fig. 3.14. The ideal temperature cycle is represented as a black bold line, labelled as “Oven input”. In practice the plate never reaches the programmed temperature, so a prediction was performed to ensure that the desired temperature was reached; this estimation, represented as a bold violet line, was performed using data from two preliminary tests, where the plate was heated at two different temperature rates. This violet line was also used for the numerical simulation of the plate. Using the differences between programmed and obtained temperature rates in both experiments, for a desired plate temperature rate an oven input program rate can be extrapolated.

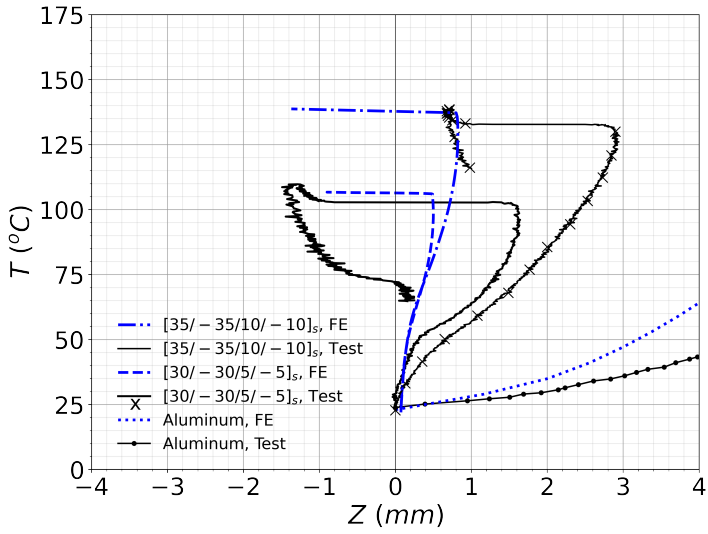


Figure 3.13: Temperature vs. out-of-plane deformation for the three plates.

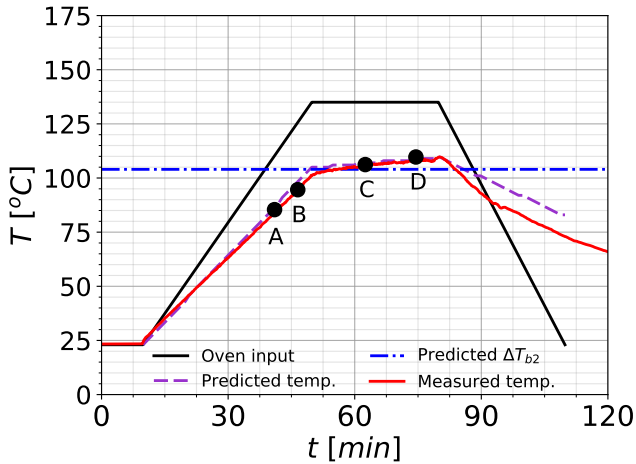


Figure 3.14: Heating cycle for for [30/-30/5/-5]_s plate.

The expected value for mode jumping is plotted in the graph as a horizontal dot-dashed blue line. The temperature measured in the plate with the thermocouple is depicted as a red bold line. It closely matches the predicted temperature curve, in violet, and crosses it at the numerically expected temperature ΔT_{b2} . In Fig. 3.15 experimental and numerical plots are reported. Temperature points A and B correspond to the points in which the plate is heated and the out-of-plane displacements are clearly visible in the form of a (1, 1) buckling shape. At temperature values C and D a change in mode buckling into a (1, 2) shape is registered. When observing the FE simulations at point C the mode jump has still not happened.

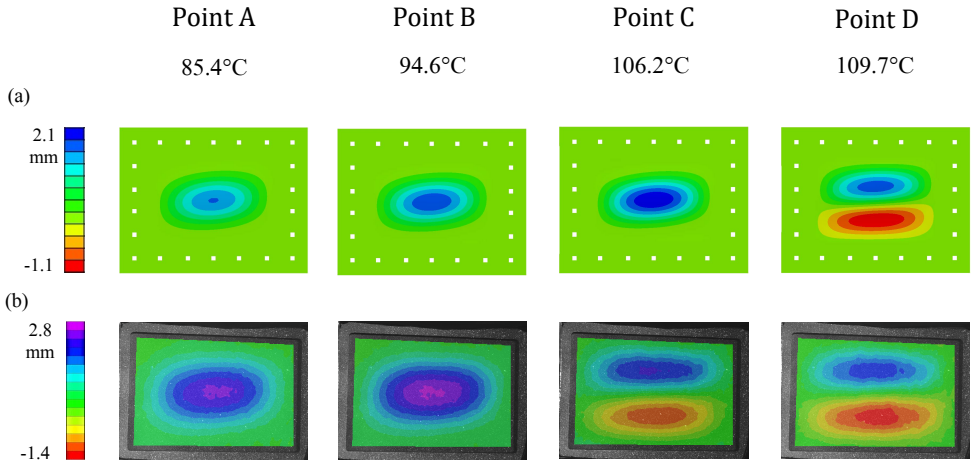


Figure 3.15: Out-of-plate deformation for $[30/-30/5/-5]_s$ composite plate: (a) FE analysis; (b) Test.

This difference becomes evident when observing Fig. 3.13, where plate Z-position is measured at $(a/2, b/4)$. In the two curves for laminate $[30/-30/5/-5]_s$, the black line for the test and the dot-dashed blue line for the FE analysis are displayed. A change on sign in Z coordinate takes place at 107°C for the numerical prediction and at 102.5°C for the experimental result. Thus, the mode jump took place slightly earlier than what the FE simulation indicates. Additionally, 7.5 minutes after point D the temperature in the plate becomes maximum and after that it starts decreasing. When the plate cools down to the mode jump temperature $\Delta T_{b2} = 102.5^\circ\text{C}$, it does not spontaneously jump back into the original one half-wave configuration but it remains at a (1, 2) shape till $T = 72^\circ\text{C}$ showing some sort of hysteresis behavior.

The third test was performed on the composite plate with $[35/-35/10/-10]_s$ laminate. The heating diagram in Fig. 3.16 shows that the curves for experimental temperature and estimated mode jump temperature do not cross, hence the temperature estimation was not accurate enough. However, in Fig. 3.17, the experimental image of point D shows that a mode jump is indeed captured, differing from FE prediction which still shows a (1, 1) buckling mode. This mode jump is also observable in Fig. 3.13, where, although the sign of Z does not change, it experiences a sudden drop at 122.5°C .

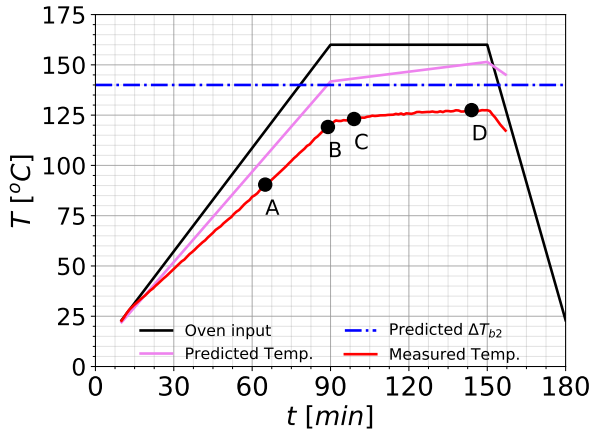


Figure 3.16: Heating cycle for for $[35/-35/10/-10]_s$ plate.

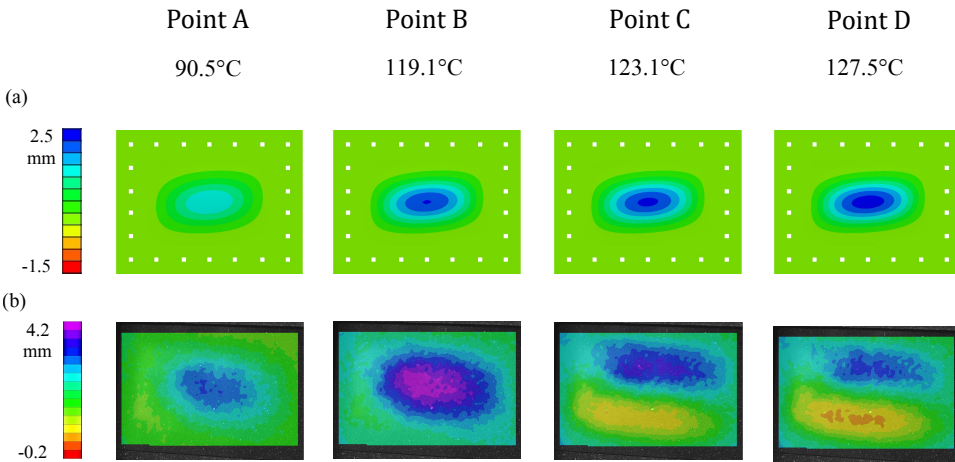


Figure 3.17: Out-of-plate deformation for $[35/-35/10/-10]_s$ composite plate: (a) FE analysis; (b) Test.

As occurred with previous plate $[30/-30/5/-5]_s$, the predicted mode jump temperature happens at a larger temperature, at 137°C .

A brief comparison of the three plates is here presented. The curves in Fig. 3.13 indicate that for all cases plates show larger deflections than in the FE predictions: they are 33% higher for the $[30/-30/5/-5]_s$ plate and 68% for the $[35/-35/10/-10]_s$ plate. In the case of the two tested composite plates, the plate with layup $[35/-35/10/-10]_s$ shows much larger deflections than the plate with $[30/-30/5/-5]_s$ layup. Both plates present a mode jump, being the temperature ΔT_{b2} higher for the $[35/-35/10/-10]_s$ plate. For both composite plates the mode jump manifests at a slightly lower temperature than in the numerical prediction.

The discrepancies found between predictions and experimental results can be attributed to multiple factors. In the FE models, possible source of uncertainty is mainly the temperature dependency of material properties. While it is assumed that residual stresses due to the curing process were present in the tested laminates, their contribution was expected not to be significant. Also, the effect of moisture was also not considered, since it becomes relevant when composite parts have been subjected to humidity rich environments for a sustained period of time. Due to this, these factors were not taken into account into the FE model. Regarding the tests, the discrepancy sources can be different: deviation from nominal values in material properties, change in material properties due to sustained heating, small variations in the ply angles due to the manufacturing process, relaxation in the boundary conditions due to the thermal expansion in the steel bolts, irregular heating in the specimen and geometrical imperfections of the plate. Even though the differences with the prediction are evident, the dynamic explicit procedure successfully captures the tendency to show mode jumping in the studied composite plates when these are under heating loading condition. Numerical predictions can be improved by individually addressing all previously mentioned factors. However, even though these deserve independent attention, they bring complexity and they therefore remain out of scope for the present investigation. Only the initial imperfection over ΔT_{b2} is addressed here: as shown in Section 3, 1^{st} mode imperfection patterns with a 5% amplitude tend to stabilize the nonlinear range of the plate rising ΔT_{b2} , while plate imperfections dominated by other modes shapes may decrease the mode jumping temperature or even neutralize the effect completely. All FE predictions reported in Fig. 3.14 used a 1^{st} mode, 10% imperfection amplitude for all cases, while more adverse imperfections may have been present. Indeed, buckling fixtures can imprint a certain imperfection in the plate which can influences its buckling shape. Finally, the position of the heating source is also noteworthy: the tested plate is heated only from one side, and due to this, a through-thickness temperature gradient appears in the plate. This creates a thermal moment that can help the plate overcoming potentially disruptive initial imperfections, buckling into a (1, 1) mode shape, as all three experiments buckle under a (1, 1) shape, with the maximum deflection area directed towards the interior of the oven.

Based on previous results, 1^{st} mode geometrical imperfections and slight panel curvatures could be used deliberately to stabilize the post-buckling shape in composite panels and help better control the mode jumping effect. Mild geometrical patterns such as panel beadings have been successfully used in the past for structural stabilization of

thermally post-buckled structures [32], and may offer interesting properties towards applications of mode jumping. Also, morphing applications using mode jumping should take advantage of heating asymmetries present in aerospace applications such high-speed aircraft or satellites, where the structure is heated in only one side due to aerodynamic friction or solar radiation.

3.6. CONCLUSIONS

In this study the thermal buckling and post-buckling behavior of composite plates was investigated. Plates were studied using both numerical and experimental techniques. A methodology for selecting composite plates showing mode jumping under heating was presented. Linear buckling eigenvalue analysis proved useful for the identification of desired secondary mode shapes, while dynamic explicit analysis was able to capture this event and give estimations for mode jumping temperatures. Additionally, parametric analysis predicted a stabilizing influence of 1st mode imperfections with diverse amplitudes over the post-buckling shape increasing the mode jumping temperature, while 2nd mode imperfections of comparable amplitude appeared to have a destructive effect over it. Thus, inducing (1,1) imperfections on composite panels could be advantageous if mode jumps are sought. As a result of the preliminary analysis, two plates made in AS4/8552 composite material with layups $[30/-30/5/-5]_s$ and $[35/-35/10/-10]_s$ were selected for experimentation in a novel test setup. An additional plate made in 2024T3 aluminum alloy was selected as a benchmark case and to demonstrate the functionality of the setup. The post-buckling behavior was successfully reproduced in all plates, while mode jumping was successfully captured for both composite plates. The experimental deflections resulted larger than the predicted values for all three tested plates. For the composite plates, mode jumping happened at temperatures lower than predicted, being the largest difference limited to 13%. Even if discrepancies with numerical predictions are reported, nonlinear numerical procedures succeeded in capturing the trends and overall behavior in all plates. It is believed that sources for discrepancies may range from temperature dependent material properties, manufacturing or assembly defects. Also, potential morphing applications using mode jumping should take advantage of heating asymmetries present in aerospace applications. These results can be valuable as a preliminary study when considering applications of thermally triggered buckling shape change in aerospace applications.

BIBLIOGRAPHY

- [1] Z. Wu, P. M. Weaver, and G. Raju, "Postbuckling optimisation of variable angle tow composite plates", *Composite Structures*, vol. 103, pp. 34–42, 2013, ISSN: 02638223. DOI: [10.1016/j.compstruct.2013.03.004](https://doi.org/10.1016/j.compstruct.2013.03.004). [Online]. Available: <http://dx.doi.org/10.1016/j.compstruct.2013.03.004%20http://dx.doi.org/10.1016/j.tws.2012.07.008>.
- [2] R. Vescovini and C. Bisagni, "Two-step procedure for fast post-buckling analysis of composite stiffened panels", *Computers and Structures*, vol. 128, pp. 38–47, 2013, ISSN: 00457949. DOI: [10.1016/j.compstruc.2013.06.002](https://doi.org/10.1016/j.compstruc.2013.06.002). [Online]. Available: <http://dx.doi.org/10.1016/j.compstruc.2013.06.002>.
- [3] N. Hu and R. Burgueño, "Buckling-induced smart applications: recent advances and trends", *Smart Materials and Structures*, vol. 24, no. 6, p. 063001, Jun. 2015, ISSN: 0964-1726. DOI: [10.1088/0964-1726/24/6/063001](https://doi.org/10.1088/0964-1726/24/6/063001). [Online]. Available: <http://dx.doi.org/10.1088/0964-1726/24/6/063001%20https://iopscience.iop.org/article/10.1088/0964-1726/24/6/063001>.
- [4] R. Vos, R. Barrett, R. D. Breuker, and P. Tiso, "Post-buckled precompressed elements: a new class of control actuators for morphing wing UAVs", *Smart Materials and Structures*, vol. 16, no. 3, pp. 919–926, Jun. 2007, ISSN: 0964-1726. DOI: [10.1088/0964-1726/16/3/042](https://doi.org/10.1088/0964-1726/16/3/042). [Online]. Available: <https://iopscience.iop.org/article/10.1088/0964-1726/16/3/042>.
- [5] F. Runkel, U. Fasel, G. Molinari, A. F. Arrieta, and P. Ermanni, "Wing twisting by elastic instability: A purely passive approach", *Composite Structures*, vol. 206, no. June, pp. 750–761, 2018, ISSN: 02638223. DOI: [10.1016/j.compstruct.2018.07.095](https://doi.org/10.1016/j.compstruct.2018.07.095).
- [6] E. Eckstein, A. Pirrera, and P. M. Weaver, "Thermally driven morphing and snap-through behavior of hybrid laminate shells", *AIAA Journal*, vol. 54, no. 5, pp. 1778–1788, May 2016, ISSN: 00011452. DOI: [10.2514/1.J054648](https://doi.org/10.2514/1.J054648). [Online]. Available: <http://arc.aiaa.org/doi/10.2514/1.J054648>.
- [7] E. Eckstein, A. Pirrera, and P. M. Weaver, "Morphing high-temperature composite plates utilizing thermal gradients", *Composite Structures*, vol. 100, pp. 363–372, 2013, ISSN: 0263-8223. DOI: [10.1016/j.compstruct.2012.12.049](https://doi.org/10.1016/j.compstruct.2012.12.049).
- [8] P. Nali and E. Carrera, "Accurate buckling analysis of composite layered plates with combined thermal and mechanical loadings", *Journal of Thermal Stresses*, vol. 36, no. 1, pp. 1–18, 2013, ISSN: 01495739. DOI: [10.1080/01495739.2012.663679](https://doi.org/10.1080/01495739.2012.663679). [Online]. Available: <http://www.tandfonline.com/doi/abs/10.1080/01495739.2012.663679>.

- [9] I. Tawk, P. Navarro, J. F. Ferrero, J. J. Barrau, and E. Abdullah, "Composite delamination modelling using a multi-layered solid element", *Composites Science and Technology*, vol. 70, no. 2, pp. 207–214, 2010, ISSN: 02663538. DOI: [10.1016/j.compscitech.2009.10.008](https://doi.org/10.1016/j.compscitech.2009.10.008). [Online]. Available: <http://dx.doi.org/10.1016/j.compscitech.2009.10.008>.
- [10] F. Fabbrocino, M. F. Funari, F. Greco, P. Lonetti, R. Luciano, and R. Penna, "Dynamic crack growth based on moving mesh method", *Composites Part B: Engineering*, vol. 174, no. 5, p. 107053, Oct. 2019, ISSN: 13598368. DOI: [10.1016/j.compositesb.2019.107053](https://doi.org/10.1016/j.compositesb.2019.107053). [Online]. Available: <https://doi.org/10.1016/j.compositesb.2019.107053%20https://linkinghub.elsevier.com/retrieve/pii/S1359836819320062>.
- [11] L.-c. Shiau and S.-y. Kuo, "Free vibration of thermally buckled composite sandwich plates", *Journal of Vibration and Acoustics*, vol. 128, no. 1, p. 1, 2006, ISSN: 07393717. DOI: [10.1115/1.2149388](https://doi.org/10.1115/1.2149388). [Online]. Available: <http://link.aip.org/link/JVACEK/v128/i1/p1/s1%7B%5C%7Dagg=doi>.
- [12] B. Falzon and D. Hitchings, "Capturing mode-switching in postbuckling composite panels using a modified explicit procedure", *Composite Structures*, vol. 60, pp. 447–453, 2003, ISSN: 02638223. DOI: [10.1016/S0263-8223\(03\)00019-9](https://doi.org/10.1016/S0263-8223(03)00019-9).
- [13] B. Falzon and M. Cerini, "A study of secondary instabilities in postbuckling composite aerostructures", *The Aeronautical Journal*, vol. 111, pp. 715–729, Nov. 2007, ISSN: 0001-9240. DOI: [10.1017/S0001924000004899](https://doi.org/10.1017/S0001924000004899). [Online]. Available: <https://www.cambridge.org/core/product/identifier/S0001924000004899/type/journal%7B%5C%7Darticle>.
- [14] M. A. Arbelo, S. F. M. De Almeida, M. V. Donadon, *et al.*, "Vibration correlation technique for the estimation of real boundary conditions and buckling load of unstiffened plates and cylindrical shells", *Thin-Walled Structures*, vol. 79, pp. 119–128, 2014, ISSN: 02638231. DOI: [10.1016/j.tws.2014.02.006](https://doi.org/10.1016/j.tws.2014.02.006).
- [15] M. A. Arbelo, K. Kalnins, O. Ozolins, E. Skukis, S. G. Castro, and R. Degenhardt, "Experimental and numerical estimation of buckling load on unstiffened cylindrical shells using a vibration correlation technique", *Thin-Walled Structures*, vol. 94, pp. 273–279, 2015, ISSN: 02638231. DOI: [10.1016/j.tws.2015.04.024](https://doi.org/10.1016/j.tws.2015.04.024).
- [16] C. Bisagni, "Dynamic buckling of fiber composite shells under impulsive axial compression", *Thin-Walled Structures*, vol. 43, no. 3, pp. 499–514, 2005, ISSN: 02638231. DOI: [10.1016/j.tws.2004.07.012](https://doi.org/10.1016/j.tws.2004.07.012).
- [17] C. Bisagni and P. Cordisco, "Post-buckling and collapse experiments of stiffened composite cylindrical shells subjected to axial loading and torque", *Composite Structures*, vol. 73, no. 2, pp. 138–149, 2006, ISSN: 02638223. DOI: [10.1016/j.compstruct.2005.11.055](https://doi.org/10.1016/j.compstruct.2005.11.055).
- [18] E. Labans, H. Abramovich, and C. Bisagni, "An experimental vibration-buckling investigation on classical and variable angle tow composite shells under axial compression", *Journal of Sound and Vibration*, vol. 449, pp. 315–329, 2019, ISSN: 10958568. DOI: [10.1016/j.jsv.2019.02.034](https://doi.org/10.1016/j.jsv.2019.02.034). [Online]. Available: <https://doi.org/10.1016/j.jsv.2019.02.034>.

- [19] D. A. Ehrhardt and L. N. Virgin, "Experiments on the thermal post-buckling of panels, including localized heating", *Journal of Sound and Vibration*, vol. 439, pp. 300–309, Jan. 2019, ISSN: 0022460X. DOI: [10.1016/j.jsv.2018.08.043](https://doi.org/10.1016/j.jsv.2018.08.043).
- [20] W. Percy and R. Fields, "Buckling analysis and test correlation of hat stiffened panels for hypersonic vehicles", in *2nd International Aerospace Planes Conference*, Reston, Virginia: American Institute of Aeronautics and Astronautics, Oct. 1990. DOI: [10.2514/6.1990-5219](https://doi.org/10.2514/6.1990-5219). [Online]. Available: <http://arc.aiaa.org/doi/10.2514/6.1990-5219>;
<https://arc.aiaa.org/doi/10.2514/6.1990-5219>.
- [21] R. C. Thompson and W. L. Richards, "Thermal-structural panel buckling tests", *NASA Technical Memorandum 104243*, no. December 1991, 1991. [Online]. Available: <https://ntrs.nasa.gov/citations/19920006186>.
- [22] J. F. Rakow and A. M. Waas, "Thermal buckling of metal foam sandwich panels for convective thermal protection systems", *Journal of Spacecraft and Rockets*, vol. 42, no. 5, pp. 832–844, Sep. 2005, ISSN: 0022-4650. DOI: [10.2514/1.9741](https://doi.org/10.2514/1.9741). [Online]. Available: <http://arc.aiaa.org/doi/abs/10.2514/1.9741>;
<https://arc.aiaa.org/doi/10.2514/1.9741>.
- [23] K. D. Murphy, L. Virgin, and S. A. Rizzi, "The effect of thermal prestress on the free vibration characteristics of clamped rectangular plates: theory and experiment", *Journal of Vibration and Acoustics*, vol. 119, no. 2, p. 243, 1997, ISSN: 07393717. DOI: [10.1115/1.2889710](https://doi.org/10.1115/1.2889710). [Online]. Available: <http://vibrationacoustics.asmedigitalcollection.asme.org/article.aspx?articleid=1469874>.
- [24] M. Amabili and M. R. S. Tajahmadi, "Thermal post-buckling of laminated and isotropic rectangular plates with fixed edges: Comparison of experimental and numerical results", *Proceedings of the Institution of Mechanical Engineers, Part C: Journal of Mechanical Engineering Science*, vol. 226, no. 10, pp. 2393–2401, Oct. 2012, ISSN: 0954-4062. DOI: [10.1177/0954406211434496](https://doi.org/10.1177/0954406211434496). [Online]. Available: <http://journals.sagepub.com/doi/10.1177/0954406211434496>.
- [25] E. A. Thornton, "Thermal buckling of plates and shells", *Applied Mechanics Reviews*, vol. 46, no. 10, pp. 485–506, Oct. 1993, ISSN: 0003-6900. DOI: [10.1115/1.3120310](https://doi.org/10.1115/1.3120310). [Online]. Available: <https://asmedigitalcollection.asme.org/appliedmechanicsreviews/article/46/10/485/400818/Thermal-Buckling-of-Plates-and-Shells>.
- [26] N. L. Breivik and M. W. Hyer, "Buckling and postbuckling behavior of curved composite panels due to thermal and mechanical loading", *Journal of Reinforced Plastics and Composites*, vol. 17, no. 14, pp. 1292–1306, Sep. 1998, ISSN: 07316844. DOI: [10.1177/073168449801701404](https://doi.org/10.1177/073168449801701404).
- [27] R. A. Fields, W. L. Richards, and M. V. DeAngelis, "Combined loads test fixture for thermal-structural testing of aerospace vehicle panel concepts", *NASA Technical Memorandum TM-2004-212039*, no. February, 2004. [Online]. Available: <https://ntrs.nasa.gov/citations/20040031531>.

- [28] K. Wu and Z. Gurdal, "Thermal testing of tow-placed, variable stiffness panels", in *19th AIAA Applied Aerodynamics Conference*, Reston, Virginia: American Institute of Aeronautics and Astronautics, Jun. 2001. DOI: [10.2514/6.2001-1190](https://doi.org/10.2514/6.2001-1190). [Online]. Available: <https://arc.aiaa.org/doi/10.2514/6.2001-1190>.
- [29] Y. Xu, S. Ren, W. Zhang, Z. Wu, W. Gong, and H. Li, "Study of thermal buckling behavior of plain woven C/SiC composite plate using digital image correlation technique and finite element simulation", *Thin-Walled Structures*, vol. 131, no. October 2017, pp. 385–392, Oct. 2018, ISSN: 02638231. DOI: [10.1016/j.tws.2018.07.023](https://doi.org/10.1016/j.tws.2018.07.023). [Online]. Available: <https://doi.org/10.1016/j.tws.2018.07.023> [20https://linkinghub.elsevier.com/retrieve/pii/S0263823117312788](https://linkinghub.elsevier.com/retrieve/pii/S0263823117312788).
- [30] Hexcel Corporation, *HexPly 8552*, 2016. [Online]. Available: <https://www.hexcel.com/Resources/DataSheets/Prepreg> (visited on 10/15/2020).
- [31] Department of Defense, "Military Handbook Metallic Materials and Elements for Aerospace Structures (MIL-HDBK-5H)", no. December, 1998.
- [32] J. Lee and M. Bhatia, "Impact of corrugations on bifurcation and thermoelastic responses of hat-stiffened panels", *Thin-Walled Structures*, vol. 140, no. October 2018, pp. 209–221, Jul. 2019, ISSN: 02638231. DOI: [10.1016/j.tws.2019.03.027](https://doi.org/10.1016/j.tws.2019.03.027). [Online]. Available: <https://linkinghub.elsevier.com/retrieve/pii/S0263823118311273> [20https://doi.org/10.1016/j.tws.2019.03.027](https://doi.org/10.1016/j.tws.2019.03.027).

4

INVESTIGATION ON BUCKLING AND MODE JUMPING OF COMPOSITE PLATES UNDER THERMOMECHANICAL LOADS

To see what is in front of one's nose needs a constant struggle.

George Orwell

This paper presents an experimental and numerical study of composite plates, analyzing the interaction between mechanical and thermal loads related to buckling and the occurrence of mode jumping. A novel experimental setup for thermomechanical testing was developed. The setup is conceived around a frame with a low coefficient of thermal expansion, so that the plate can experience buckling and mode jumping when heated; and when compressed, interactions between the two loading states can be studied. Experimental results of plates loaded under diverse load cases are delivered in the form of load vs out-of-plane deflection graphs, deflection plots and buckling charts, where all buckling and mode jumping bifurcation points are registered. The influence of combined loading over mode jumping phenomena was successfully captured. Numerical predictions are able to estimate general tendencies in the occurrences of both buckling and mode jumping and in the mutual influence of thermal and mechanical loads

This chapter has been adapted from: J. G. Álvarez and C. Bisagni, "Investigation on buckling and mode jumping of composite plates under thermomechanical loads", International Journal of Non-Linear Mechanics, vol. 138, no. August 2021, p. 103 837, Jan. 2022, ISSN: 00207462. DOI: 10.1016/j.ijnonlinmec.2021.103837.

4.1. INTRODUCTION

AEROSPACE STRUCTURES are often required to work under conditions that involve combinations of mechanical and thermal loads, while accomplishing conflicting requirements such as robustness and being lightweight. Such requisites often yield thin-walled structural designs which are highly mass efficient but also vulnerable to buckling. Buckling has been traditionally considered as a liability or as a “no-go” area, even though, under specific circumstances, buckling can be used to enhance the aircraft structural performance [1]. In these cases, post-buckling regime states are considered as an extension of the original operative range of a given structure. While mechanically buckled structures have been successfully exploited in the past to improve structural performance, thermal buckling has traditionally been avoided [2]. However, thermally post-buckled states have been also successfully applied through the use of beaded panels or corrugated structures [3], [4], seeking aims such as increasing buckling stiffness or relaxation for thermal stresses. Structural elements as plates have potential for such applications, because of their stable behavior in post-buckling regime. Carbon fibre reinforced plastics (CFRP) materials can greatly contribute to this aim due to the high structural performance they offer and their material behavior that allows for large elastic deformations. They also offer high design flexibility thanks to the possibility to optimize their stacking orientation. Good knowledge of thermomechanically buckled states can help structural designers to identify potential advantage opportunities, make better choices and eventually contribute to better future designs.

On the other hand, new research trends are putting traditional conceptions about buckling under revision, as they are willing to observe buckling as a structural state with potentially advantageous features [5]–[7]. Gutiérrez Álvarez and Bisagni [8] performed experiments in heated, rectangular, symmetric and balanced angle-ply composite plates. The plates were able to display shape changes in the form of mode jumps when assembled in a stiff constraining fitting with low coefficient of thermal expansion (CTE). Cases in which plate size remains constant are, however, an idealization: a plate attached to an airframe is subjected to stretching and compression due to service loads. Plate size variation has a direct impact over the buckling temperature [9], while the impact over the mode jumping temperature is unknown.

Taking a look over previous work, the interest in thermal buckling emerged with the beginning of supersonic flight [10], [11]. Throughout the decades, the focus evolved, ranging from innovative structural configurations and geometries to the introduction of new generation aerospace materials. Thermal buckling experiments can be roughly divided in two types. The first type refers to tests in which the specimens buckle by stresses arisen due to constrained size variations. During the test, the specimen, typically a flat plate, is installed within a restraining fixture, sometimes water-cooled, and subjected to a typically uniform temperature increase. Examples are the tests on metallic plates performed by Murphy and Ferreira [12] or the tests on metal foam core sandwich panels done by Rakow and Waas [13]. In composite materials, Amabili et al [14] tested the buckling of cooled composite plates; Wu and Gurdal tested heated steered fiber panels, and more recently Xu et al [15] tested the buckling C/SiC woven composite plates. A subtype of test is the case where free, unrestrained plates buckle merely due to thermal

gradients [16]. Ehrhardt and Virgin [17] found the presence of alternative equilibrium states in rectangular, metallic, thermally buckled plates, Bhagat and Yeyaraj [18] studied the effect of non-uniform temperature distributions on the thermal buckling of shallow curved metallic panels, and Gutiérrez Álvarez and Bisagni [8] achieved buckling and mode jumping in carbon composite plates. The second type of thermal buckling tests available in literature consists on specimens being placed in a compression device and subsequently being subjected to combinations of compression and heat. Substantial experimental efforts were made during the early test campaigns of Ross et al. [19], Anderson and Card [20], Mayers and Jaworski [21], Bushnell [22], Frum and Baruch [23] and Ari-Gur and Baruch [24]. All these experiments were performed considering metallic cylinders, heated either uniformly or along two opposite cylinder generators. Percy and Fields [25], and Thompson and Richards [26] tested identical hat stiffened panels made in titanium and titanium matrix composite under the simultaneous effect of compression and heat. Still, the most sophisticated experimental setups available are based in multi-actuator concepts, such as the one developed by Fields [27] who developed a test setup for combined thermomechanical loading using an 8-engine system capable of exerting compression, tension and/or shear with heating loads over a flat stiffened panel, or the Nasa Langley Combined Loads Testing System [28]. The amount of available literature on experiments on thermomechanical buckling is, however, not extensive, being this scarcity even more pronounced for CFRP structures. On shallow shells, Breivik and Hyer [29] tested shallow shells made in composite material, with different layup under either heating or compression. Even if considerable efforts have been made in the field of buckling and post-buckling of composite structures [30]–[33], understanding instabilities triggered by thermomechanical loads [34], and also in understanding the mode changes in thin-walled structures [35], [36], no experimental attempts can be easily found on understanding mode changes in thermally and mechanically loaded composite plates.

The goal of this research is to perform an exploratory investigation to evaluate the effects of combined thermal and mechanical loads over buckling and mode jumping in CFRP plates. During this investigation both numerical and experimental techniques were used, even if the principal focus is the development and implementation of a novel experimental methodology and the presentation of a set of preliminary results. The proposed setup is based on the previously used concept of utilizing a low CTE invar frame to restrain thermal expansion [8], which is upgraded by incorporating the novel concept of applying compression to the frame using a compression machine. The proposed setup is therefore capable to simultaneously apply compression and heat. Tested plates have a laminate stacking that can both buckle and show mode jumps when heated, compressed, or under combination of these two loading conditions.

In Section 4.2, the main concepts related to the analyzed phenomena are introduced; in Section 4.3, numerical predictions performed using the Finite Element software Abaqus are presented and discussed. Section 4.4 contains a description of the experimental setup. In Section 4.5, a set of preliminary experimental results are presented: in particular, results for each type of performed test are reported in the form of load vs. displacement graphs and out-of-plane deflection shapes. A final experimental buckling chart for combined loading is also reported with the results of all performed tests. A dis-

discussion about the obtained results and the deviations from the numerical predictions is presented in Section 4.6, and potential sources of error are discussed.

4.2. BUCKLING AND MODE JUMPING ON HEATED AND MECHANICALLY LOADED COMPOSITE PLATES

A mode jump can be described as a change in the buckling shape of a panel as a consequence of variations in the load. This phenomenon often occurs in an abrupt manner and can be thus considered a dynamic event. In order to better explain this phenomenon, it is convenient to use an idealized plate such as the one represented in Fig. 4.1.

4

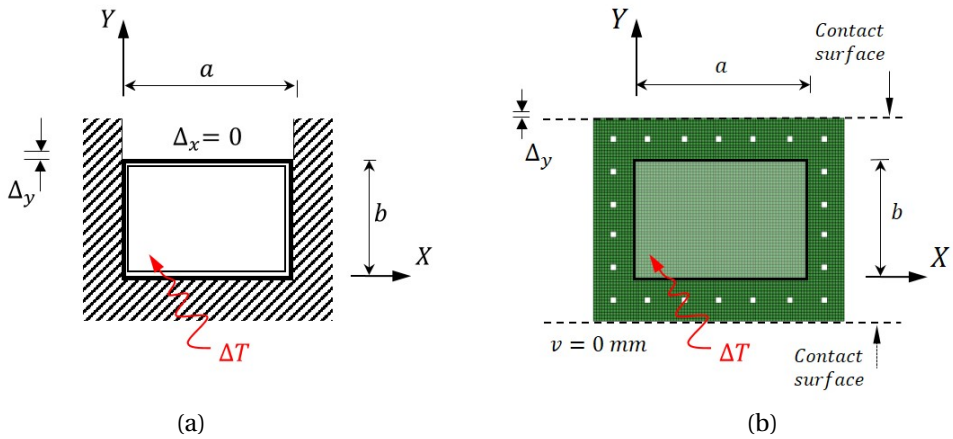


Figure 4.1: Plate under thermal and mechanical loads: (a) Plate boundary conditions; (b) FE model.

A rectangular flat plate of width a , height b and thickness t , made in composite laminate material, with a symmetric and balanced stacking orientation is considered. A XYZ coordinate system is placed in the lower left corner of the plate, coinciding the XY plane with the mid plane of the plate. Each ply is oriented at a generic angle θ which is defined with respect to the X reference axis and is assumed to be counter-clockwise positive. Displacements along the axis are characterized as U, V, W . Rotations around the four plate edges are constrained, and also the out-of-plane displacements of the edges are constrained. The plate is not allowed to experience change in size along X direction i.e. $\Delta_x = 0$, while external mechanical load along Y can be introduced in the form of a prescribed vertical displacement Δ_y . The plate can also be loaded by introducing uniform temperature increments ΔT . Positive values of ΔT correspond to temperatures over the in-plane stress free temperature, while negative values of Δ_y correspond to a shortening of the plate, i.e. compression. Plate edges remain straight during the whole loading process. The plate can therefore be subjected to combinations of loading conditions ΔT

and Δ_y , from now on referred as load cases.

Different load cases are analyzed. A “pure heating” load case assumes that a ΔT is applied while Δ_y remains fixed at 0 mm ; in a “pure compression” load case Δ_y is applied while ΔT is zero. A combined “compression + heating” load case consists of two load phases: during the first one a compressive Δ_y is introduced, and in the second loading phase a ΔT is applied on top of the initial Δ_y . The order of load application is relevant. During this investigation, two combined load cases are considered, “compression + heating” and “heating + compression”. When the plate is subjected to an homogeneous, monotonically increasing ΔT in a “pure heating” load case, stresses arise as a consequence of restrained thermal expansion. The typical path of the deflection at the plate center can be followed in Fig. 4.2. With temperature increasing, the plate remains flat till a bifurcation point, known as buckling temperature ΔT_{b1} , is reached. Once buckling temperature is surpassed, the plate starts to deform out of plane following the path reported as a bold black line, usually in a shape with a sinusoidal half-wave in the X direction and a sinusoidal half wave in the Y direction, denoted as a (1,1) shape. If the value of ΔT keeps growing, plates with certain layups may encounter bifurcations and change into different stable buckling shapes, typically into a (1,2) or (2,1) shape. This occurrence is commonly known as a mode jump or mode change and it is reported in the figure as temperature ΔT_{b2} . This is a well-known occurrence, which has been extensively documented for mechanically loaded metallic and composite panels [37]–[41]. The magnitude of ΔT_{b2} and also the mode shape obtained after the jump are heavily dependent on the dimensions, stacking orientation and boundary conditions of the plate.

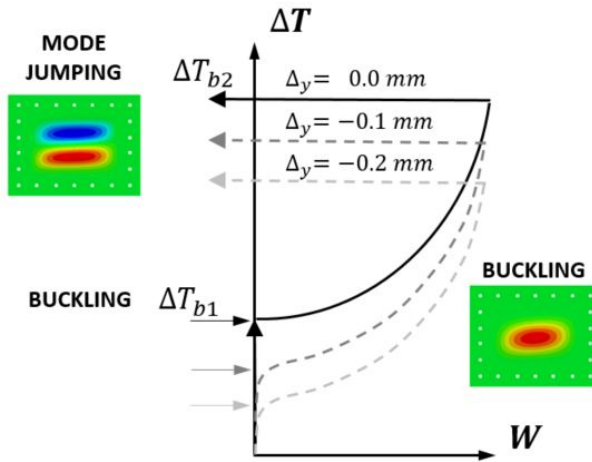


Figure 4.2: Mode jumping under thermal and mechanical loads.

If the plate is instead subjected to a “compression + heat” load case, a compressive Δ_y is first applied, and then a ΔT is gradually introduced. Buckling temperature ΔT_{b1} is expected to decrease with the magnitude of initial compression Δ_y [9]; this mechanical pre-load is expected to have also an impact over the mode jumping temperature ΔT_{b2} ,

typically a decrease, as shown in Fig. 4.2. However, the relation between the applied Δy and the obtained reduction of ΔT_{b2} is a priori unknown, and such phenomenon happens in the nonlinear regime where linear load superposition is not expected to hold.

When the plate is loaded under a “pure compression” load case, the plate deflections may describe a trajectory analogue to the “pure heating” case: buckling is reached at displacement Δy_{b1} , and a mode jump may occur at Δy_{b2} . Contrary to the “pure heating” load case, the orientation of the mode jump is strongly preconditioned by the direction of the compressive load: an initial (1, 1) buckling shape can be followed by a (1, 2) buckling shape, as the main compressive load comes from that direction. Preloads in the form of initial ΔT , in the “heat + compression” load case, are expected to reduce Δy_{b1} and Δy_{b2} . These deflection paths correspond to the behavior of a perfectly flat plate. In reality, plate imperfections are unavoidable and have a substantial effect over the overall plate behavior [8]. Real boundary conditions are also to be taken into consideration: the material of the boundary conditions may be sensitive to temperature changes, and thus experience size variations when subjected to a ΔT . This can have an impact on both buckling and mode jumping temperatures of the plate.

4.3. PRELIMINARY ANALYSIS: MODE JUMPING IN PLATES SUBJECTED TO THERMAL AND MECHANICAL LOADS.

Two different types of numerical procedures were conducted as preliminary analysis of the considered structure: a linear eigenvalue analysis and a dynamic explicit analysis.

Both types of simulation were performed using the same finite element (FE) model performed in Abaqus, shown in Fig. 4.1 (b). The model is a simplification of the proposed experimental configuration: the compression machine in the real test setup was not represented in the model; instead, only the plate and the frame were modelled. The FE model represents a plate of size 440 mm x 340 mm, made in composite material AS4/8552 with a ply thickness of 0.181 mm, fixed on a surrounding structural frame made in Invar 36. The frame and the plate have the same width and height of 440 mm x 340 mm; when they are assembled together, a smaller area of the plate with dimensions 300 mm x 200 mm remains accessible; this area corresponds to the region with width a and height b reported in Fig. 4.1 (b). The material properties are reported in Table 4.1. The plate has a stacking orientation [35/ - 35/10/ - 10]_s. This stacking was successfully used in previous experimental campaigns to reproduce thermal buckling and mode jumping in composite plates [8]. The FE model consists of standard quadrilateral shell elements S4R with a size of 5 mm. The elements of the plate and the frame have nodes at identical positions, and thus were tied together, therefore seamlessly connected, which means no slipping due to gripping loss nor effect of friction between frame and specimen were considered. Vertical displacements V in the lower contact surface of the frame were constrained; out-of-plane deflections W were constrained at both lateral edges. Load introduction was performed by enforcing Δy as vertical displacement V over the upper contact surface of the frame, and/or by enforcing ΔT in all nodes in the model.

For a given FE simulation, the corresponding load case is implemented by introducing the different loading phases as steps in the analysis. In a linear eigenvalue analysis,

Material	E_{11} [GPa]	E_{22} [GPa]	G_{12} [GPa]	ν_{12}	α_1 [$\frac{\mu m}{m^{\circ}C}$]	α_2 [$\frac{\mu m}{m^{\circ}C}$]	t_{ply} [mm]	ρ [kg/m ³]
AS4/8552	135	9.68	5.6	0.30	0.28	28.0	0.181	1.58
Invar 36		140		0.33		1.5		8.05

Table 4.1: Material properties.

the first load phase is introduced as a general static load step, and the second load phase is introduced in the form of an eigenvalue analysis over the preloaded structure. In a dynamic explicit analysis, loading phases are implemented as load steps where the load is introduced as loading ramps, with loading speeds of -0.05 mm/s and 3°C/s for compression and heating phases, respectively. These loading rates are significantly higher than the experimental counterparts, and were verified to decrease the analysis time without affecting the final result. An imperfection with the shape of the first eigenvalue analysis, with amplitude of 0.5% of plate thickness, was assumed. Such imperfection amplitude is comparatively small, and thus grants a behavior close to the perfectly flat plate.

The results of the eigenvalue analysis and the dynamic explicit analysis are reported in Fig. 4.3, where ΔT is plotted versus Δ_y . White and magenta colored markers indicate buckling and mode change bifurcations, respectively. Marker shape provides information about the loading condition operating at the moment of bifurcation: circular and triangular marker shapes denote compression and heat loading, respectively.

Considering a “pure compression” load case, the loading path starts at the origin and follows the horizontal axis till a bifurcation point is found at $\Delta_{y,b1} = -0.120 \text{ mm}$; this is reported in the graph with a white, circular marker at position $(-0.120 \text{ mm}, 0^{\circ}\text{C})$. Under “pure heating” conditions, the loading path overlaps with the vertical axis and buckling is reached at $\Delta T_{b1} = 43.81^{\circ}\text{C}$; reported over the vertical axis as a white triangular marker. The other white markers reported in the graph represent buckling results for combined load cases: for instance, when an initial load of $\Delta_y = -0.02 \text{ mm}$ is applied and temperature is increased, buckling is found for $\Delta T_{b1} = 36.68^{\circ}\text{C}$; the analysis is registered at position $(-0.02 \text{ mm}, 36.68^{\circ}\text{C})$ using a white marker with triangular shape, as buckling was reached under heating. In an analogous manner, if an initial $\Delta T = 10^{\circ}\text{C}$ is applied, buckling can be reached by applying $\Delta_{y,b1} = -0.093 \text{ mm}$. The reported buckling analysis results indicate a well-defined linear decrease of buckling temperature for increasing values of loading condition Δ_y , and the same tendency manifests when the order of load application is inverted. This is in accordance with the principle of load superposition, which holds in plate linear regime, making the order of load application not relevant until the buckling load. All presented eigenvalues correspond to a (1,1) buckling shape. It can also be noted that the regression curve divides the loading diagram in two areas, corresponding to buckled and unbuckled states.

Numerical predictions for the plate post-buckling behavior obtained by dynamic explicit analysis are presented in Fig. 4.4 (a) and (b), where two graphs for “compression + heating” and “heating + compression” load cases are reported. These graphs capture only the last loading phase. Curves for varying amounts of initial preload are reported. For instance, in Fig. 4.4 (a) the curve labeled as $\Delta_y = -0.08 \text{ mm}$ indicates a displace-

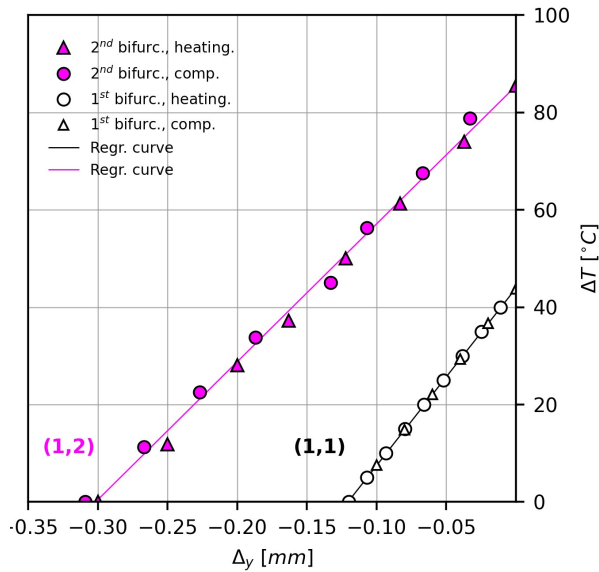


Figure 4.3: FE predictions: Buckling chart for combined loading.

ment of -0.08 mm previous to heating phase, while in Fig. 4.4 (b) the curve labeled as $\Delta T = 22.5^\circ\text{C}$ represents an initial heating phase of 22.5°C . Looking now at Fig. 4.4 (a), the “pure heating” case, labeled as $\Delta y = 0.000 \text{ mm}$, is the curve reaching the highest temperature. During heating phase, plate deflections are zero till a critical value of ΔT is reached and the plate starts deflecting out of plane. For a plate with no imperfections, the buckling temperature is close to the previously calculated linear eigenvalue, $\Delta T_{b1} = 43.81^\circ\text{C}$, plotted in Fig. 4.3 on the vertical axis. If temperature continues rising beyond ΔT_{b1} , deflection W starts growing under a (1, 1) buckling shape. When temperature reaches a value $\Delta T = 85.5^\circ\text{C}$, the plate experiences an abrupt mode jump into a (1, 2) buckling shape. The point of maximal deflection previous to the jump marks a change in slope in the curve, and is considered as the indicator of mode jump. The mode jump is registered in Fig. 4.4 (a) as a blue triangular marker over the ΔT vertical axis, and is also reported in Fig. 4.3 as a magenta circular marker at $(0.000 \text{ mm}, 85.5^\circ\text{C})$. For increasing values of compressive preload Δy , the deflection curves shift downwards and mode jumping temperatures decrease: an initial amount of preload $\Delta y = -0.040 \text{ mm}$ reduces the mode change temperature to $\Delta T_{b2} = 73.95^\circ\text{C}$. Looking now at the curve for $\Delta y = -0.120 \text{ mm}$, it can be noted that deflection W is already present at $\Delta T = 0.0^\circ\text{C}$: the Δy pre-load introduced during the compression phase is larger than the pure compression buckling load $\Delta y_{b1} = -0.120 \text{ mm}$, and thus buckling occurred during the first loading phase.

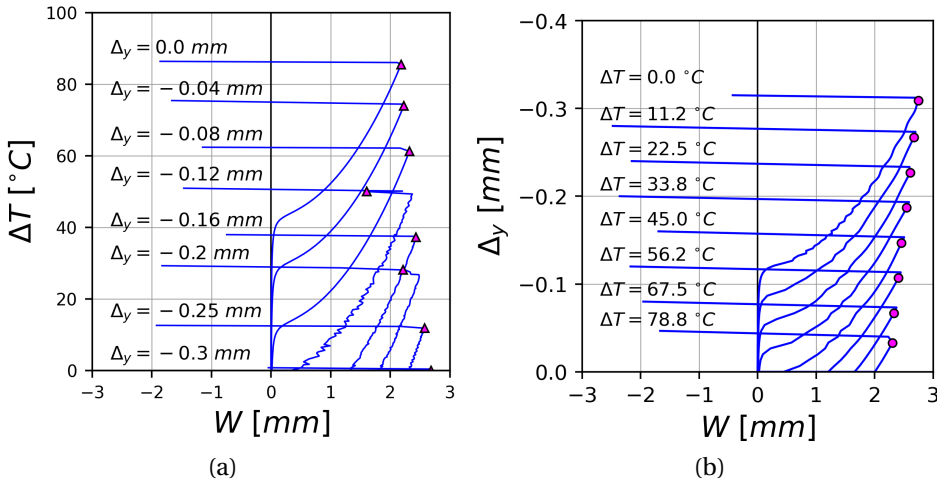


Figure 4.4: FE Load vs deflection curves: (a) Heating + Compression ; (b) Compression + Heating.

In an analogous manner, in Fig. 4.4 (b) the “pure compression” load case is labeled as $\Delta T = 0.0^\circ C$ and is the curve reaching the highest compressive values. At the beginning of the compression load phase, plate deflections are zero till a critical value of Δ_y is reached and out-of-plane deflections start increasing. $\Delta_{y,b1}$ is close to the ideal value for the perfect plate, given by previously calculated eigenvalue analysis $\Delta_{y,b1} = -0.120\text{ mm}$, plotted in Fig. 4.3 . If compression increases beyond $\Delta_{y,b1}$, deflections keep growing under a (1, 1) buckling shape, and, as previously seen for pure heating cases, when the compression reaches $\Delta_{y,b2}$, the plate experiences an abrupt mode jump, changing into a (1, 2) buckling shape. Mode jumps can be obtained under both "pure heating" and "pure compression" load cases. The point of maximal deflection W demarcates the mode transition. The mode jump is reported in Fig. 4.4 (b) as a magenta circular marker and is also reported in Fig. 4.3 at $(0.309\text{ mm}, 0.00^\circ C)$. For increasing values of pre-heating ΔT , mode jumps appear at lower temperature. For example, an initial amount of preload $\Delta T = 22.5^\circ C$ reduces the mode change compression to $\Delta_{y,b2} = -0.198\text{ mm}$. Observing now the curve for preload $\Delta T = 45.0^\circ C$, it can be noted that deflections W are already present at $\Delta_y = 0.000\text{ mm}$; this is because the Δ_y pre-load introduced during the compression phase is larger than the pure heating buckling temperature $\Delta T_{b1} = 43.81^\circ C$, and therefore buckling occurs during the first loading phase. Reporting this, Fig. 4.3 is populated of magenta, circular and triangular markers which seem to be distributed approximately along a line. Performing a least square linear regression over these values reveals a well-defined linear correlation between compressive preload and mode jumps. In particular, decreasing values of initial load Δ_y decrease ΔT_{b2} in “compression + heating” cases, while increasing values of initial load ΔT seems to reduce $\Delta_{y,b2}$ in “heating + compression” cases.

It is possible to note in Figs. 4.4 (a) and (b) that the first and second bifurcations may happen during different load phases, so representing only one load phase in the diagram may leave out valuable information.

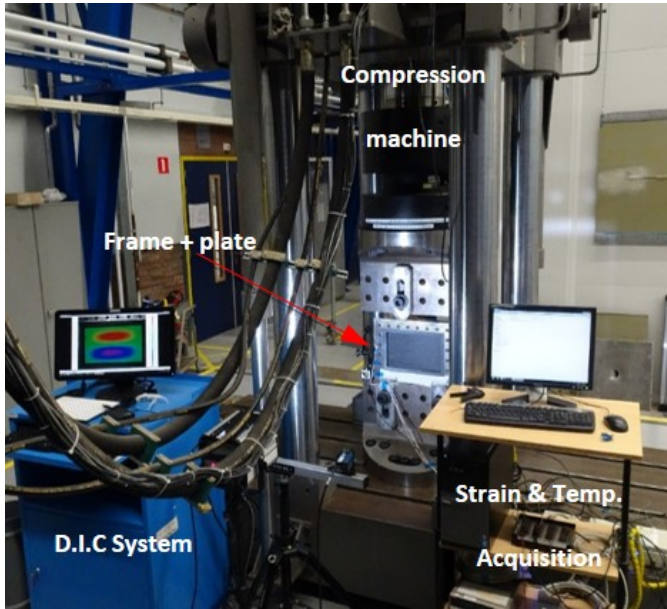
4.4. TEST SETUP

The main goal of the tests is studying the buckling and mode jumping of a plate that is subjected to combinations of compressive load and heat. The test setup is shown in Fig. 4.5. The composite plate is bolted to a frame. The frame is made in Invar 36 material [42] which has a low CTE, see properties in Table 1. Low CTE fittings are useful for two purposes: restraining thermal expansion of the plate and reducing the chances of non-uniform compression due to irregular thermal expansion.

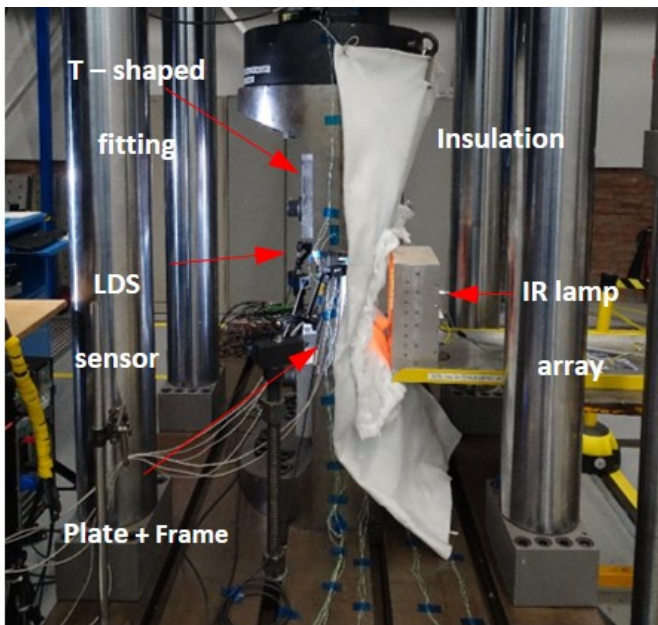
Prior to the testing, the composite plate is placed between the two symmetric parts of the frame. Originally, the plate and the frame have same length and width of 440 mm x 340 mm; when assembled, the exterior edge of the plate remains gripped by the frame, leaving an accessible inner region of 300 mm x 200 mm. The holes in both plate and frame are large enough to avoid contact of the bolts with the plate. The assembly is completed by following a cross- sequence to bolt the assembly in three levels up to the maximal level of 60 Nm. This torque guarantees uniform constraining of the plate in-plane displacements. The alignment of both frame parts was ensured by the use of alignment pins. The test setup is built in a compression machine, with a maximal compressive force of 3500 kN. The machine consists of a canopy structure in which four columns support a high-stiffness crosshead with adjustable height. The crosshead has an integrated load actuator and hydraulic manifold, which support the loading cylinder and a load transducer for force monitoring. The machine is equipped with an LVDT sensor that monitors the vertical displacements of the cylinder.

Six strain gauges were placed at six different positions, as shown in Fig. 4.6, to monitor longitudinal strain during compression tests. At positions 1 and 4, two strain gauges were placed at the front and back of the frame, labelled as “F” and “B”, respectively. The gauges were connected in a half-bridge, for self-compensation of temperature. Once installed in the frame, the tested plate acquired an inherent initial imperfection, caused by the gripping surfaces and the torquing operation.

The load transfer between compression machine and frame was done through two T-shaped stainless steel fittings: they were attached to the loading cylinder and to the base of the test machine, and the invar frame was placed in-between. The load introduction process is regulated by a fully automated computer system that allows for displacement-controlled loading. Additionally, two external laser LDS sensors were used to monitor the vertical displacement of the compression fitting to account for machine compliance during testing. The FE analysis had also the function to provide estimations of maximum expected loading Δ_y . It should be clarified that the low CTE of the frame makes it less sensitive to temperature changes. Ultimately, and because the plate is attached to the frame, almost the totality of the size variation in height b experimented by the plate is originated by the compression applied to the frame and not by thermal expansion caused by heating loads.



(a)



(b)

Figure 4.5: Test setup: (a) Front view; (b) Side view.

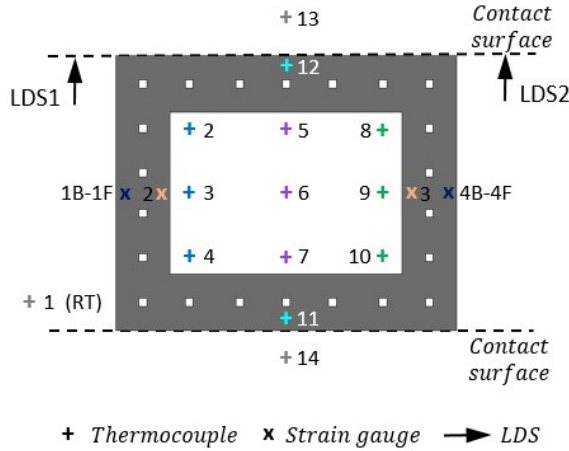


Figure 4.6: Test setup: sensor distribution

The source used to heat the plate was an IR lamp array, shown in Fig. 4.5 (b). It consists of eight lamps with a maximum power of 1000 W at 200 V. The lamps were used with a power source able to deliver 120 V and 50 A. The heat provided by the IR array was regulated by manually increasing the input power. The heat lamps were placed vertically, distributed in a 4 + 4 configuration in an attempt to achieve uniform heat distribution. Temperatures were monitored with "K" - type thermocouples in diverse positions of the setup: one measuring point for room temperature, nine measuring points on the plate, two on the T-shaped compression fittings, as reported in Fig. 4.6. Readings for thermocouples, strain gauges, LDS lasers and load cell were simultaneously acquired by a "Keythley" multimeter. Out of plane displacements were monitored using a DIC equipment from the brand Correlated Solutions, model Vic3D; two different sets of cameras were used, with 30 mm and 50 mm objective lenses. In Fig. 4.5(a) it can be observed the uniform speckle distribution of white dots over black background that was applied on the plate. In order to protect the LSD laser sensors from the heat radiated by the lamps, a layer of aluminum wool was used, as shown in Fig 4.5 (b).

For the implementation of the four described load cases, four different testing protocols were followed. During the "pure compression" tests, the vertical position of the T-shaped adaptor was set to enter in contact with the frame, and the Y position of the machine was set to zero. Then, a displacement of $\Delta_y = -0.4 \text{ mm}$ was enforced to the frame. This was done along a period of 3 minutes, during which the strains in the frame were monitored, as shown in Fig. 4.7 (a) where strains are plotted versus reaction force in the compression machine. Once reached, the maximal load is maintained for 30 seconds and after that gradually released. These data are used to ensure compression uniformity in the frame. Finite element simulations have also been included in the plot. It can be observed that compression is not fully uniform, as gauges 1F and 1B deliver

slightly larger strains than gauges $4F$ and $4B$. An approximate difference of $60 \mu\epsilon$ between left and right sides is captured in the gauges at almost all loading states. Even though attempts were made to solve this issue, it could not be improved due to the limited adaptability of the compression head of the loading machine. This alignment error is percentage-wise larger at low compression levels, while it is smaller when the load increases. It needs to be noted that the test setup is an approximation of an ideal condition: during the experiments, plate height experiences a shortening while plate length remains constant. In reality, the compressed elements of the frame experience a small sideways deflection: the columns experience a small lateral arching deflection, which was never larger than 0.04 mm at maximal compressive $\Delta_{y,max} = 0.4 \text{ mm}$, that means, 10% of the maximal compressive $\Delta_{y,max}$. It can therefore be assumed that the effect of lateral distortion, even if present, is not dominant in the experiment.

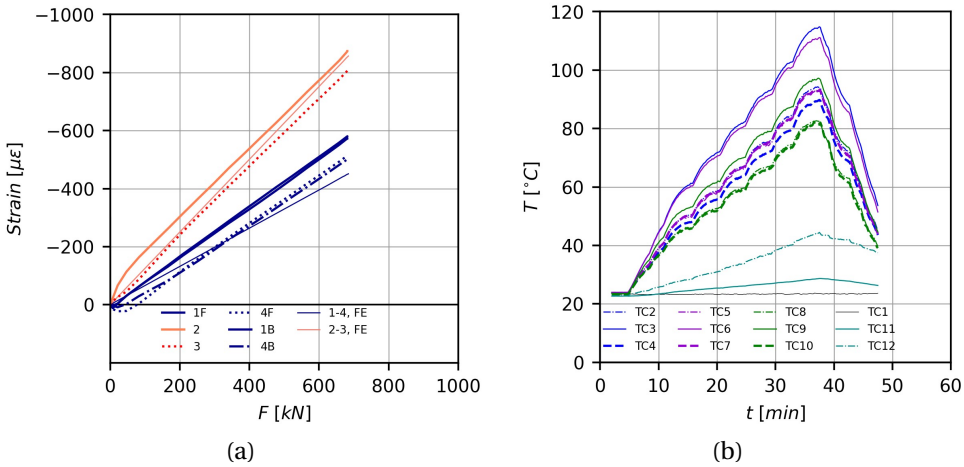


Figure 4.7: Example of sensor measurements: (a) Strain gauges in pure compression test; (b) Thermocouples in pure heating test.

Prior to a “pure heating” test, the T-shaped adaptor is set in contact with the frame as in the “pure compression” case, and is kept at a fixed position for the duration of the test. Once this is done, the IR lamp array is turned on, and the heating of the plate starts. This operation is performed manually, at a speed of approximately $3^\circ\text{C}/\text{min}$. Once the goal temperature is reached, the lamps are turned off and the whole setup is let to cool down. In Fig. 4.7 (b), measurements of the thermocouples are reported. From the data collected for sensors $TC2$ to $TC10$, on the plate, a large dispersion can be observed, reaching these up to 30°C at large temperatures. Attempts were made to solve the issue of the temperature non-uniformity in the plate by changing the distribution of the heat lamps, however, no improvement was achieved. It can be appreciated from the sensors $TC11$ and $TC12$ that there is a temperature gradient within the invar frame itself of approximately 23°C ; but due to its low CTE the effects of this variation are non-significant. Temperatures for thermocouples $TC13$ and $TC14$, placed at the T-shaped

fittings, are indistinguishable from the $TC1$, measuring room temperature, and are not reported in the graph.

The procedures followed for “compression + heating” and “heating + compression” tests keep the essence of the procedures. In the “compression + heating”, the compression head is first adjusted to the frame, and the vertical position is set to zero. Once preload Δ_y is applied, the heat lamp array is turned on and heat is gradually applied to the specimen. When the pre-fixed goal temperature is reached, the lamps are turned off and the specimen is unloaded. Conversely, during “heating + compression”, the position of the compression is set to zero, then heat is applied, and after a goal ΔT is reached, a fixed Δ_y compression phase, similar to the one in the “pure compression” test.

4.5. EXPERIMENTAL RESULTS

4

A total of 22 tests were conducted and a few examples of typical results for each type of performed tests are reported. Due to asymmetries in the obtained buckling shapes, it was found convenient to monitor out-of-plane displacements W at three plate positions, referred as $P0$, $P1$ and $P2$: position $P0$ corresponds to the plate center, with coordinates $(a/2, b/2)$, and positions $P1$ and $P2$ are placed over the vertical symmetry axis of the plate, at positions $(a/2, 3b/4)$ and $(a/2, b/4)$, respectively. The graphical notation for depicting each position is the same for all experiments: deflections at $P0$ or plate center are represented by a bold continuous gray curve, while curves for points $P1$ and $P2$ are reported as dashed and dash-dotted gray bold lines, respectively.

4.5.1. PURE HEATING AND PURE COMPRESSION LOAD CASES

Results of “pure heating” and “pure compression” loading tests are represented in Fig. 4.8 (a) and (b). These are reported as graphs representing applied ΔT versus W and applied Δ_y versus W , respectively. Finite element simulations for both loading cases are also represented in the graphs. Regression curves and cross-shaped markers present in both figures are used for the extraction of buckling loads, and are discussed later in this section. Plots for both experimental and numerical deflection shapes are reported in Fig. 4.9.

For the “pure heating” tests, the observed behavior is in line with the numerical simulations: when ΔT is gradually applied, the plate remains flat up to the point where the buckling temperature is reached; beyond that point, the plate starts deflecting out of plane, in a (1, 1) buckling shape. Out of plane deflections W have negative values, which means that the plate moves towards the heat source. Deflections W continue growing, occurring the largest plate deflections approximately at the plate center.

The obtained buckling shape is not fully symmetric, as position $P1$ reaches much larger deflections than its counterpart $P2$; however, a (1, 1) mode is clearly predominant, as seen in Fig. 4.9 (a). If ΔT keeps increasing, the current buckling shape abruptly changes its shape into a (1, 2) buckling mode at around $\Delta T_{b2} = 80.0^\circ C$. At that moment, deflections at $P0$ shift towards zero, as this point changes from having nearly maximal plate deflections to be in the proximity of a nodal line of the new buckling shape with almost zero deflections. Plate behavior is comparable to numerical predictions, even

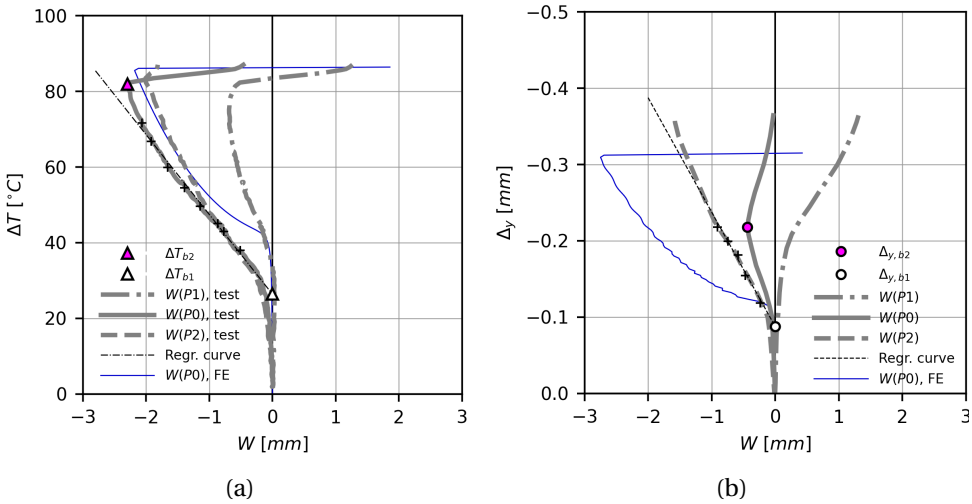


Figure 4.8: Test results: (a) Pure heating case ; (b) Pure compression case.

though buckling happened much earlier than the predicted $\Delta T_{b1} = 43.81^{\circ}\text{C}$, and the numerical mode jump happened at $\Delta T_{b2} = 85.81^{\circ}\text{C}$. FE predicted deflection shapes deliver reasonably well with experimental results, as shown in Fig. 4.9 (a).

For the “pure compression” test, differences can be noted with respect to the heating case. When compression loads were applied, plate displacements slowly increased up to a point where they started growing faster and the plate could be considered as buckled. Maximal deflections were not reached at the plate center, but at both $P1$ and $P2$ positions, as shown in Fig. 4.9 (b). The asymmetry of the initial buckling shape was much more pronounced than in pure heating tests. Out-of-plane displacements started happening much earlier at $P2$, than at $P1$ or at the plate center $P0$. The obtained buckling shape resembles a (1, 2) mode where one of the half-waves is much larger than the other. This is consistent with previously shown results for pure heating tests, where $P2$ deflections were consistently much larger than at its symmetric counterpart $P1$. When load kept increasing, deflections at $P0$ and $P2$ kept growing up to a point where $P0$ finds a maximum value; after that point, deflection in the plate center started decreasing till it went to zero, and deflections at $P1$ started to grow, gradually shifting into a fully developed (1, 2) mode. Also, clear differences can be observed with the numerical simulation: even if the simulation appears to capture well the buckling onset, the test showed a progressive transition into (1, 2) mode rather than an abrupt, dynamic mode jump.

Even though pure heating and pure compression tests showed clear differences in their buckling shapes, there are similarities between them. For both experiments, the half-wave showing maximal deflections at buckling is not in the center of the plate, but rather displaced towards plate position $P2$.

Choosing criteria for the identification of bifurcation points is a challenging task. For comparability, these criteria need to be applicable to all four types of performed tests.

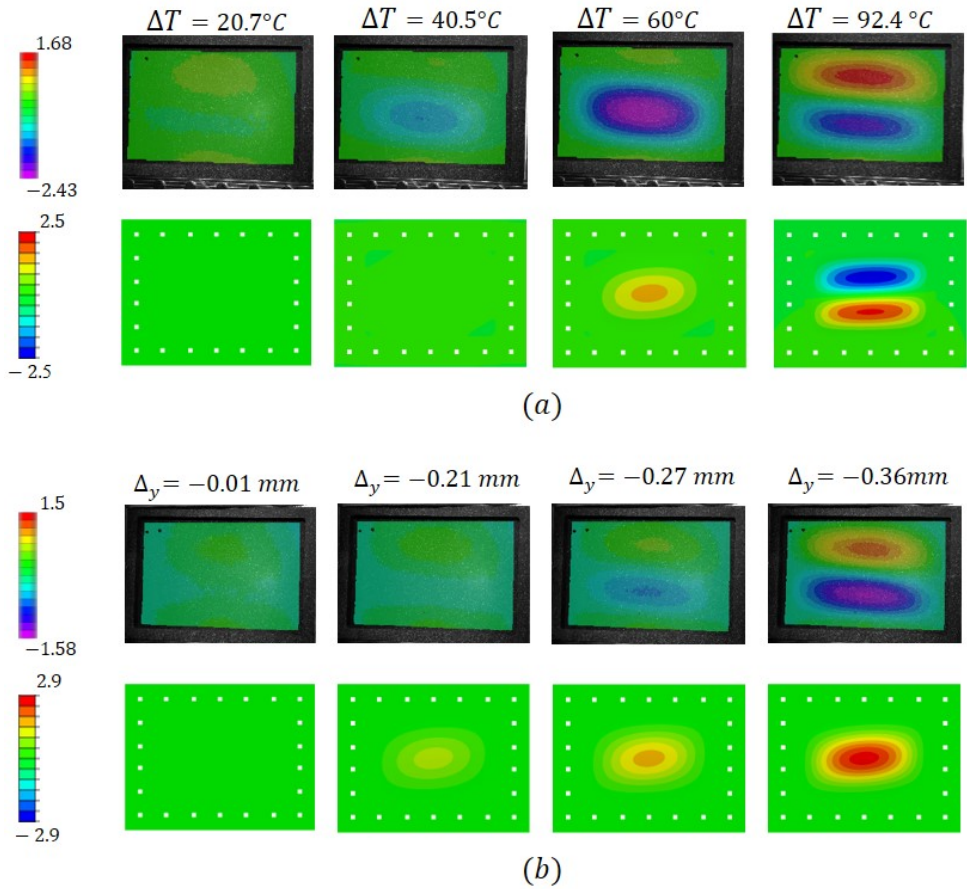


Figure 4.9: Experimental and numerical deflection shapes: Pure heating; (b) Pure compression.

First, defining buckling in a plate is not a evident occurrence, as plates do not show a clear behavior at buckling onset. A classical way to perform this operation is using so-called “direct” methods [43], where the critical buckling load is extracted from a test output curve such as “load versus out-of-plane deflection” or “load versus strain”. The buckling load can be then determined in two ways: automatically assigning buckling to a recognizable point in the curve, such as a slope or a curvature change, or performing a fitting curve/regression curve over points in the stable post-buckling region. The buckling load is then assigned to the intersection of this regression curve with the load vertical axis.

Regarding the identification of a mode jump, it can be easier when it happens suddenly, such as in a typical pure heating test, while it can be more unclear when it happens gradually, as in a pure compression test. Methods available in literature involve monitoring plate strains at certain plate positions, using back-to-back strain gauges, but due to

the chosen sensor layout this methodology cannot be applied.

Thus, two methodologies for the identification of bifurcations are here presented. For the extraction of buckling bifurcation points, a method referred as “load vs. displacement” is used: from the three deflection curves at $P0 - P1 - P2$ positions, the one showing highest deflections is selected; points from the deep post-buckling are chosen and then a least-square linear fitting is performed over them. The plate is considered buckled at the load value at which the regression line intersects the vertical axis. An example can be seen in Fig. 4.8 (a) and (b), where selected points are reported as black markers with a “+” shape. These points should be located at the stable post-buckling range and at a loading state inferior to the second bifurcation load, as curve stiffness varies after mode change. For instance, in Fig. 4.8 (a) the method is applied on the curve $P0$ yielding $\Delta T_{b1} = 27^\circ C$, while in Fig. 4.8 (b) the method is applied at $P1$ and yields a $\Delta_{y,b1} = -0.093 \text{ mm}$. The obtained bifurcation points are registered in Fig. 4.8 (a) and (b) as white markers, with triangular shape for the “pure heating” test, and circular shape for the “pure compression” test.

For the extraction of mode jump bifurcations, a method referred as “slope vs. displacement” is proposed. This method relies on the fact that during the test, deflections W at plate center increase till the moment when a mode change happens, and then they go back to zero, as position $P0$ is close to a nodal position in the new (1,2) buckling configuration. The point of maximal W , that marks a change in slope sign, is used here to mark the transition into the (1,2) mode. This transition may either be sudden, such as in Fig. 4.8 (a), or a gradual change, as in Fig. 4.8 (b). The result of applying this methods yields $\Delta T_{b2} = 82^\circ C$ for the “pure heating” case, and $\Delta_{y,b2} = -0.220 \text{ mm}$ for the “pure compression” case. These new bifurcation points are reported in Fig. 4.8 (a) and (b) as magenta colored markers, with either circular or triangular shape depending on loading condition acting at the moment of bifurcation.

For any performed test, either pure or combined, the obtained bifurcation points can be documented in an overview chart such as Fig. 4.10, where load condition ΔT is plotted versus applied Δ_y . Fig. 4.10 contains an overview of all experiments performed in this campaign: two clouds of colored markers are reported, corresponding to buckling and mode jumping bifurcations. For the tests presented in this section, only one load type was applied, and therefore their bifurcation points lay approximately along the axis lines, i.e. X axis for pure compression and Y axis for pure heating tests, respectively. Thus, for the pure compression test, two bifurcation points, labeled as $PC01$ are reported at $(-0.091 \text{ mm}, 0.0^\circ C)$ and $(-0.220 \text{ mm}, 0.0^\circ C)$, and are reported as white and magenta circular markers. In the same way, for the pure heating test two triangular, white and magenta colored markers labeled as $PH01$ are registered at locations $(0.000 \text{ mm}, 27.0^\circ C)$ and $(0.000 \text{ mm}, 82.0^\circ C)$.

4.5.2. COMBINED LOAD CASES

Fig. 4.11 (a) and (b) represent two examples of “compression + heating” combined test. Each graph is divided in two halves where the lower and upper parts represent the first and second loading phases, respectively. The plate deflections at the end of the first load phase are the initial deflections for the second load phase. It can be observed how the test in Fig. 4.11 (a) begins with an initial compression load of $\Delta_y = -0.028 \text{ mm}$, while the

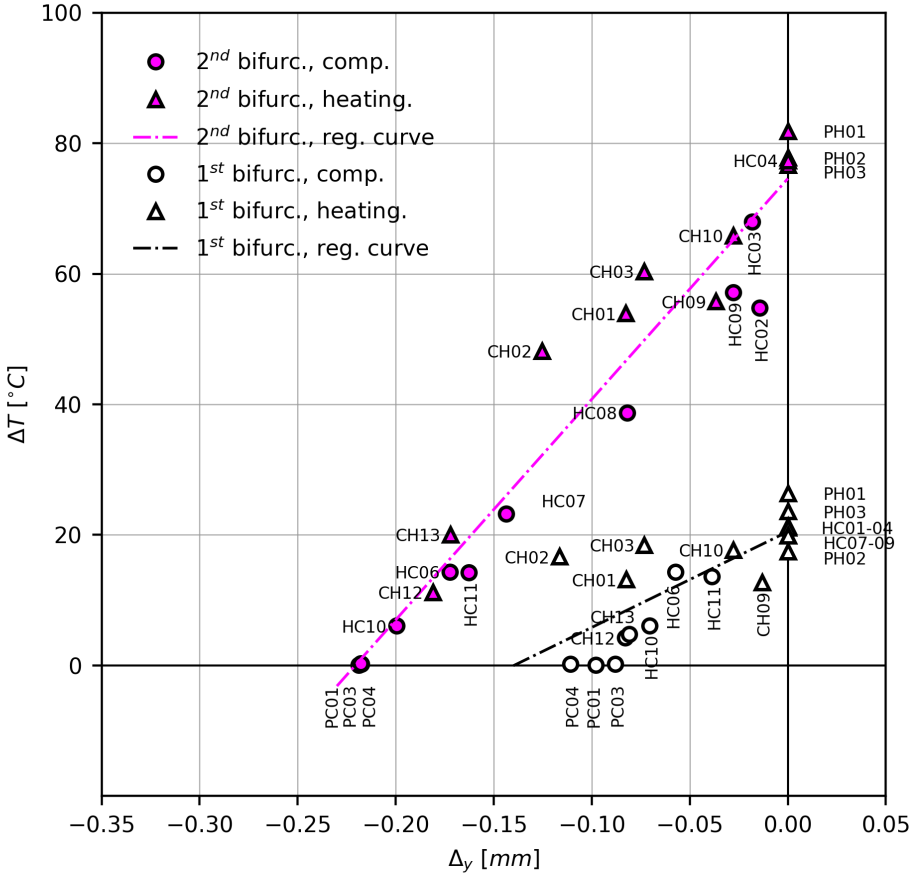
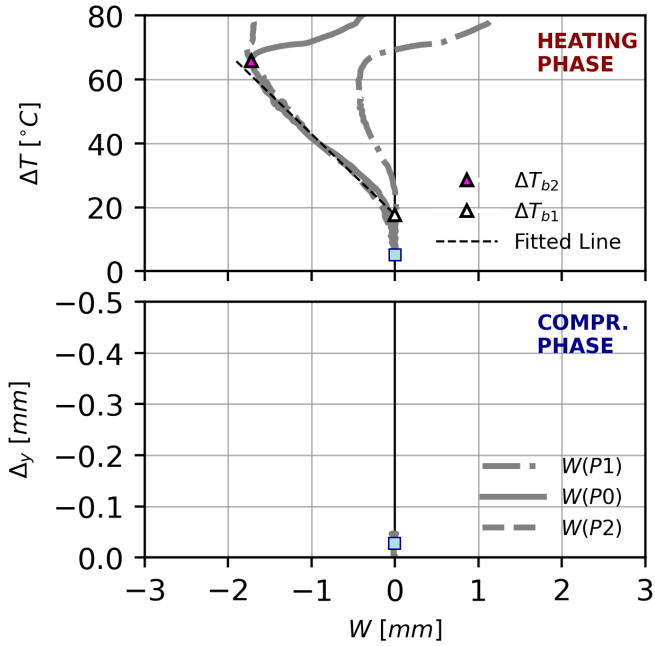
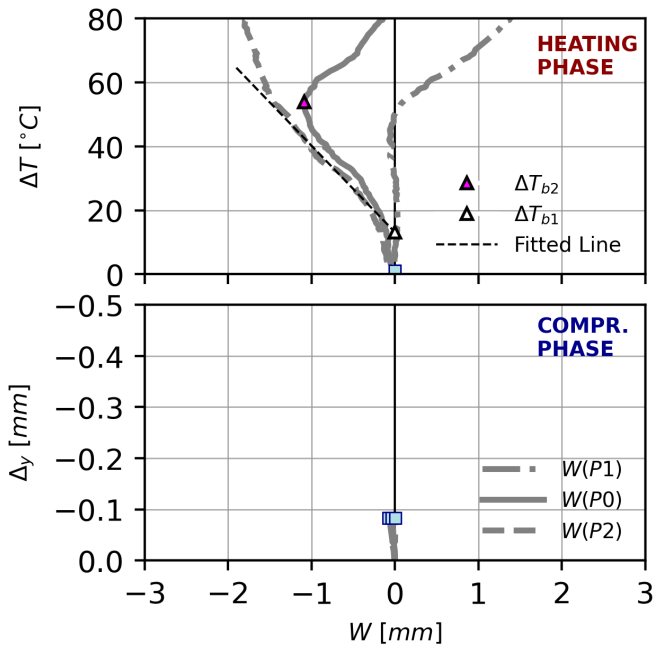


Figure 4.10: Experimental buckling chart.

preload in Fig. 4.11 (b) is equal to $\Delta y = -0.0821 \text{ mm}$. Once the entire compression load is applied, the lamps are turned on and the plate is heated up to $\Delta T = 80.00^\circ \text{C}$ in both cases.



(a)



(b)

Figure 4.11: Test results for "Compression + Heating" case: (a) $\Delta y = -0.028$ mm; (b) $\Delta y = -0.081$ mm

It can be seen that for both tests, the plate remained flat during the compression phase and started deflecting during the heating phase. Thus, buckling and mode change bifurcations take place during the heating phase and the corresponding markers are located in the upper half of the diagram. For the first test, which results are reported in Fig. 4.11 (a), $\Delta T_{b1} = 17.69^\circ\text{C}$ is found, while lower $\Delta T_{b1} = 13.1^\circ\text{C}$ is found for the second test, recorded in Fig. 4.11 (b). Values of $\Delta T_{b2} = 65.8^\circ\text{C}$ and $\Delta T_{b2} = 53.9^\circ\text{C}$ are found, respectively. Plate deflections show a clear resemblance with pure heating tests. The effect of preload is evident as ΔT_{b1} and ΔT_{b2} have decreased with respect to the pure heating test. This tendency becomes more evident for increasing values of preload Δ_y . The maximal deflections W decrease with Δ_y , and the trajectories followed by the three control points $P0$, $P1$ and $P2$ come to resemble more those observed in “pure compression” cases.

In Fig. 4.12 (a) - (d), four examples of “Heating + Compression” experiments are reported. These four experiments were performed sequentially. In all of them the same procedure was followed: First, the plate is heated up to a given temperature, reaching a loading state $(0, \Delta T)$; this process is from now on referred as “heating phase”. Second, a compression load Δ_y is applied on top, reaching a loading state $(\Delta_y, \Delta T)$; after that, the load Δ_y is retired, returning to loading state $(0, \Delta T)$; the operation of applying and removing Δ_y is referred as “compression phase”. Subsequently, the plate is heated to a higher value of ΔT and the compression procedure is repeated. It was found that independent of the amount of preload ΔT , in every case, the plate returned to the buckling configuration before the compression Δ_y was applied. This occurrence was found to be consistent and repeatable. The starting ΔT of these compression phases can be identified at the lower part of graphs while the evolution of the plate deflections can be followed in the upper part. It can also be seen that the initial deflections for each one of these compression phases increases with the applied ΔT . DIC deflection shapes are reported in Fig. 4.13 for each one of these compression phases.

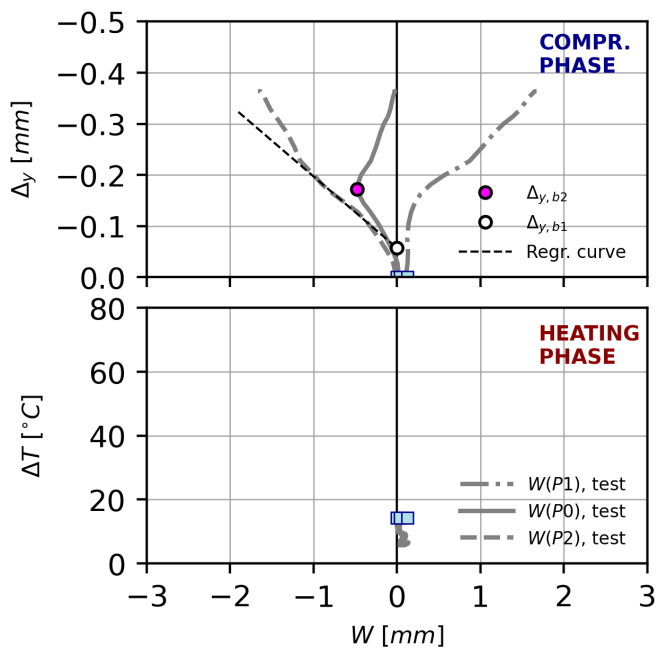
The first compression phase is documented in Fig. 4.12 (a) and in the upper row of images in Fig. 4.13. First, temperature is increased and stabilized at $\Delta T = 14.3^\circ\text{C}$, and then a compression phase is applied. The starting point of the compression phase is registered in the bottom part of the graph as a blue square dot. The compression phase can be followed in the upper part of the graph, where deflections continue to grow for increasing values of loading condition Δ_y . During this loading phase the plate finds both buckling and mode change bifurcations, registered in the graph as white and magenta circular markers at $\Delta_{y,b1} = -0.057\text{ mm}$ and $\Delta_{y,b2} = -0.172\text{ mm}$. In Fig. 4.13, obtained deflections shapes show how at $\Delta_y = -0.100\text{ mm}$ a mild (1,2) mode is present, while at $\Delta_y = -0.175\text{ mm}$, a (1,2) shape can be appreciated and at $\Delta_y = -0.300\text{ mm}$ a fully developed (1,2) mode is clearly identifiable. The two obtained bifurcation points are then registered in Fig. 4.10 at positions $(-0.057\text{ mm}, 14.3^\circ\text{C})$ and $(-0.172\text{ mm}, 14.3^\circ\text{C})$ respectively, both of them labeled as *HC06*. As both bifurcations happen during the same loading phase, both points are located over the same isothermal line. Once the load Δ_y is retired, the plate returns to its initial (1,1) shape.

For the second compression test, the heating phase is documented in Fig. 4.12 (b) and in the second row of images in Fig. 4.13. Prior to compression, the temperature is first risen from $\Delta T = 14.3^\circ\text{C}$ up to $\Delta T = 23.23^\circ\text{C}$, and then a new compression phase is applied. The first bifurcation is reached during the new heating phase, at $\Delta T_{b1} = 12.15^\circ\text{C}$, and it is reported in the lower part of the figure as a triangular white marker. However, there are still not enough points in the post-buckling region and this prediction is still unreliable. The second bifurcation is reached during the compression phase at $\Delta_{y,b2} = -0.144\text{ mm}$, and it is registered as a magenta circular marker in the upper part of the diagram. DIC plots at Fig. 4.13 show how for temperature values of $\Delta T = 23.23^\circ\text{C}$, mild deflections are already present for $\Delta_y = -0.010\text{ mm}$, and how the switch into a (1,2) shape starts happening already at $\Delta_y = -0.100\text{ mm}$. The effect of the initial ΔT manifests in the earlier occurrence of bifurcation points. Second bifurcation point is also registered in the buckling chart in Fig. 4.10, at position $(-0.144\text{ mm}, 23.23^\circ\text{C})$ labeled as *HC07* with a magenta circular marker. After the load decreases, the plate returns back to (1,1) mode.

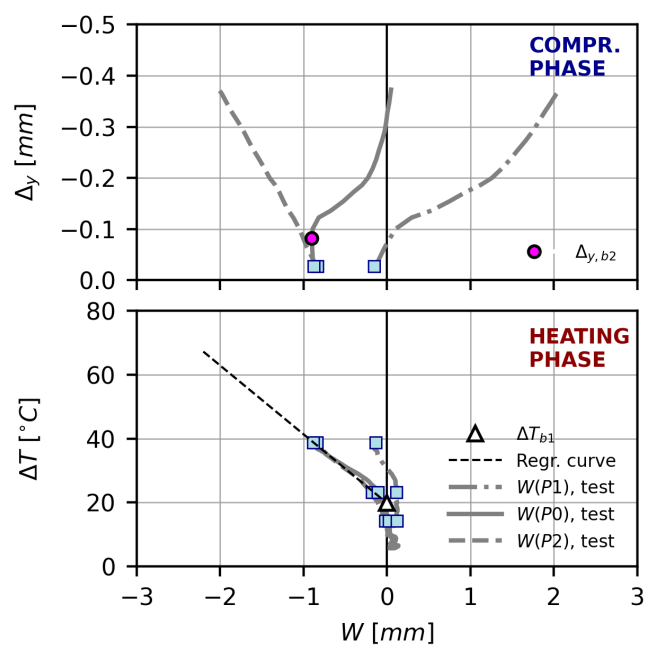
Results for the third compression phase are reported in Fig. 4.12 (c) and in the third row of Fig. 4.13. The compression cycle is performed after temperature is increased from $\Delta T = 23.23^\circ\text{C}$ to $\Delta T = 38.54^\circ\text{C}$. A linear regression can now yield much more reliable results for buckling. Indeed, the regression yields a ΔT_{b1} equal to 19.85°C . Mode change is reached under compression at $\Delta_{y,b2} = -0.082\text{ mm}$, and is then registered in Fig. 4.10 at position $(-0.082\text{ mm}, 38.71^\circ\text{C})$, labeled as *HC08*. In the DIC plots it can be seen that the mode change happens at even smaller values than at previous compression phases.

For the fourth and last compression phase results are reported in Fig. 4.12 (d) and in the fourth row of DIC images in Fig. 4.13. It can be observed that the buckling shape for $\Delta_y = -0.010\text{ mm}$ is a fully developed (1,1) mode with the crest peak slightly off the plate center. As soon as compression phase starts, deflections at point *P0* start decreasing very fast, instead of decreasing gradually like in previous compression phases. Then, the plate remains at a (1,2) mode shape indefinitely as long as ΔT is maintained. The second bifurcation is then assigned to $(-0.028\text{ mm}, 57.12^\circ\text{C})$, reported in Fig. 4.10 as *HC09*.

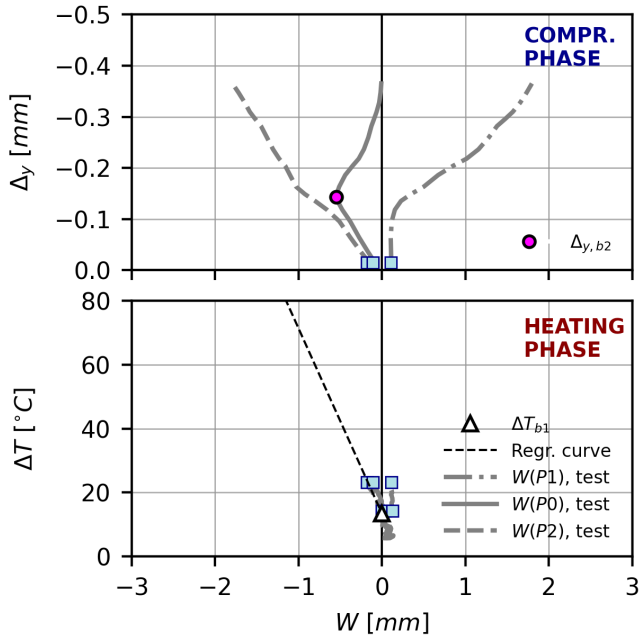
An overview of all performed experiments can be observed in Fig. 4.10, where two clouds of colored markers are reported, corresponding to buckling and mode jumping bifurcations. Linear regressions for both point clouds, performed using the “least squares” procedure, are reported as dot-dashed lines in the graph. A Pearson correlation for both point clouds yields *R* factors of 0.793 for the buckling bifurcation cloud points and 0.967 for the cloud of mode jumping points. It can be concluded that linear relation between Δ_y and ΔT is well defined for buckling bifurcation and very good for the mode change bifurcations. These lines confirm the tendencies predicted by the numerical analysis, also for the mode change bifurcations. For pure heating and pure compression cases, the dispersion among bifurcation points is larger for buckling than for the mode jumping temperatures. The bifurcation points reached under compression are mostly below their corresponding regression lines, while bifurcation points reached under heating are mostly placed above them. Besides, buckling values show large dispersions for all tested load combinations, while for mode jumping large dispersion happens at large temperatures and decreases almost totally for pure compression cases. It is believed this occurrence is caused by the gradients in the plate at high temperatures, documented in Fig. 4.7 (b).



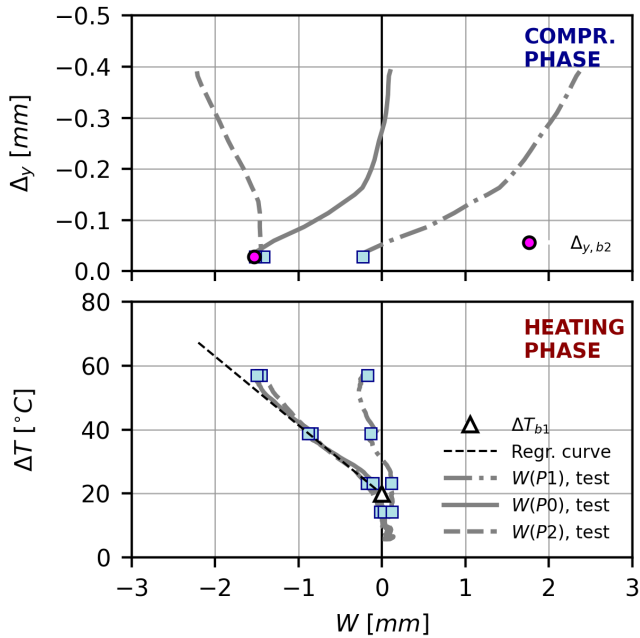
(a)



(c)



(b)



(d)

Figure 4.12: Test results for “Heating + Compression” cases: $\Delta T = 14.3^\circ\text{C}$; (b) $\Delta T = 23.1^\circ\text{C}$; (c) $\Delta T = 38.5^\circ\text{C}$; (d) $\Delta T = 56.9^\circ\text{C}$.

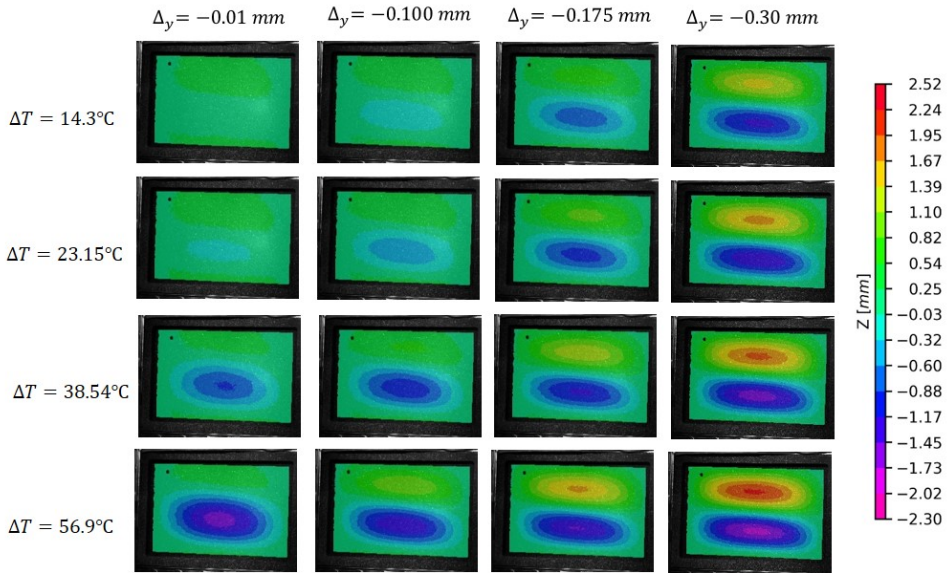


Figure 4.13: Experimental deflection shapes under combined loading.

In Fig. 4.14, experimental regression lines are plotted against numerical predictions: two lines representing the regression curves from FE simulations are reported as thin continuous lines, while experimental regressions are represented as dot-dashed lines. Large differences on the magnitude of the buckling loads can be observed: all experimental values are significantly lower than their numerical counterparts. In the pure compression, predictions appear to underestimate compression buckling loads, while in pure heating predictions appear to overestimate them. For mode jumping values, FE simulations are consistently higher than their experimental counterparts, being the differences larger for values with a higher compressive component.

One of the principal sources of discrepancy with the behavior of the ideal plate in any buckling test are the initial imperfections. In Fig. 4.15, a plot of a typical imperfection shape measured during the test campaign is reported; this imperfection shape was found to be consistent throughout all reported tests. The reported imperfection had one fully developed half-wave in the upper half of the specimen, while in the lower half, a second half-wave and a partially developed third half-wave along the Y axis can be appreciated; also, it can be perceived how there is a large area the upper left and right corners of the specimen which has a negative value, while in the center of that upper horizontal edge is positive: it would appear that the upper horizontal edge of the plate was slightly bent outwards. The maximal amplitude of the imperfection had a maximal amplitude of 20% of plate thickness, however the shape was highly distorted. Such initial shape would explain the consistent tendency in compression dominated tests to almost

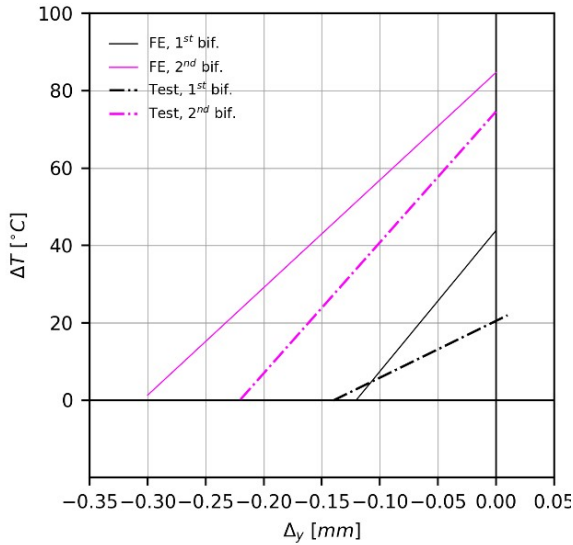


Figure 4.14: Comparison between experimental results and numerical predictions.

skip the (1, 1) buckling shape and go directly into a (1, 2) shape. This sort of imperfection could have been originated during the assembly operation of the frame: torquing the frame could yield an initial out-of-plane deformation due to the squeezing of the plate and derivate Poisson's transverse effects, or due to irregular application of torque. Initial imperfections, however, are only one of the multiple reasons for divergence. Differences between experimental results and numerical predictions could have been originated by multiple sources: variability of material properties, change of material properties due to heating, plate geometrical imperfections, irregular torquing of the frame, asymmetries in load distribution due to non-perfectly straight boundary conditions, overstretching of bolts during compression phases, through-thickness temperature gradients and non-uniform in-plane temperature distributions, differences in temperatures between frame and specimen. Residual stresses due to the curing process are assumed to be present, however their contribution is not expected to be significant. In equal manner, the effect of moisture was also not included in the FE model, since it they become relevant when composite parts have been subjected to humidity rich environments for a sustained period of time. The quality of the predictions could be improved by separately tacking any of these potential discrepancy sources.

Even though the setup can certainly benefit from refinement in some aspects of its design, such as compression uniformity or improvement in temperature distributions, insight about the interaction of mechanical and thermal loads was gained. Several phenomena were successfully captured experimentally: decreases in both buckling and

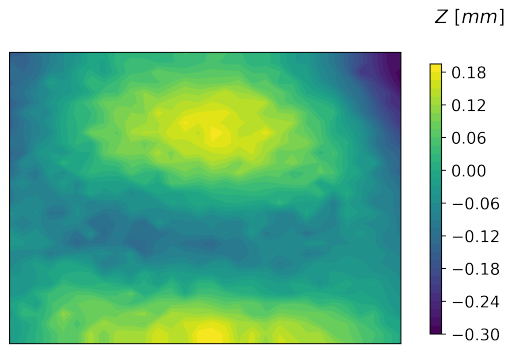


Figure 4.15: Measurement of initial imperfections in the plate.

4

mode jumping loads were successfully captured for different amounts of pre-load; and it was also found that in “heat + compression” load cases, the mode jump was reversible once the mechanical load decreased. This experimental work contributes to expand previous gained experimental knowledge about mode jumps in heated composite plates [8]. Better understanding on the appearance of mode jumps plates under heat and compression could be valuable knowledge for future designs when considering aerospace components operating in thermomechanical post-buckling regime, as well as for future research fields such as morphing, as mode jumps in composite plates could potentially be used as a source for shape change.

4.6. CONCLUSIONS

During this research, the buckling and mode jumping behavior of thermally and mechanically loaded composite plates was studied. A novel experimental setup for combined tests was proposed. The setup is conceived around a frame with a low coefficient of thermal expansion, so that the plate can experience buckling and mode jumping when heated, and also when subjected to mechanical load by compressing the frame. Experimental results were delivered as load vs out-of-plane deflection graphs, deflection plots and an overview buckling chart in the form of temperature variation ΔT vs. displacement Δy . Even if there are differences between experimental results and numerical predictions, the finite element analysis managed to anticipate the most critical trends. Reported data appear to confirm a linear relation between the two loading conditions ΔT and Δy for the mode jumping bifurcations. However, for the occurrence of buckling the same linear tendency could not be confirmed, even if the results are encouraging of the existence of such trend. Potential sources of difference between numerical and experimental data are the variability of plate geometrical imperfections, irregularity in temperature distributions and potential changes in material properties. These experimental results are still, however, preliminary, and should be seen as a proof of concept.

It is expected this research to contribute to the extension of the operative range of composite panels into the thermomechanical post-buckling regime, as well as open the door for potential passive, heat/compression-triggered shape change of aircraft composite thin structures.

BIBLIOGRAPHY

- [1] J. Williams and M. Stein, “Buckling behavior and structural efficiency of open-section stiffened composite compression panels”, in *17th Structures, Structural Dynamics, and Materials Conference*, vol. 14, Reston, Virginia: American Institute of Aeronautics and Astronautics, May 1976, pp. 1618–1626. DOI: [10.2514/6.1976-1727](https://doi.org/10.2514/6.1976-1727). [Online]. Available: <https://arc.aiaa.org/doi/10.2514/6.1976-1727>.
- [2] S. Y. Kuo, “Flutter of thermally buckled angle-ply laminates with variable fiber spacing”, *Composites Part B: Engineering*, vol. 95, pp. 240–251, 2016, ISSN: 13598368. DOI: [10.1016/j.compositesb.2016.04.009](https://doi.org/10.1016/j.compositesb.2016.04.009).
- [3] W. Ko, “Thermal analysis stiffened and mechanical buckling of hypersonic aircraft panels with varying hat-face sheet geometry and fiber orientation”, *NASA Technical Memorandum 4770*, 1996. [Online]. Available: <https://ntrs.nasa.gov/citations/19970005336>.
- [4] J. Lee and M. Bhatia, “Impact of corrugations on bifurcation and thermoelastic responses of hat-stiffened panels”, *Thin-Walled Structures*, vol. 140, no. October 2018, pp. 209–221, Jul. 2019, ISSN: 02638231. DOI: [10.1016/j.tws.2019.03.027](https://doi.org/10.1016/j.tws.2019.03.027). [Online]. Available: <https://linkinghub.elsevier.com/retrieve/pii/S0263823118311273%20https://doi.org/10.1016/j.tws.2019.03.027>.
- [5] P. M. Reis, “A perspective on the revival of structural (in) stability with novel opportunities for function: from buckliphobia to buckliphilia”, *Journal of Applied Mechanics*, vol. 82, no. 11, Nov. 2015, ISSN: 0021-8936. DOI: [10.1115/1.4031456](https://doi.org/10.1115/1.4031456). [Online]. Available: <https://asmedigitalcollection.asme.org/appliedmechanics/article/doi/10.1115/1.4031456/474193/A-Perspective-on-the-Revival-of-Structural>.
- [6] N. Hu and R. Burgueño, “Buckling-induced smart applications: recent advances and trends”, *Smart Materials and Structures*, vol. 24, no. 6, p. 063001, Jun. 2015, ISSN: 0964-1726. DOI: [10.1088/0964-1726/24/6/063001](https://doi.org/10.1088/0964-1726/24/6/063001). [Online]. Available: <http://dx.doi.org/10.1088/0964-1726/24/6/063001%20https://iopscience.iop.org/article/10.1088/0964-1726/24/6/063001>.
- [7] A. R. Champneys, T. J. Dodwell, R. M. J. Groh, *et al.*, “Happy catastrophe: recent progress in analysis and exploitation of elastic instability”, *Frontiers in Applied Mathematics and Statistics*, vol. 5, no. July, pp. 1–30, Jul. 2019, ISSN: 2297-4687. DOI: [10.3389/fams.2019.00034](https://doi.org/10.3389/fams.2019.00034). [Online]. Available: <https://www.frontiersin.org/article/10.3389/fams.2019.00034/full>.

- [8] J. Gutiérrez Álvarez and C. Bisagni, "A study on thermal buckling and mode jumping of metallic and composite plates", *Aerospace*, vol. 8, no. 2, p. 56, Feb. 2021, ISSN: 2226-4310. DOI: [10.3390/aerospace8020056](https://doi.org/10.3390/aerospace8020056). [Online]. Available: <https://www.mdpi.com/2226-4310/8/2/56>.
- [9] J. Gutiérrez Álvarez and C. Bisagni, "Closed-form solutions for thermomechanical buckling of orthotropic composite plates", *Composite Structures*, vol. 233, no. May 2019, p. 111 622, Feb. 2020, ISSN: 02638223. DOI: [10.1016/j.compstruct.2019.111622](https://doi.org/10.1016/j.compstruct.2019.111622). [Online]. Available: <https://linkinghub.elsevier.com/retrieve/pii/S0263822319318835%20https://doi.org/10.1016/j.compstruct.2019.111622>.
- [10] R. D. Kotanchik, J. N. and Johnson A.E. and Ross, "Rapid radiant heating tests of multiweb beams", *NACA Technical Note 3474*, no. June, 1956. [Online]. Available: <https://ntrs.nasa.gov/citations/19930084251>.
- [11] R. Heldenfels and W. Roberts, "Experimental and theoretical determination of thermal stresses in a flat plate", Langley Field, Va., Tech. Rep., 1952, pp. 1–35. [Online]. Available: <https://ntrs.nasa.gov/citations/19930081138>.
- [12] K. D. Murphy and D. Ferreira, "Thermal buckling of rectangular plates", *International Journal of Solids and Structures*, vol. 38, no. 22-23, pp. 3979–3994, May 2001, ISSN: 00207683. DOI: [10.1016/S0020-7683\(00\)00240-7](https://doi.org/10.1016/S0020-7683(00)00240-7). [Online]. Available: <https://linkinghub.elsevier.com/retrieve/pii/S0020768300002407>.
- [13] J. F. Rakow and A. M. Waas, "Thermal buckling of metal foam sandwich panels for convective thermal protection systems", *Journal of Spacecraft and Rockets*, vol. 42, no. 5, pp. 832–844, Sep. 2005, ISSN: 0022-4650. DOI: [10.2514/1.9741](https://doi.org/10.2514/1.9741). [Online]. Available: <http://arc.aiaa.org/doi/abs/10.2514/1.9741%20https://arc.aiaa.org/doi/10.2514/1.9741>.
- [14] M. Amabili and M. R. S. Tajahmadi, "Thermal post-buckling of laminated and isotropic rectangular plates with fixed edges: Comparison of experimental and numerical results", *Proceedings of the Institution of Mechanical Engineers, Part C: Journal of Mechanical Engineering Science*, vol. 226, no. 10, pp. 2393–2401, Oct. 2012, ISSN: 0954-4062. DOI: [10.1177/0954406211434496](https://doi.org/10.1177/0954406211434496). [Online]. Available: <http://journals.sagepub.com/doi/10.1177/0954406211434496>.
- [15] Y. Xu, S. Ren, W. Zhang, Z. Wu, W. Gong, and H. Li, "Study of thermal buckling behavior of plain woven C/SiC composite plate using digital image correlation technique and finite element simulation", *Thin-Walled Structures*, vol. 131, no. October 2017, pp. 385–392, Oct. 2018, ISSN: 02638231. DOI: [10.1016/j.tws.2018.07.023](https://doi.org/10.1016/j.tws.2018.07.023). [Online]. Available: <https://doi.org/10.1016/j.tws.2018.07.023%20https://linkinghub.elsevier.com/retrieve/pii/S0263823117312788>.
- [16] E. A. Thornton, M. F. Coyle, and R. N. McLeod, "Experimental study of plate buckling induced by spatial temperature gradients", *Journal of Thermal Stresses*, vol. 17, no. 2, pp. 191–212, Apr. 1994, ISSN: 0149-5739. DOI: [10.1080/01495739408946255](https://doi.org/10.1080/01495739408946255). [Online]. Available: <http://www.tandfonline.com/doi/full/10.1080/01495739408946255>.

- [17] D. A. Ehrhardt and L. N. Virgin, "Experiments on the thermal post-buckling of panels, including localized heating", *Journal of Sound and Vibration*, vol. 439, pp. 300–309, Jan. 2019, ISSN: 0022460X. DOI: [10.1016/j.jsv.2018.08.043](https://doi.org/10.1016/j.jsv.2018.08.043).
- [18] V. Bhagat, J. P., and P. Jeyaraj, "Experimental investigation on buckling strength of cylindrical panel: Effect of non-uniform temperature field", *International Journal of Non-Linear Mechanics*, vol. 99, no. December 2017, pp. 247–257, Mar. 2018, ISSN: 00207462. DOI: [10.1016/j.ijnonlinmec.2017.12.005](https://doi.org/10.1016/j.ijnonlinmec.2017.12.005). [Online]. Available: <https://doi.org/10.1016/j.ijnonlinmec.2017.12.005>.
- [19] B. Ross, N. J. Hoff, and W. H. Horton, "The buckling behavior of uniformly heated thin circular cylindrical shells", *Experimental Mechanics*, vol. 6, no. 11, pp. 529–537, Nov. 1966, ISSN: 0014-4851. DOI: [10.1007/BF02327232](https://doi.org/10.1007/BF02327232). [Online]. Available: <http://link.springer.com/10.1007/BF02327232>.
- [20] M. Anderson and M. Card, "Buckling of ring-stiffened cylinders under a pure bending moment and a nonuniform temperature distribution", Tech. Rep. November, Nov. 1962. [Online]. Available: <https://ntrs.nasa.gov/citations/19630000305>.
- [21] B. Ross, J. Mayers, and A. Jaworski, "Buckling of thin cylindrical shells heated along an axial strip", *Experimental Mechanics*, vol. 5, no. 8, pp. 247–256, 1965, ISSN: 0014-4851. DOI: [10.1007/bf02327148](https://doi.org/10.1007/bf02327148).
- [22] D. Bushnell and S. Smith, "Stress and buckling of nonuniformly heated cylindrical and conical shells", *AIAA Journal*, vol. 9, no. 12, pp. 2314–2321, Dec. 1971, ISSN: 0001-1452. DOI: [10.2514/3.6515](https://doi.org/10.2514/3.6515). [Online]. Available: <https://arc.aiaa.org/doi/10.2514/3.6515>.
- [23] Y. Frum and M. Baruch, "Buckling of cylindrical shells heated along two opposite generators combined with axial compression", *Experimental Mechanics*, vol. 16, no. 4, pp. 133–139, Apr. 1976, ISSN: 0014-4851. DOI: [10.1007/BF02321107](https://doi.org/10.1007/BF02321107). [Online]. Available: <http://link.springer.com/10.1007/BF02321107>.
- [24] J. Ari-Gur, M. Baruch, and J. Singer, "Buckling of cylindrical shells under combined axial preload, nonuniform heating and torque", *Experimental Mechanics*, vol. 19, no. 11, pp. 406–410, Nov. 1979, ISSN: 0014-4851. DOI: [10.1007/BF02324506](https://doi.org/10.1007/BF02324506). [Online]. Available: <http://link.springer.com/10.1007/BF02324506>.
- [25] W. Percy and R. Fields, "Buckling analysis and test correlation of hat stiffened panels for hypersonic vehicles", in *2nd International Aerospace Planes Conference*, Reston, Virginia: American Institute of Aeronautics and Astronautics, Oct. 1990. DOI: [10.2514/6.1990-5219](https://doi.org/10.2514/6.1990-5219). [Online]. Available: <http://arc.aiaa.org/doi/10.2514/6.1990-5219> <https://arc.aiaa.org/doi/10.2514/6.1990-5219>.
- [26] R. C. Thompson and W. L. Richards, "Thermal-structural panel buckling tests", *NASA Technical Memorandum 104243*, no. December 1991, 1991. [Online]. Available: <https://ntrs.nasa.gov/citations/19920006186>.
- [27] R. A. Fields, W. L. Richards, and M. V. DeAngelis, "Combined loads test fixture for thermal-structural testing of aerospace vehicle panel concepts", *NASA Technical Memorandum TM-2004-212039*, no. February, 2004. [Online]. Available: <https://ntrs.nasa.gov/citations/20040031531>.

- [28] M. Rouse and D. Jegley, "Testing a multi-bay box subjected to combined loads", in *Conference Proceedings of the Society for Experimental Mechanics*, Springer, Cham, 2016, pp. 173–182. DOI: [10.1007/978-3-319-22449-7_21](https://doi.org/10.1007/978-3-319-22449-7_21). [Online]. Available: http://link.springer.com/10.1007/978-3-319-22449-7%7B%5C_%7D21.
- [29] N. L. Breivik and M. W. Hyer, "Buckling and postbuckling behavior of curved composite panels due to thermal and mechanical loading", *Journal of Reinforced Plastics and Composites*, vol. 17, no. 14, pp. 1292–1306, Sep. 1998, ISSN: 07316844. DOI: [10.1177/073168449801701404](https://doi.org/10.1177/073168449801701404).
- [30] C. Bisagni and P. Cordisco, "An experimental investigation into the buckling and post-buckling of CFRP shells under combined axial and torsion loading", *Composite Structures*, vol. 60, no. 4, pp. 391–402, 2003, ISSN: 02638223. DOI: [10.1016/S0263-8223\(03\)00024-2](https://doi.org/10.1016/S0263-8223(03)00024-2).
- [31] C. Bisagni and C. Walters, "Experimental investigation of the damage propagation in composite specimens under biaxial loading", *Composite Structures*, vol. 85, no. 4, pp. 293–310, Oct. 2008, ISSN: 02638223. DOI: [10.1016/j.compstruct.2007.10.029](https://doi.org/10.1016/j.compstruct.2007.10.029). [Online]. Available: <https://linkinghub.elsevier.com/retrieve/pii/S0263822307002620>.
- [32] C. Bisagni and G. Sala, "Buckling and shape control of composite laminates using embedded shape memory alloys wires", in *Collection of Technical Papers - AIAA/ASME/ASCE/AHS/ASC Structures, Structural Dynamics and Materials Conference*, vol. 2, Reston, Virginia: American Institute of Aeronautics and Astronautics, Apr. 2004, pp. 1515–1529, ISBN: 978-1-62410-079-6. DOI: [10.2514/6.2004-1648](https://doi.org/10.2514/6.2004-1648). [Online]. Available: <http://arc.aiaa.org/doi/abs/10.2514/6.2004-1648>.
- [33] K. K. Shukla and Y. Nath, "Analytical solution for buckling and post-buckling of angle-ply laminated plates under thermomechanical loading", *International Journal of Non-Linear Mechanics*, vol. 36, no. 7, pp. 1097–1108, 2001, ISSN: 00207462. DOI: [10.1016/S0020-7462\(00\)00074-3](https://doi.org/10.1016/S0020-7462(00)00074-3).
- [34] F. Alijani and M. Amabili, "Non-linear dynamic instability of functionally graded plates in thermal environments", *International Journal of Non-Linear Mechanics*, vol. 50, pp. 109–126, 2013, ISSN: 00207462. DOI: [10.1016/j.ijnonlinmec.2012.10.009](https://doi.org/10.1016/j.ijnonlinmec.2012.10.009). [Online]. Available: <http://dx.doi.org/10.1016/j.ijnonlinmec.2012.10.009>.
- [35] S. Faghfouri and F. G. Rammerstorfer, "Mode transitions in buckling and post-buckling of stretched-twisted strips", *International Journal of Non-Linear Mechanics*, vol. 127, no. 5, p. 103 609, 2020, ISSN: 00207462. DOI: [10.1016/j.ijnonlinmec.2020.103609](https://doi.org/10.1016/j.ijnonlinmec.2020.103609). [Online]. Available: <https://doi.org/10.1016/j.ijnonlinmec.2020.103609>.
- [36] Y. Kiani, "Axisymmetric static and dynamics snap-through phenomena in a thermally postbuckled temperature-dependent FGM circular plate", *International Journal of Non-Linear Mechanics*, vol. 89, no. June 2016, pp. 1–13, 2017, ISSN: 00207462. DOI: [10.1016/j.ijnonlinmec.2016.11.003](https://doi.org/10.1016/j.ijnonlinmec.2016.11.003). [Online]. Available: <http://dx.doi.org/10.1016/j.ijnonlinmec.2016.11.003>.

- [37] M. Stein, “The phenomenon of change in buckle pattern in elastic structures”, *NASA-MEMO-5-13-59L*, 1959. [Online]. Available: https://archive.org/details/nasa%7B%5C_%7Dtechdoc%7B%5C_%7D19980228195.
- [38] W. J. Supple, “Changes of wave-form of plates in the post-buckling range”, *International Journal of Solids and Structures*, vol. 6, no. 9, pp. 1243–1258, 1970, ISSN: 00207683. DOI: [10.1016/0020-7683\(70\)90100-9](https://doi.org/10.1016/0020-7683(70)90100-9). [Online]. Available: [http://dx.doi.org/10.1016/0020-7683\(70\)90100-9](http://dx.doi.org/10.1016/0020-7683(70)90100-9).
- [39] F. Stoll, *Analysis of the snap phenomenon in buckled plates*, 1994. DOI: [10.1016/0020-7462\(94\)90031-0](https://doi.org/10.1016/0020-7462(94)90031-0).
- [40] B. Falzon and G. P. Steven, “Buckling mode transition in hat-stiffened composite panels loaded in uniaxial compression”, *Composite Structures*, vol. 37, no. 2, pp. 253–267, 1997, ISSN: 02638223. DOI: [10.1016/S0263-8223\(97\)80017-7](https://doi.org/10.1016/S0263-8223(97)80017-7).
- [41] M. Cerini and B. Falzon, “Use of the arc-length method for capturing mode jumping in postbuckling aerostructures”, *AIAA Journal*, vol. 43, no. 3, pp. 681–689, 2008, ISSN: 0001-1452. DOI: [10.2514/1.7914](https://doi.org/10.2514/1.7914).
- [42] Re-Steel, *Invar 36 for Composite Tooling (commercial catalog)*, 2021. [Online]. Available: <https://re-steel.com/invar-plate/invar-36/>.
- [43] J. Singer, J. Arbocz, and T. Weller, *Buckling Experiments: Experimental Methods in Buckling of Thin-Walled Structures*. Hoboken, NJ, USA: John Wiley & Sons, Inc., 2002, vol. 2, ISBN: 9780470172995. DOI: [10.1002/9780470172995](https://doi.org/10.1002/9780470172995). [Online]. Available: <http://doi.wiley.com/10.1002/9780470172995>.

5

VIBRATION-BUCKLING TESTS ON HEATED COMPOSITE PLATES

Experiment is the sole judge of the validity of any idea.

Richard P. Feynman

This paper presents an experimental investigation on vibrations of heated composite plates leading to thermal buckling. The tests were performed considering two main goals: the application of the Vibration Correlation Technique for the detection of thermal buckling in composite plates; and the exploration of the frequency variations before and after the occurrence of a mode jumping in post-buckling regime. Two test setups were used. The setups shared a low thermal expansion frame, while they differentiate on the type of heating source and mechanical boundary conditions. Two composite plates with layups $[30/-30/5/-5]_s$ and $[35/-35/10/-10]_s$ were tested. The plates were excited acoustically using a loudspeaker, and the vibration frequencies were monitored and stored using a laser vibrometer. Buckling temperatures were successfully detected using the Vibration Correlation Technique. Frequency changes, potentially related to the mode jumping, were also detected.

5.1. INTRODUCTION

STRUCTURAL plates under heating can engage in typically stable, reversible post-buckled states and can operate under post-buckling conditions, as long as no material failure occurs. Structural situations reached after buckling may have potentially interesting

This chapter has been adapted from: J. G. Álvarez, H. Abramovich and C. Bisagni, "J.G. Álvarez, Haim Abramovich, Chiara Bisagni, Vibration-buckling tests on heated composite plates, Journal of Sound and Vibration, Volume 536, 2022, 117145, ISSN 0022-460X, <https://doi.org/10.1016/j.jsv.2022.117145>.)

applications, for instance, as a source for shape change [1]. An example of such deformed states are the so-called mode jumps, i.e. sudden changes in shape experienced in post-buckling, during which the buckled plates increase the number of half-waves as a response to load variations [2]. However, during buckling and post-buckling, plates experience variations in the vibration frequencies, which can have an impact on structural integrity. Plates intended to operate in those situations should have well-understood vibration behaviour throughout all their operative ranges. Additionally, plates made of carbon fibre reinforced plastics can even make a better use of these states thanks to their strength and elastic behaviour, which allows for highly deformed shapes [3]. Modal testing can be an excellent tool for understanding the vibration changes in heated plates in post-buckling. First, it can help in the prediction of buckling, using the Vibration-Correlation Technique (VCT). Second, it can allow the exploration of deep post-buckling states, included those after the occurrence of mode jumping.

VCT technique relies on the principle that, often, a relation between changes in the vibration frequencies and buckling can be established. This relation can allow to obtain reliable estimations for the occurrence of buckling by monitoring the evolution on the frequencies in the loaded structure. VCT has successfully been applied to different kinds of structures, such as columns, plates, and more recently to cylinders. Labans et al. [4] performed vibration correlation studies on conventional laminated cylinders and fibre steering cylinders. VCT was applied by Arbelo et al. [5], [6] for the estimation of buckling load of perfect and imperfect flat metallic plates and cylindrical shells. Examples of the VCT method applied to different structures were also reported by Abramovich [7]. On recent studies, the technique has also been successfully applied to grid-stiffened cylindrical shells [8], and to isotropic cylinders with reinforced circular cutouts [9], which suggests that the applicability of the method can be extended to more complex structures.

Even though it is well understood that changes in the vibration signature of plates can be used to predict buckling, it is not known whether a similar procedure can be used to predict their mode jumpings. This possibility can, however, be explored via modal testing. A reasonably large amount of studies on the vibration of heated, post-buckled plates is available in literature. The approaches are heterogeneous, since they comprise analytical, numerical and experimental studies, and consider plates made of various materials and under diverse boundary conditions. Chung and Clevenson [10] investigated how acoustic emissions would affect the resonance frequencies and induce mode jumping in stiffened, pre-heated plates; Thompson and Virgin [11] performed experimental studies on the mode jumping in metallic plates subjected to noise and pulses; while Jacobson [12] tested multi-bay, curved and flat composite panels under thermal and high intensity acoustic excitation. More recently, Sun et al. [13] performed an experiment where the mode jumping on heated, acoustically excited C/Si plates were studied. Ehrhardt and Virgin [14] tested heated metallic plates and verified the existence of alternative equilibrium states by using a poking bar as external perturbation source. There are also several numerical studies in plate vibration and mode changes in metallic and composite plates: Kuo [15] performed studies on the changes of vibration patterns after the mode jumping in composite plates; Xia and Shen [16] investigated the vibration of heated post-buckled sandwich plates with functionally graded material facesheets;

Chen and Virgin [17] performed dynamic analysis of modal shifting and mode jumping in rectangular, metallic, thermally buckled plates; and Murphy et al. [18] characterized the buckling and snap-through phenomena in heated, fully clamped rectangular plates.

While there seems to be a lot of available research on the application of VCT to mechanically compressed composite structures, there appears to be a gap in the study of the application of VCT to heated composite plates, as well as in the investigation of their frequency changes after a mode jumping has occurred.

During the present investigation, modal testing of rectangular, laminated, heated plates were performed. In these experiments, two plates were tested under both unbuckled and post-buckled states, including the plate configurations reached after a mode jumping. Two goals were pursued: first, the application of VCT technique for the capture of buckling on heated composite plates; second, the investigation of any potential change in the frequency signature of the plates at the moment of the mode jumping. To achieve these objectives, two experimental configurations were used. The main difference between the two setups was the used heat source, being these an oven for the test setup No. 1 and an Infrared (IR) lamp array for the test setup No. 2.

The structure of this paper is here presented. In Section 5.2, the fundamentals of the VCT are briefly explained. In Section 5.3, the two experimental configurations are described, while the test methodology followed for the execution of the experiments is presented in Section 5.4. In Sections 5.5 and 5.6 the results are reported and evaluated, while Section 5.7 contains a summary of all obtained results. The conclusions are reported in Section 5.8.

5.2. VIBRATION CORRELATION TECHNIQUE IN HEATED PLATES: BUCKLING AND MODE JUMPING

The vibration correlation technique (VCT) is an experimental, non-destructive technique that allows the prediction of the buckling load in a slender, axially loaded structure. This technique consists on monitoring the variation in the vibration frequencies of the structure with respect to the applied compressive load. Based on the evolution of these frequencies, good estimations of the buckling load can often be obtained by using data acquired at load levels below the 60% of the originally predicted buckling load. This is, therefore, a valuable technique when dealing with structures liable to fail due to buckling. The same principle can also be applied to structures under the effect of thermal loads. In a heated structure, stresses often arise due to restrained thermal expansion, sometimes being large enough to buckle the structure. Such stresses are a function of the coefficients of thermal expansion (CTE), the laminate in-plane and bending stiffness, the boundary conditions and the temperature distributions in the structure [19]. When temperature changes are present, assessing the loads in a structure becomes a difficult task. In those cases, VCT can be a valuable alternative for the estimation of buckling load.

The VCT methodology is rooted on the similarity between the equations for buckling and vibration, investigated early on by Lurie [20], [21], and later by Souza et al. [22]. Given the case that a given vibration mode is comparable in shape to the buckling mode, a linear relation between the square of the frequencies and the applied load can often be

established. In order to illustrate this concept, a flat, rectangular plate is now considered. The plate is placed in a coordinate system XYZ , and the XY plane coincides with the mid-surface of the plate, with the lower left corner of the plate as the origin of the coordinate system, as shown in Fig. 5.1. The plate has length a , height b and thickness h , is made of carbon composite material, and has a symmetric and balanced angle-ply layup. Each ply is oriented at a generic angle θ , which is defined with respect to the X reference axis and is assumed to be counter-clockwise positive. The plate is loaded under a uniform temperature increment ΔT , which is applied gradually. Plate length and width variations are constrained, and rotations around the edges are also constrained.

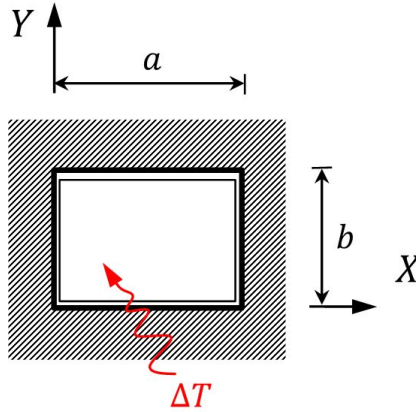


Figure 5.1: Plate reference system.

The vibration-buckling behaviour of an orthotropic composite plate can be represented by the differential equation reported as Eq. 5.1:

$$D_{11}w_{,xxxx} + 2(D_{12} + 2D_{66})w_{,xxyy} + D_{22}w_{,yyyy} + \bar{\rho}\ddot{w} - N_x w_{,xx} - N_y w_{,yy} = 0 \quad (5.1)$$

where the comma-preceded sub-indexes represent partial derivatives with respect to the specified variables, and the double dot represents double time derivative; $\bar{\rho}$ represents the equivalent density, calculated as $\bar{\rho} = \sum_{k=1}^N \rho_k h_k$, where N is the total amount of stacked layers, and h_k, ρ_k are the height and density of the corresponding layers; the D_{ij} ($i, j = 1, 2, 6$) represent the laminate bending stiffness, and N_x, N_y, N_{xy} are the edge force reactions along X, Y axes. The appearance of thermal loading in Eq. 5.1 takes place through the membrane constitutive equations:

$$\begin{Bmatrix} N_x \\ N_y \\ N_{xy} \end{Bmatrix} = \begin{bmatrix} A_{11} & A_{12} & 0 \\ A_{12} & A_{22} & 0 \\ 0 & 0 & A_{66} \end{bmatrix} \begin{Bmatrix} \epsilon_{xx}^0 \\ \epsilon_{yy}^0 \\ \gamma_{xy}^0 \end{Bmatrix} - \begin{Bmatrix} \hat{N}_x^T \\ \hat{N}_y^T \\ \hat{N}_{xy}^T \end{Bmatrix} \Delta T \quad (5.2)$$

Where the terms A_{ij} ($i, j = 1, 2, 6$) represent the laminate in-plane stiffness, $\epsilon_{xx}^0, \epsilon_{yy}^0, \gamma_{xy}^0$ are the engineering strains, and \hat{N}_x^T, \hat{N}_y^T and \hat{N}_{xy}^T are the unitary thermal force re-

sultants, which depend uniquely on laminate properties. Thermal forces vanish when $\Delta T = 0$. Eq. 5.1 captures the interaction effects of thermal and mechanical load over both plate vibration and buckling phenomena.

The typical vibration-buckling behaviour of such plate is described in Fig. 5.2 where two graphs are presented in a stacked form. The upper graph represents the out-of-plane deflections W measured at the plate center versus the applied ΔT , while the lower graph represents the square of the frequencies f^2 versus ΔT . In both graphs, two lines in colour black and blue are plotted, representing the typical behaviour of plates without and with geometric imperfections. In order to differentiate buckling shapes from vibration modes, buckling shapes are represented as pairs of integer values between parenthesis such as (m, n) , meaning m and n the number of half-waves in X and Y directions, respectively. For plate vibration modes the same notation holds, however the integer pair is between angle brackets, i.e. $\langle m, n \rangle$.

Taking now the bold black line for the plate without imperfections at $\Delta T = 0^\circ$ the plate is under a stress-free state. If temperature increases, in-plane stresses appear in the plate, and the plate remains flat. If temperature keeps increasing, the plate finds a bifurcation point at ΔT_{b1} , beyond which it starts deflecting out-of-plane, typically in a $(1, 1)$ buckling shape. This point is known as buckling temperature, represented here as ΔT_{b1} . Meanwhile, in the lower graph, the bold black line represents the vibration mode $\langle 1, 1 \rangle$ for the plate without imperfections, which is the lowest frequency mode at $\Delta T = 0^\circ$. This vibration mode is also comparable in shape to the previously described $(1, 1)$ buckling mode, and is the relevant vibration mode for the application of VCT. At $\Delta T = 0^\circ$ the intersection of the black curve with the vertical axis yields the square of the frequencies of the plate at room temperature. When ΔT increases, f^2 experiences a linear decrease, up to a certain value of ΔT for which f^2 becomes zero, an event that characterizes buckling [23]. This point coincides with the buckling temperature ΔT_{b1} . It constitutes the conceptual basis of the VCT methodology: for the plate without imperfections, when the applied load equals the buckling load, the frequency of the vibration mode, which more closely resembles the buckling shape, is equal to zero.

However, in reality, plates have geometric imperfections and their buckling and vibration behaviour deviate from the ideal behaviour. Regarding plate deflections, in Fig. 5.2 it can be seen that plates with geometric imperfections do not show a perfectly defined bifurcation temperature ΔT_{b1} , as the plate deflects gradually, describing a trajectory that asymptotically approaches the deflection curve for the ideal plate [23]. The presence of geometrical imperfections manifests in the vibration signature of the plate in several ways. First, vibration frequencies for plates with geometric imperfections are inherently higher than for their ideal counterparts. This is illustrated in the lower graph of Fig 2: for $\Delta T = 0^\circ$ the intersection of the blue curve with the vertical axis is slightly higher than for the curve of the ideal plate, and this tendency accentuates as ΔT increases, because the out-of-plane deflections grow larger with the temperature, producing a stiffening effect over the plate [24]. Second, the evolution of f^2 vs. ΔT is not a line anymore, since the linear decrease only holds up to a load level close to buckling. The vibration frequency is not zero at buckling temperature ΔT_{b1} , but instead it reaches a local minimum at approximately the same location. Identifying the local minimum on this curve is a reliable method to identify the buckling load in plates [5]. However, an

estimation of the buckling load can be done by performing a linear extrapolation of the linear segment in the f^2 vs. ΔT curve and finding its intersection with the horizontal axis.

When the plate is in post-buckling and the temperature keeps on increasing, the plate can experience a mode jump, changing the buckling shape from (1, 1) into a (1, 2) mode. It is difficult to estimate when a mode jumping is going to occur even because VCT is based on plate linear behaviour, and the relation between the frequencies and buckled states ends up at the point of buckling.

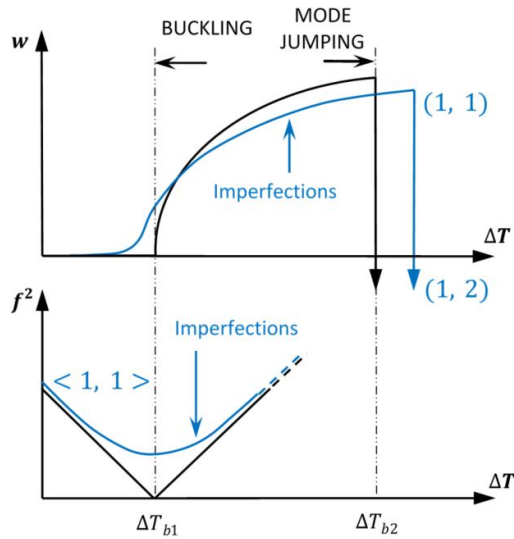


Figure 5.2: Behaviour of a heated composite plate: Out-of-plane deflection and squared frequency as function of the temperature variation.

5.3. EXPERIMENTAL SETUPS

The present experimental investigation was performed using two different test setups. The first test setup, here called test setup No. 1, was in part based on a previous research by the authors [25], while the second one, here called test setup No. 2, was developed as a novel test configuration. The two test setups are represented in Fig. 5.3 and Fig. 5.4, respectively.

In both setups the composite plate was fixed within a low coefficient of thermal expansion (CTE) frame. The plate and the frame are subjected to heat increments and, due to restrained thermal expansions, the plate experiences buckling and eventually mode jumping. The heating operation is performed gradually, by increasing the temperature in small steps, so that the temperature can stabilize at the desired values, and then the vibration modes and the frequencies can be measured through modal tests.

The tested plates were made of carbon unidirectional composite material. Hints for design of laminates displaying mode jumping under heating can be found in a previous work by the authors [25]. The plates were made of AS4/8552 [26] composite material, and have a stacking orientation of $[30/-30/5/-5]_s$ and $[35/-35/10/-10]_s$. The plies were cut using an automatic cutting machine and were subsequently stacked manually, and the laminate was cured in an autoclave. The frame was constructed using Invar 36 material [27]. The material properties of the composite and the Invar 36 material are presented in Table 5.1. The low CTE of the frame contributes to restrain the thermal expansion of the plate and to have low sensitivity to thermal gradients in the fixture. Prior to testing, the composite plate was placed between the two parts of the frame and assembled, following a cross sequence to bolt the assembly in three levels up to the maximal level of 60 Nm.

Material	E_{11} [GPa]	E_{22} [GPa]	G_{12} [GPa]	ν_{12}	α_1 [$\frac{\mu m}{m^{\circ}C}$]	α_2 [$\frac{\mu m}{m^{\circ}C}$]	t_{ply} [mm]	ρ [kg/m ³]
AS4/8552	135	9.68	5.6	0.30	0.28	28.0	0.181	1.58
Invar 36		140		0.33		1.5		8.05

Table 5.1: Material properties.

During the modal tests, a POLYTEC PSV 500 XTRA system was used to capture both the vibration frequencies and deflection shapes of the plates at different temperatures. The scanning head of the vibrometer was equipped with a full optics and camera setup with a laser beam, which allowed to perform the calibration and measurements directly from a fully dedicated acquisition and processing unit system. In order to measure the frequency response, the plate and the frame were acoustically excited using a loudspeaker. The test setup No. 1 is presented in Fig. 5.3. In this configuration, the assembled plate and frame were placed on top of a metallic support inside an oven, which acted as heating source. The oven can contain specimens up to 600 mm x 600 mm x 600 mm. The oven door was substituted with a replacement door, which had a rectangular aperture, slightly larger than the plate, so to allow direct access to the measurement devices. In order to close the gap between the frame and the oven door, an aluminum sheet was used. The temperatures on the plate and the frame were monitored using thermocouples, which positions are reported in Fig 5 (a), and thermocouple readings were acquired by a Keythley multimeter. During the experiment, the temperature was increased by manually regulating the temperature in the oven. Due to the test configuration, it was not possible to use both Digital Image Correlation (DIC) and vibrometry at the same time. In this setup, a plate with layup $[30/-30/5/-5]_s$ was tested.

In the test setup No. 2, reported in Fig. 5.4, the frame was kept suspended in the air with the help of two chains, to recreate as much as possible free-free boundary conditions. For convenience, the test setup was assembled within the working space of a MTS 3500 compression machine. The heating operation was performed using a quartz infrared (IR) lamp array. The temperatures on the plate and frame were monitored using thermocouples, which positions are reported in Fig. 5.5 (b). A total of nine thermocouples were placed on the plate. The out-of-plane deflections of the plates were measured using a DIC system, using two cameras with 50 mm lenses. The plate tested in this setup

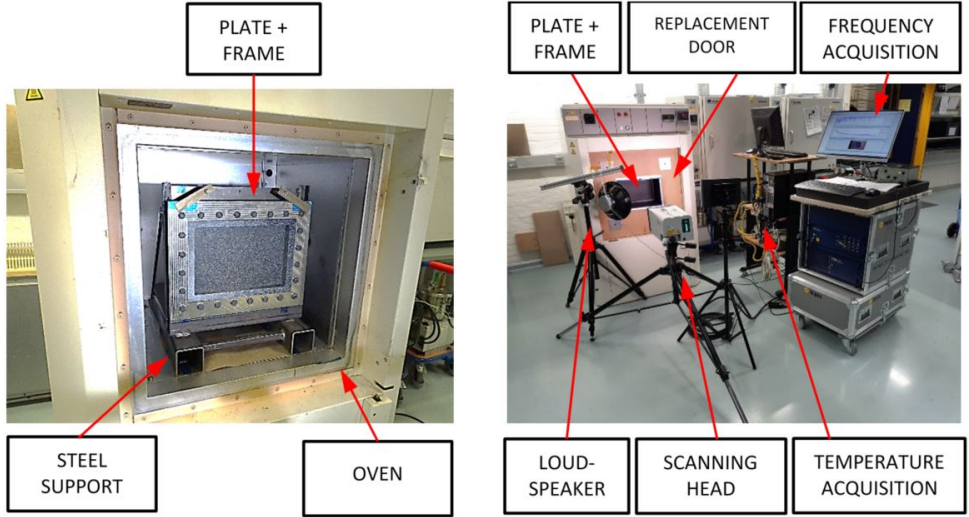


Figure 5.3: Test setup No. 1: (a) Details of plate fixture; (b) Complete setup.

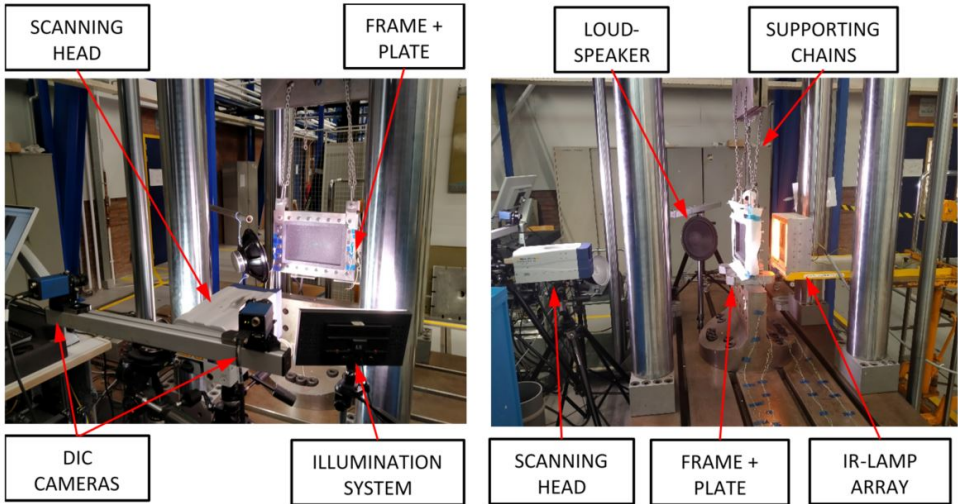


Figure 5.4: Test setup No. 2: (a) Front view; (b) Lateral view.

had a stacking orientation of $[35/ - 35/10/ - 10]_s$.

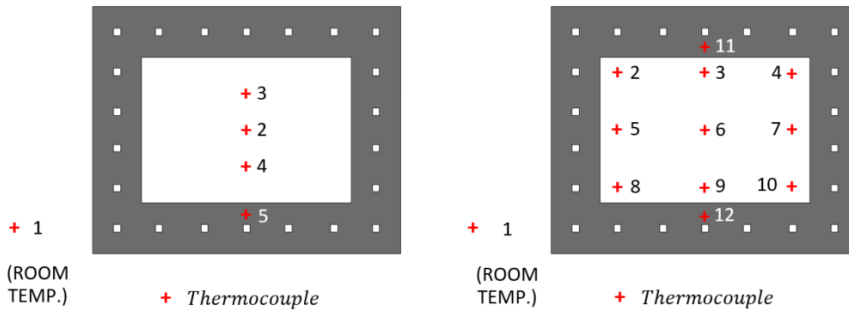


Figure 5.5: Thermocouple distribution: (a) Test setup No. 1; (b) Test setup No. 2

5.4. TESTING METHODOLOGY

5

Due to the differences of the two test setups, the testing protocol had to be slightly different. The test setup No. 1 had the limitation of not being able to capture both DIC deflections and vibration data simultaneously, and consequently the frequency data could not be exactly related to the experimental plate deflections. In order to be able to obtain comparative information, two tests were consecutively performed. During the first test, the plate and the frame were monotonically heated, reaching both buckling and mode jumping, and acquiring DIC deflection shapes and temperatures in the plate. After that, the setup was let to cool down. During the second test, the plate and the frame were subjected to temperature increments. Once the temperature was stabilized, the vibration frequencies were measured, repeating this measurement at different temperatures. The buckling and mode jumping temperatures measured during the second test, together with the deflection shapes acquired during the first test, closely resembled a VCT test. The test setup No. 2 could conveniently fit all the instrumentation around the plate, and therefore DIC and vibration data could be acquired during the same experiment. The plate and the frame were subjected to temperature increments and, once the temperature was stabilized, both DIC and vibration frequencies were measured, repeating these measurements at different temperatures.

Unfortunately, during the tests performed using the two different test setups, the temperature distributions were not homogeneous and consequently the temperature at the centre of the plate was considered as a reference. The frequency measurements were performed using the laser vibrometer and measuring the response to acoustic excitation at each position of an array of points located on the surface of the plate. The scanning head measured the response to the external excitation at each position of the preselected matrix of points. The excitation was performed with a loudspeaker placed in the proximities of the plate. The signal used for excitation with the loudspeaker was an acoustic, “burst chirp” type signal, sweeping the frequency range of 1-600 *Hz* and 1-800 *Hz* for test setups 1 and 2, respectively. In the test setup 2, a Hanning window was applied in order to improve measurement coherence. An averaging of three measurements per

scanned point was performed.

5.5. EXPERIMENTAL RESULTS FOR TEST SETUP NO. 1

For the test setup No. 1, deflections plots are presented in Fig. 5.6 in two rows, where the plots reported in the upper row represent the buckling, and the plots in the lower row the mode jumping. In the first row it can be appreciated how a (1,1) buckling shape started to be incipient at 56°C . Then, it gradually conformed as the temperature increased, and became fully developed at 76°C . The buckling temperature was extracted graphically by applying the Southwell method [23]. For this, the data for the first test was plotted in a $w/\Delta T$ vs. w graph, as shown in Fig. 5.7. The experimental data points, represented as circles, were fitted to a line, reported as a thin blue line with the label “fitted line”. Finally, the buckling temperature was obtained by extracting the inverse of the slope of the fitted line. For this case, it yields a buckling temperature of $T_{b1}(Exp) = 71^\circ\text{C}$. Regarding the mode jumping, in the second row of Fig. 5.6 it can be seen that at 89°C the plate still showed a (1,1) buckling shape, being the maximum deflection equal to 1.4 mm . A secondary (1,2) buckling shape appeared at 93°C being the lower half-wave smaller in size than the upper one. At 106°C , the two half waves became approximately equal in size. The mode jumping temperature $T_{b2}(Exp)$ is considered to have happened around 93°C .

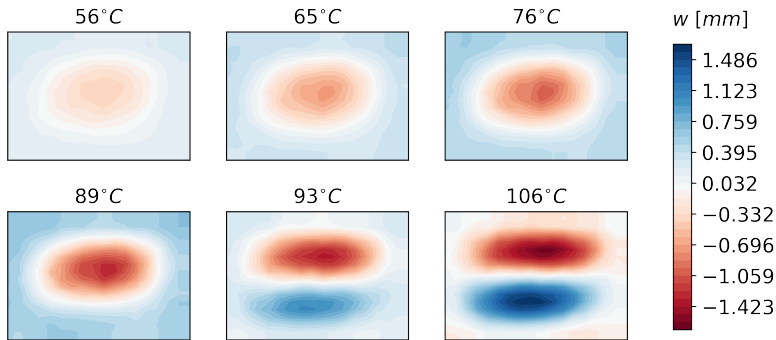


Figure 5.6: Out-of-plane displacements w for $[30/ -30/5/ -5]_s$ plate.

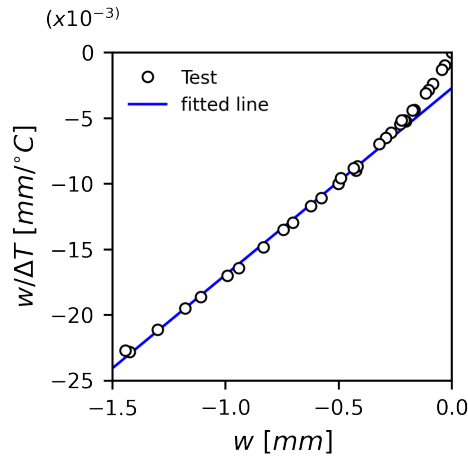
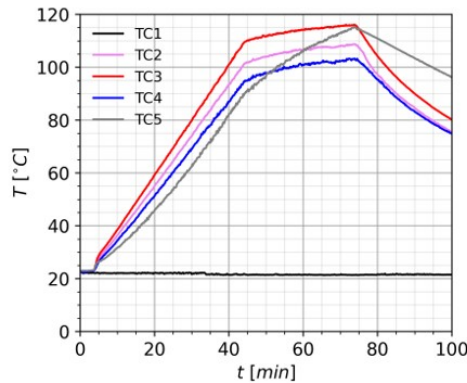
Figure 5.7: Southwell plot for $[30/-30/5/-5]_s$ plate.

Fig. 5.8 reports the temperature readings. Temperature differences among the different thermocouple measurements were approximately 10°C when the reading of $TC2$ is 60°C and around 15°C when the reading of $TC2$ is 105°C . Such temperature distributions were far from the ideal, uniform temperature distribution which was desired. They were caused by an inherent characteristic of the test setup: air convection flows upwards, and due to this the hotter air concentrated in the upper areas of the oven. Thus, the temperature distribution could not be completely uniform.

Figure 5.8: Thermocouple measurements for $[30/-30/5/-5]_s$ plate

In Fig. 5.9, eight measured frequency spectra are reported. In these graphs, the dis-

placement measured in μm is plotted versus the excitation frequency, measured in Hz. The peaks indicate relevant vibration modes at a given frequency. A black label indicates the first relevant mode, that is $\langle 1,1 \rangle$; red and blue labels identify the second and third plate vibration modes, respectively; fourth modes and higher are reported in violet. The lowest measured vibration mode $\langle 1,1 \rangle$ in Fig. 5.8 closely resembles the $(1,1)$ buckling mode displayed by the plate.

The lowest measured vibration mode $\langle 1,1 \rangle$ closely resembles the $(1,1)$ buckling mode. This vibration mode can be identified in Fig. 5.9, at the graph acquired at $23^\circ C$, as a peak at 215 Hz. First, this vibration mode experienced a decrease in frequency as the temperature increased: for temperatures $33^\circ C$, $42^\circ C$, $53^\circ C$ and $67^\circ C$ the frequency sank down to the values 188 Hz, 168 Hz, 140 Hz, and 97 Hz, respectively. The lowest frequency value of 94 Hz was measured at approximately $83^\circ C$ after which it increased again. The mode $\langle 1,2 \rangle$ in red is the mode which resembled the $(1,2)$ post-buckling shape after the mode jumping. It can be seen that this mode is not present between $42^\circ C$ and $83^\circ C$. Conversely, the mode $\langle 2,1 \rangle$ identified in blue is present in all performed modal tests. At room temperature, i.e. at $23^\circ C$ it shows a vibration frequency of 416 Hz, gradually decreasing as temperature increases; the frequency for this mode finds a minimum at $67^\circ C$ after which it increases again, reaching 511 Hz at $110^\circ C$.

In Fig. 5.10, some examples of vibration shapes are displayed. These were obtained at three different temperature levels, $23^\circ C$, $33^\circ C$ and $53^\circ C$. In the upper row, corresponding to $23^\circ C$ the three first captured vibration modes are reported. These were the $\langle 1,1 \rangle$, $\langle 2,1 \rangle$ and $\langle 1,2 \rangle$, with frequencies 215 Hz, 416 Hz and 457 Hz, respectively. The frequency of the first vibration mode $\langle 1,1 \rangle$ decreased with the temperature, becoming 187 Hz at $33^\circ C$ and 140 Hz at $53^\circ C$. The vibration modes $\langle 2,1 \rangle$ and $\langle 1,2 \rangle$ appeared to experience rotations of 33° and -33° respectively, as temperature was risen. In order to represent skew or rotated vibration mode shapes, the notation $\langle m,n \rangle_\theta$ was used, where the sub-index θ indicates the angle of rotation of that mode with respect to the X axis. In this way, at $T = 33^\circ C$, the $\langle 2,1 \rangle_{33^\circ}$ mode shape captured at 389 Hz represents a $\langle 2,1 \rangle$ vibration mode shape with two half-waves along the line at $\theta = 33^\circ$, approximately the diagonal of the plate connecting the lower left and upper right corners in the plate. Thus, at 33° the vibration modes $\langle 2,1 \rangle_{33^\circ}$ and $\langle 2,1 \rangle_{-33^\circ}$ were captured, and they appeared to merge into a $\langle 2,1 \rangle$ vibration mode at $53^\circ C$.

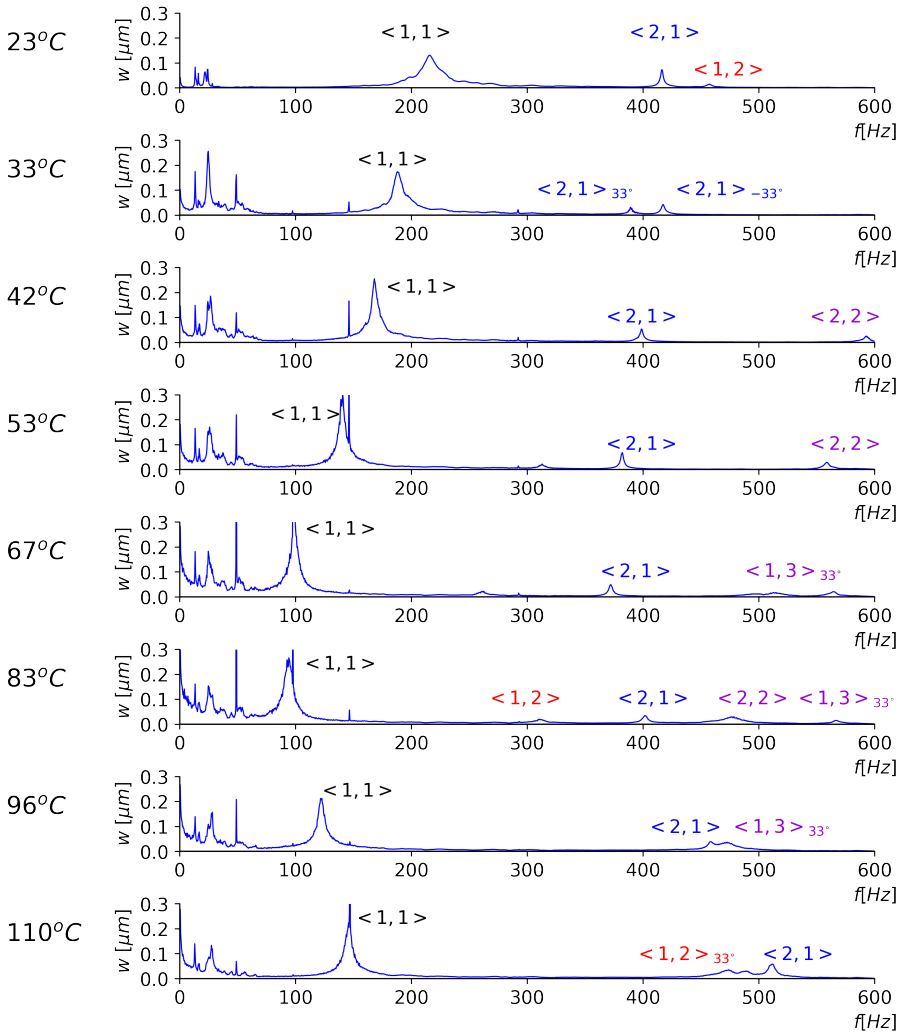


Figure 5.9: Frequency spectra for $[30/-30/5/-5]_s$ plate

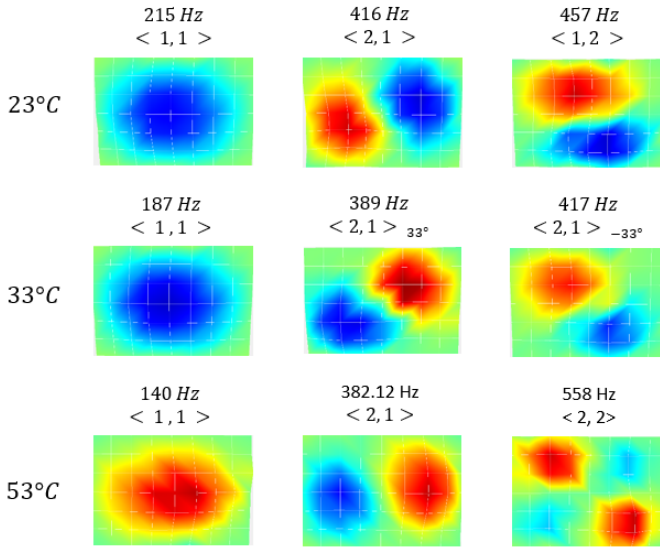


Figure 5.10: Examples of vibration mode shapes at various temperatures for test setup No. 1.

5.5.1. PREDICTION OF BUCKLING USING VCT

The evolution of the first vibration mode $\langle 1,1 \rangle$ is summarized in a graph where f^2 is plotted versus T , reported in Fig. 5.11 (a). A black thin line with "+" markers labelled as " $\langle 1,1 \rangle$ " represents the measured frequencies for mode $\langle 1,1 \rangle$, and the positions of each individual marker represents a single frequency measurement. It can be seen how from 23°C up to 67°C the frequency squared f^2 decreased almost linearly and then, after 83°C it increased again. The first four frequency measurements located in the linear portion of the curve were used to extract a fitted line using the least-square method.

This line, represented in the graph as a blue dotted line labelled as "VCT", yields an intersection point with the horizontal axis that can be used as a prediction for the buckling temperature. This prediction value will from now on be referred as $T_{b1}(VCT)$, yielding for this particular case $T_{b1}(VCT) = 75^\circ\text{C}$. This prediction can be verified by using the minimum of the f^2 vs T curve, located between the measurements at 67°C and 83°C. A fitted polynomial curve, represented in the figure as a brown dashed line, was used to extract this minimum. This curve finds a minimum at 77°C that is, only 2°C apart from the obtained $T_{b1}(VCT)$. Deflections reported in Fig. 5.6 indicate that, indeed, the plate has a clear $\langle 1,1 \rangle$ buckling shape around 65°C and that this is fully conformed at 75°C. The VCT predicted temperature $T_{b1}(VCT)$ appears therefore to correctly point towards the buckling temperature. It must be noted that determining a precise value for the experimental buckling load in plates is a difficult task, since buckling is a gradual procedure and the out-of-plane deflections increase gradually.

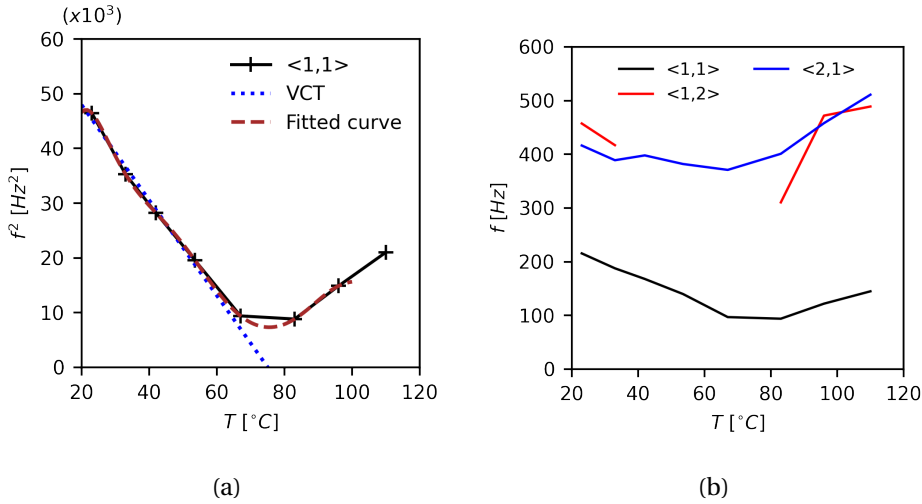


Figure 5.11: Frequencies vs. temperature for $[30/-30/5/-5]_s$ plate: (a) Lowest vibration mode; (b) Three lowest vibration modes.

5.5.2. DETECTION OF THE MODE JUMPING

The vibration signature of the plate was then investigated to see if it could be related to the mode jumping. For this, the evolution of modes $\langle 1,1 \rangle$, $\langle 2,1 \rangle$ and $\langle 1,2 \rangle$, which are the first three modes of the plate at room temperature, are shown in Fig. 5.11 (b), reporting f versus T . While the vibration modes $\langle 1,1 \rangle$ and $\langle 2,1 \rangle$ could be tracked throughout all temperatures, the mode $\langle 1,2 \rangle$ disappeared after 33° and did not reappear till 83°. None of the aforementioned curves showed either maxima or minima at temperatures close to the mode jumping. At temperatures close to the mode jumping there is some overlapping between modes $\langle 1,2 \rangle$ and $\langle 2,1 \rangle$. Already in Fig. 5.9 it can be seen how these two modes appear to change their order at frequencies in the [450 – 550] Hz range. However, the definition of these modes was insufficiently captured.

The test setup No. 1 presented some issues regarding the acquisition of vibration frequencies. When acoustically excited, not only the frame and plate but the complete assembly i.e. oven, metallic support, door, etc. vibrated, so the vibration modes originated from the assembly appeared in the measurements. This can be observed in the first graph of Fig. 5.9, which corresponds to the modal test at 23°C. Most of the frequency readings registered within the frequency band 0-60 Hz correspond to the vibration of the test hardware, and not only the plate-frame assembly. For this reason, the measurements in this frequency band should be neglected. Additionally, the noise generated by the oven fan introduced an additional excitation in the test setup, so the acoustic signal emitted by the loudspeaker had to be loud enough to overcome it. It is suspected

that mode $\langle 1, 2 \rangle$ and other higher modes could not be accurately captured throughout all temperatures due to lack of resolution in the frequency sampling during acquisition. The vibrometer acquisition unit uses a Fast Fourier Transform (FFT) algorithm, which allows for separation of the plate response into individual frequency components. This procedure requires a discretization of the frequency range of interest, where both the range and the resolution of such discretization parameters have to be selected by the user. Lowering this resolution allows for smaller measuring and processing times, but can yield defects in the measurements such as aliasing or leaking. While the used resolution proved enough to capture the buckling of the plate via VCT, it would appear not to be sufficient to capture the higher modes, $\langle 1, 2 \rangle$ and $\langle 2, 1 \rangle$ in detail, where it is believed that potentially valuable information about the mode jumping may be. The lessons learned from this setup were, however, useful for the development of test setup No. 2.

5.6. EXPERIMENTAL RESULTS FOR TEST SETUP NO. 2

5

The out-of-plane deflections measured on $[35/-35/10/-10]_s$ plate using test setup No. 2 are reported in Fig. 5.12. The three images in the upper row capture the occurrence of buckling, while the bottom row presents the occurrence of the mode jumping. Observing the upper row, it can be seen how at 23°C , that is the room temperature, the plate remained flat, while at 46°C an incipient (1, 1) buckling shape can be appreciated, and at 67°C the same shape appeared fully developed. The experimental buckling temperature could not be extracted via the Southwell method since there were not enough measurements for the displacement to apply this method reliably. The buckling temperature was estimated to be $T_{b1}(Exp) = 50^\circ\text{C}$, using the “top-of-the-knee” qualitative method [23]. In the bottom row of Fig. 5.12, it can be observed that at 90°C the plate presented a fully developed (1,1) buckling shape, while at 102°C the change of mode had already happened, being the bottom half-wave smaller than the one at the top, and later at 113°C a (1,2) buckling shape with two equal half-waves was completely defined. The three plots show how there is no sudden occurrence of the mode change: it happens in a rather gradual transition. In Fig. 5.12, the temperature labels reported on top of each deflection plot indicate the temperature at the centre of the plate at the time of acquisition. The temperature distribution at each of these six measurements can be found in Fig. 5.13. These temperature plots were generated using a 2D graphical interpolation of the data acquired by the nine thermocouples distributed on the plate as shown in Fig. 5.5 (b). In each temperature plot in Fig. 5.13, the position of the sensors is documented with a white cross, with a number indicating the temperature value at the instant of the measurement. At room temperature, the temperature distribution remained relatively uniform, but, as soon as heating started, temperature differences on the plate increased to 10°C at the moment of buckling, and then rose up to 16°C once the (1, 1) buckling shape was completely developed. The differences in the temperature distributions became more relevant at higher temperatures, as the temperature differences within the plate increased up to 32°C . From the six temperature plots, it becomes evident how the upper part of the plate was hotter, which is consistent with the data registered for the

test setup No. 1. Achieving uniform temperature distribution was proven to be a difficult task, and a consistent issue in all performed experiments. It was learned that, in order to avoid air convection problems, the specimen should have been placed in horizontal, being heated from below. Unfortunately, this could not be done due to the additional difficulties this arrangement would bring, such as issues with the wiring of sensors, acquisition instrumentation, and assuring a reliable calibration for the DIC cameras.

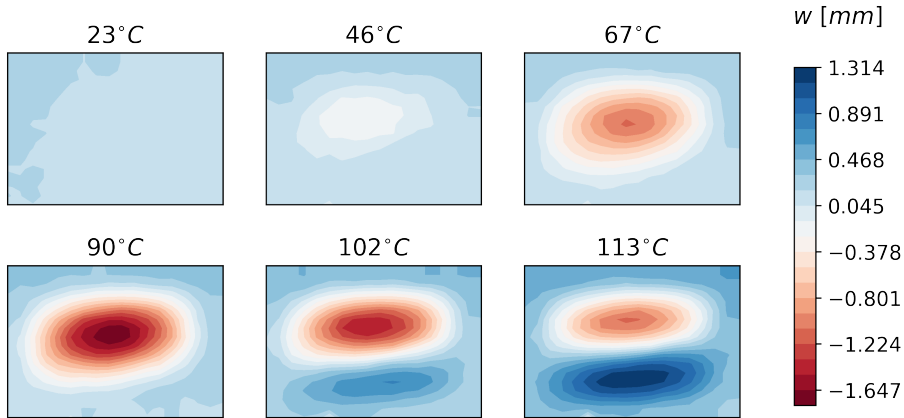


Figure 5.12: Out-of-plane displacements w for $[35/-35/10/-10]_s$ plate..

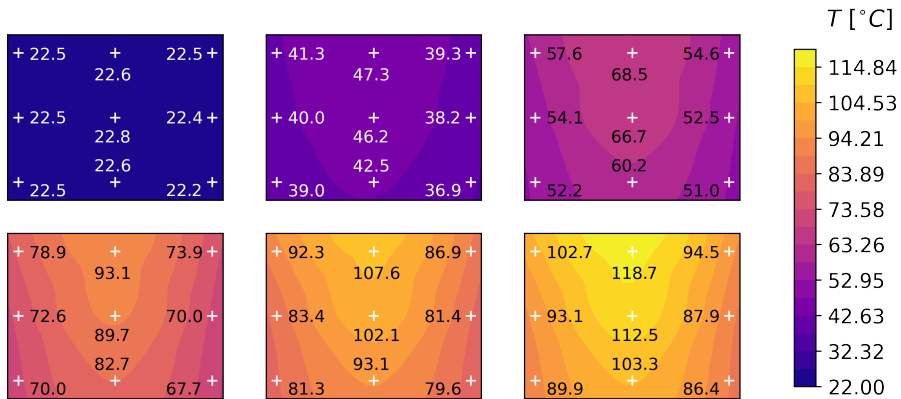


Figure 5.13: Temperature distributions for $[35/-35/10/-10]_s$ plate

The frequency spectra obtained from the modal tests in test setup No. 2 are summarized in Fig. 5.14. Almost the totality of the noise in the frequency band 0-60 Hz which was present in the frequency measurements for test setup No. 1 is not present anymore, thanks to the implemented free-free boundary conditions. The evolution of the three vibration modes, $\langle 1, 1 \rangle$, $\langle 1, 2 \rangle$ and $\langle 2, 1 \rangle$, could successfully be tracked throughout all temperature values, and also higher frequency modes were tracked. For the presentation of the frequency measurements, it was found convenient to display the spectra in terms of vibration speed in $\mu m/s$.

5.6.1. PREDICTION OF BUCKLING USING VCT

In the top graph in Fig. 5.14 it can be seen how at room temperature, i.e. $23^\circ C$, the lowest vibration mode had a $\langle 1, 1 \rangle$ shape. Also the buckling shape of the plate was a $(1, 1)$ mode. The vibration frequency of mode $\langle 1, 1 \rangle$ decreased as temperature increased, as it can be seen in the spectra for temperatures $31^\circ C$, $36^\circ C$, $41^\circ C$ and $46^\circ C$. This evolution can be better appreciated in the plot in Fig. 5.15 (a), where an overview of the variations in f^2 vs T is reported. The variation in frequencies of mode $\langle 1, 1 \rangle$ is represented as a black thin line with “+” markers labeled as “ $\langle 1, 1 \rangle$ ”, where each “+” indicates a frequency measurement. In the temperature range going from $23^\circ C$ to $46^\circ C$, the value of f^2 for mode $\langle 1, 1 \rangle$ appears to have a linear decrease. After that, it started to grow, rising up to a local maximum at $67^\circ C$, remaining stable till $83^\circ C$, after which it rapidly decreased, finding another local minimum at $102^\circ C$. The frequency measurements within $23^\circ C$ to $46^\circ C$ range were used to extract a fitted line using the least-square method, represented in Fig. 5.15 (a) as black dotted line, labelled as “VCT”. The intersection of this line with the horizontal axis yields a $T_{b1}(VCT) = 58^\circ C$. In order to find an approximate minimum reached by the f^2 vs T curve, a fitted curve was performed using the measurements within the temperature range $23^\circ C$ to $67^\circ C$. This curve is represented as a dashed, brown line with the label “fitted curve”, which finds a minimum at $51^\circ C$. This temperature has a difference of $7^\circ C$ with the VCT predicted temperature. It is believed that such difference could be originated by the lack of frequency measurements in the temperature range $51^\circ C - 67^\circ C$. The occurrence of buckling in this temperature range is also confirmed by the two deflection plots in Fig. 5.12 at $46^\circ C$ and $67^\circ C$. VCT appears therefore to correctly hint towards the occurrence of buckling.

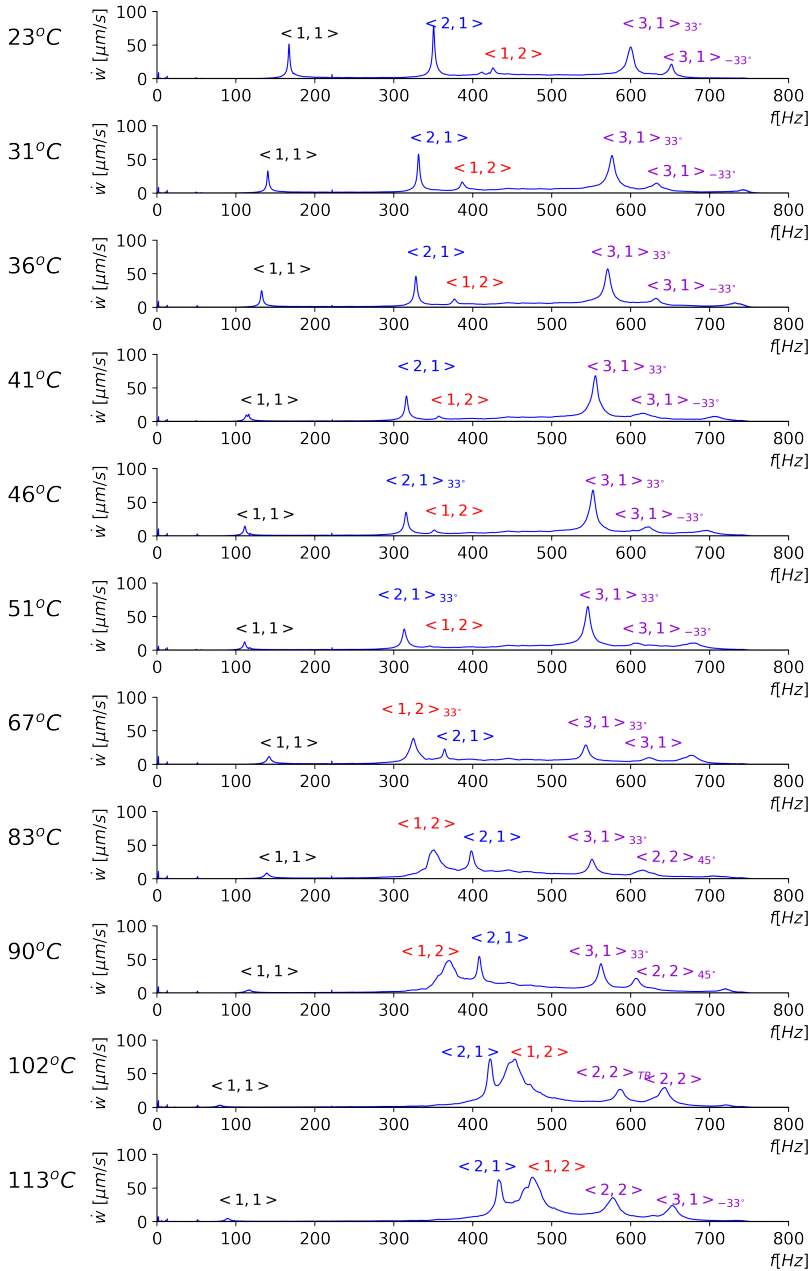


Figure 5.14: Frequency spectra for $[35/-35/10]_s$ plate

5.6.2. DETECTION OF THE MODE JUMPING

An attempt was made to identify relevant changes in the plate vibration frequencies related to the mode jumping. In the second row of DIC measurements reported in Fig. 5.12, a change from the buckling mode $(1,1)$ into mode $(1,2)$ is clearly observable, happening this between 90°C and 102°C . However, this change did not happen as a sudden event, but as a gradual transition. The evolution of three vibration modes $\langle 1,1 \rangle$, $\langle 2,1 \rangle$ and $\langle 1,2 \rangle$ is shown in Fig. 5.15 (b). The mode $\langle 2,1 \rangle$, reported as a blue curve, is the second mode present at room temperature, with a frequency of 350 Hz . When temperature increased, the frequency for this mode showed a gradual decrease, finding a minimum value of the frequency of 313 Hz at $T = 51^\circ\text{C}$. Then, it experienced an increase up to 113°C , where it reached a value of 433 Hz . The curve minimum for this mode appeared to happen at roughly the same temperature as the reported curve minimum for mode $\langle 1,1 \rangle$. The third vibration mode present at room temperature was the $\langle 1,2 \rangle$ mode at 411 Hz . The evolution of this mode is represented in Fig. 5.15 (b) as a bold red curve. When temperature increased, this mode experienced at first a gradual decrease, intersecting the line for mode $\langle 2,1 \rangle$ and becoming the second vibration mode of the plate at a point between the measurements at 51°C and 67°C . This occurred at approximately 58°C , that is shortly after the plate had buckled. After that, the frequency of mode started to increase rapidly, intersecting again the curve for $\langle 1,2 \rangle$ at around 96°C and thus becoming again the third vibration mode. This second intersection happened somewhere between the measurements at 91°C and 102°C approximately at a distance of 5°C to the occurrence of the mode change.

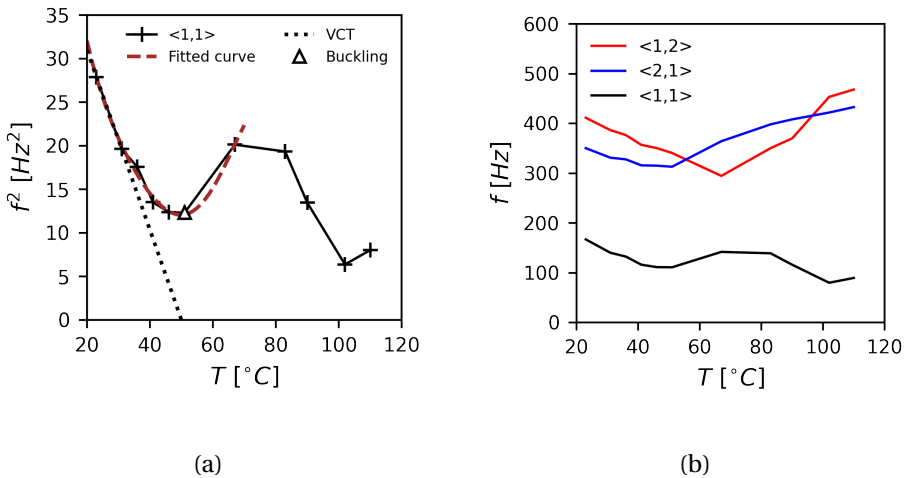


Figure 5.15: Frequencies vs. temperature for $[35/-35/10/-10]_s$ plate: (a) Lowest vibration mode; (b) Three lowest vibration modes.

Besides the three examined vibration modes, several occurrences in higher frequency modes were observed during the mode transition. Vibration mode $\langle 2,2 \rangle_{-45^\circ}$ was

present at 83°C i.e. right before the mode change, and during the buckling mode transition this mode appeared to rotate and become a $\langle 2,2 \rangle$ mode, at 102°C . Additionally, some other higher frequency vibration shapes, such as $\langle 1,3 \rangle_{33^{\circ}}$ and $\langle 1,3 \rangle_{-33^{\circ}}$, were also captured before the mode change. It should be also commented that beyond 41°C the measured speeds decrease significantly for the lowest frequency mode $\langle 1,1 \rangle$, while vibration responses for modes $\langle 1,2 \rangle$ and $\langle 2,1 \rangle$ become more relevant as temperature increases beyond 67°C . The significance of previously described events is unclear, and their relation with the mode jumping is found not yet conclusive.

For the experiments performed in test setup No. 1 and test setup No. 2, VCT achieved reasonable predictions for the buckling temperature. This was done by performing a linear extrapolation of the linear part of the f^2 vs T curve and extracting the intersection of the resulting line with the horizontal axis. The accuracy of these predictions could be verified with the minimum in the f^2 vs T curve present in the proximity of buckling. Based on these results, the VCT could be a useful tool for the prediction of buckling in heated composite plates. Events such as the inversion in order for the modes $\langle 1,2 \rangle$ and $\langle 2,1 \rangle$ were detected in the proximity of the mode jumping. However, the relation between such events and the occurrence of the mode jumping is not yet conclusive and requires a further experimental effort.

5.7. RESULTS SUMMARY

In this section, an overview of the main results of this investigation is presented. Table 2 synthesizes the results for the prediction of thermal buckling temperature with VCT, and Table 3 contains the most relevant observations for the mode jumping. For comparison, theoretical values for the buckling and mode jumping temperatures were also reported in the tables. These theoretical values were extracted from Finite Element numerical simulations performed in Abaqus, reported in previous work by the authors [25]. The FE model was performed using S4R shell elements. These are general-purpose Finite Elements, which formulation is based on Koiter-Sanders shell theory. This theory proposes simplifications on the shell kinematic equations which somewhat limits its applicability to moderately large deflections [28]. The theoretical buckling temperature is represented as $T_{b1}(Th)$, and is the result of an eigenvalue analysis, while the theoretical mode jumping temperature, represented as $T_{b2}(Th)$, was obtained by means of a nonlinear dynamic explicit simulation. While it is assumed that residual stresses are present in the tested laminates due to the curing process, no significant impact in the vibration frequencies is expected and thus it was not taken into account in the model. In equal manner, the effect of moisture was also not considered, since it they become relevant when composite parts have been subjected to humidity rich environments for a sustained period of time.

5.7.1. VCT BUCKLING PREDICTION

In Table 5.2 it can be seen how, for the test setup No. 1, the theoretical prediction $T_{b1}(Th)$ matched well with the obtained experimental buckling temperature $T_{b1}(Exp)$, showing only 3°C difference. On the other hand, the VCT prediction $T_{b1}(VCT)$ appears to have

overestimated $T_{b1}(Exp)$ in $4^{\circ}C$. This is yet considered to be a fairly close prediction of the onset of buckling. For the test setup No. 2, the experimental buckling temperature was considerably lower than the theoretical one, with $28^{\circ}C$ difference between the two. Despite this difference, VCT delivered a fair prediction of the experimental buckling temperature, with a difference of $7^{\circ}C$ between the two. For both test setups the VCT prediction is not on the conservative side since $T_{b1}(VCT)$ is larger than $T_{b1}(Exp)$. In Table 5.2, the difference in buckling temperatures percent values are calculated with respect to initial temperature $23^{\circ}C$.

Test setup	Layup	Buckling temperature [$^{\circ}C$]			
		$T_{b1}(Th)$	$T_{b1}(Exp)$	$T_{b1}(VCT)$	difference
No. 1	$[30/-30/5/-5]_s$	68	71	75	8.3%
No. 2	$[35/-35/10/-10]_s$	79	51	58	25%

Table 5.2: VCT buckling predictions.

5

5.7.2. OBSERVATIONS ABOUT MODE JUMPING

In Table 5.3, it can be seen how, for the two test setups, the theoretical prediction for the mode jumping temperature $T_{b2}(Th)$ is higher than experimentally obtained mode jumping temperature $T_{b2}(Exp)$. The differences between them were of 9° for the $[30/-30/5/-5]_s$ plate and 35° for the $[35/-35/10/-10]_s$ plate. In the last column of the table, the most relevant interactions in the higher modes are reported. However, there is no conclusive evidence about a relation between these observations and the mode jumping.

Large differences between the theoretical and experimental values for buckling and mode jumping could have been by multiple factors, such as irregularity in the temperature distributions, changes in material properties due to sustained heating, or other particularities of the test setup.

Test setup	Layup	Buckling temperature [$^{\circ}C$]		
		$T_{b2}(Th)$	$T_{b2}(Exp)$	Observations
No. 1	$[30/-30/5/-5]_s$	102	93	Switching of $\langle 1, 2 \rangle$ and $\langle 2, 1 \rangle$ modes.
No. 2	$[35/-35/10/-10]_s$	137	102	Switching of $\langle 1, 2 \rangle$ and $\langle 2, 1 \rangle$ modes and 45° rotation of mode $\langle 2, 2 \rangle_{45^{\circ}}$.

Table 5.3: Observations at mode jumping.

5.8. CONCLUSIONS

In this investigation, experiments on heated composite laminated plates were performed. Two goals were pursued: first, the application of the Vibration Correlation Technique (VCT) to detect buckling in heated composite plates; second, an exploratory measurement of the vibration frequencies of the composite plates in the proximities of a mode jumping. To this aim, two symmetric and balanced, angle ply laminates with stacking orientations $[30/-30/5/-5]_s$ and $[35/-35/10/-10]_s$, made in material AS4/8552, were tested. The plates were placed inside a frame with a low thermal expansion coefficient, and two different experimental configurations were implemented, using as heat source an oven and an infra-red quartz lamp array, respectively. The plates showed a linear decrease in the square of the frequencies f^2 with respect to the temperature T , and VCT achieved reasonable predictions for the buckling temperature by performing a linear extrapolation of the linear part of the f^2 vs T curve and extracting its intersection with the horizontal axis. The accuracy of these predictions was compared with the experimentally obtained buckling temperature. For the test setup No. 1, VCT prediction overestimated the buckling temperature of only 4°C while for the test setup No. 2 this difference rose up to 7°C . Regarding the mode jumping, changes in the vibration signature of the plates in the proximities of the mode jumping were tracked. It was found that the f vs T curves for the 2^{nd} and 3^{rd} modes intersected roughly around the temperatures at which the mode change happened. Besides, higher modes experienced a rotation. The relation of these events with the mode jumping is, however, not yet conclusive and further experimental work is required. The main contribution of this work is to show qualitatively and quantitatively the value of the VCT method for the prediction of the buckling temperature of composite plates, as well as the change of buckling and vibration mode.

BIBLIOGRAPHY

- [1] C. R. Bowen, R. Butler, R. Jervis, H. A. Kim, and A. I. T. Salo, “Morphing and shape control using unsymmetrical composites”, *Journal of Intelligent Material Systems and Structures*, vol. 18, no. 1, pp. 89–98, 2007. DOI: [10.1177/1045389X07064459](https://doi.org/10.1177/1045389X07064459). eprint: <https://doi.org/10.1177/1045389X07064459>. [Online]. Available: <https://doi.org/10.1177/1045389X07064459>.
- [2] J. G. Álvarez and C. Bisagni, “Investigation on buckling and mode jumping of composite plates under thermomechanical loads”, *International Journal of Non-Linear Mechanics*, vol. 138, no. August 2021, p. 103 837, Jan. 2022, ISSN: 00207462. DOI: [10.1016/j.ijnonlinmec.2021.103837](https://doi.org/10.1016/j.ijnonlinmec.2021.103837). [Online]. Available: <https://doi.org/10.1016/j.ijnonlinmec.2021.103837%20https://linkinghub.elsevier.com/retrieve/pii/S0020746221001712>.
- [3] L. Culliford, R. S. Choudhry, R. Butler, and A. Rhead, “Buckling and strength analysis of panels with discrete stiffness tailoring”, *Composite Structures*, vol. 234, p. 111 672, 2020, ISSN: 0263-8223. DOI: <https://doi.org/10.1016/j.compstruct.2019.111672>. [Online]. Available: <https://www.sciencedirect.com/science/article/pii/S0263822319311961>.
- [4] E. Labans, H. Abramovich, and C. Bisagni, “An experimental vibration-buckling investigation on classical and variable angle tow composite shells under axial compression”, *Journal of Sound and Vibration*, vol. 449, pp. 315–329, 2019, ISSN: 10958568. DOI: [10.1016/j.jsv.2019.02.034](https://doi.org/10.1016/j.jsv.2019.02.034). [Online]. Available: <https://doi.org/10.1016/j.jsv.2019.02.034>.
- [5] M. A. Arbelo, S. F. M. De Almeida, M. V. Donadon, *et al.*, “Vibration correlation technique for the estimation of real boundary conditions and buckling load of unstiffened plates and cylindrical shells”, *Thin-Walled Structures*, vol. 79, pp. 119–128, 2014, ISSN: 02638231. DOI: [10.1016/j.tws.2014.02.006](https://doi.org/10.1016/j.tws.2014.02.006).
- [6] M. A. Arbelo, K. Kalnins, O. Ozolins, E. Skukis, S. G. Castro, and R. Degenhardt, “Experimental and numerical estimation of buckling load on unstiffened cylindrical shells using a vibration correlation technique”, *Thin-Walled Structures*, vol. 94, pp. 273–279, 2015, ISSN: 02638231. DOI: [10.1016/j.tws.2015.04.024](https://doi.org/10.1016/j.tws.2015.04.024).
- [7] H. Abramovich, “The Vibration Correlation Technique – A reliable nondestructive method to predict buckling loads of thin walled structures”, *Thin-Walled Structures*, vol. 159, no. May 2020, p. 107 308, 2021, ISSN: 02638231. DOI: [10.1016/j.tws.2020.107308](https://doi.org/10.1016/j.tws.2020.107308). [Online]. Available: <https://doi.org/10.1016/j.tws.2020.107308>.

- [8] D. Shahgholian-Ghahfarokhi and G. Rahimi, "Buckling load prediction of grid-stiffened composite cylindrical shells using the vibration correlation technique", *Composites Science and Technology*, vol. 167, no. September, pp. 470–481, 2018, ISSN: 02663538. DOI: [10.1016/j.compscitech.2018.08.046](https://doi.org/10.1016/j.compscitech.2018.08.046). [Online]. Available: <https://doi.org/10.1016/j.compscitech.2018.08.046>.
- [9] E. Skukis, O. Ozolins, J. Andersons, K. Kalnins, and M. A. Arbelo, "Applicability of the vibration correlation technique for estimation of the buckling load in axial compression of cylindrical isotropic shells with and without circular cutouts", *Shock and Vibration*, vol. 2017, 2017, ISSN: 10709622. DOI: [10.1155/2017/2983747](https://doi.org/10.1155/2017/2983747).
- [10] C. Fai Ng and S. A. Clevenson, "High-intensity acoustic tests of a thermally stressed plate", *Journal of Aircraft*, vol. 28, no. 4, pp. 275–281, 1991, ISSN: 00218669. DOI: [10.2514/3.46023](https://doi.org/10.2514/3.46023).
- [11] J. M. T. Thompson and L. Virgin, "Predicting a jump to resonance using transient maps and beats", *International Journal of Non-Linear Mechanics*, vol. 21, no. 3, pp. 205–216, 1986, ISSN: 00207462. DOI: [10.1016/0020-7462\(86\)90004-1](https://doi.org/10.1016/0020-7462(86)90004-1).
- [12] M. J. Jacobson, "Sonic fatigue of advanced composite panels in thermal environments", *Journal of Aircraft*, vol. 20, no. 3, pp. 282–288, 1983, ISSN: 00218669. DOI: [10.2514/3.44865](https://doi.org/10.2514/3.44865).
- [13] Y. Sun, Z. Liu, J. Sun, F. Ren, H. Cheng, and L. Dong, "Snap-through response of thermally buckled C/SiC plates considering boundary elasticity and initial imperfections under progressive wave loading", *Composite Structures*, p. 114443, 2021, ISSN: 02638223. DOI: [10.1016/j.compstruct.2021.114443](https://doi.org/10.1016/j.compstruct.2021.114443). [Online]. Available: <https://doi.org/10.1016/j.compstruct.2021.114443>.
- [14] D. A. Ehrhardt and L. N. Virgin, "Experiments on the thermal post-buckling of panels, including localized heating", *Journal of Sound and Vibration*, vol. 439, pp. 300–309, Jan. 2019, ISSN: 0022460X. DOI: [10.1016/j.jsv.2018.08.043](https://doi.org/10.1016/j.jsv.2018.08.043).
- [15] S. Y. Kuo, L. C. Shiau, J. W. Chuang, and C. C. Cheng, "The relationship of buckle pattern change and vibration mode shifting: Thermal postbuckling and vibration of composite laminates", *Journal of Aeronautics, Astronautics and Aviation*, vol. 48, no. 1, pp. 65–74, 2016, ISSN: 19907710. DOI: [10.6125/15-1120-869](https://doi.org/10.6125/15-1120-869).
- [16] X. K. Xia and H. S. Shen, "Vibration of post-buckled sandwich plates with FGM face sheets in a thermal environment", *Journal of Sound and Vibration*, vol. 314, no. 1-2, pp. 254–274, 2008, ISSN: 0022460X. DOI: [10.1016/j.jsv.2008.01.019](https://doi.org/10.1016/j.jsv.2008.01.019).
- [17] H. Chen and L. Virgin, "Dynamic analysis of modal shifting and mode jumping in thermally buckled plates", *Journal of Sound and Vibration*, vol. 278, no. 1-2, pp. 233–256, 2004, ISSN: 0022460X. DOI: [10.1016/j.jsv.2003.10.054](https://doi.org/10.1016/j.jsv.2003.10.054).
- [18] K. Murphy, L. Virgin, and S. Rizzi, "Characterizing the dynamic response of a thermally loaded, acoustically excited plate", *Journal of Sound and Vibration*, vol. 196, no. 5, pp. 635–658, Oct. 1996, ISSN: 0022460X. DOI: [10.1006/jsvi.1996.0506](https://doi.org/10.1006/jsvi.1996.0506). [Online]. Available: <https://linkinghub.elsevier.com/retrieve/pii/S0022460X96905064>.

- [19] J. Gutiérrez Álvarez and C. Bisagni, “Closed-form solutions for thermomechanical buckling of orthotropic composite plates”, *Composite Structures*, vol. 233, no. May 2019, p. 111 622, Feb. 2020, ISSN: 02638223. DOI: [10.1016/j.compstruct.2019.111622](https://doi.org/10.1016/j.compstruct.2019.111622). [Online]. Available: <https://linkinghub.elsevier.com/retrieve/pii/S0263822319318835%20https://doi.org/10.1016/j.compstruct.2019.111622>.
- [20] H. Lurie, “Effective end restraint of columns by frequency measurements”, *Journal of the Aeronautical Sciences*, vol. 18, no. 8, pp. 566–567, 1951. DOI: [10.2514/8.2038](https://doi.org/10.2514/8.2038).
- [21] H. Lurie, “Lateral vibrations as related to structural stability”, *Journal of Applied Mechanics*, vol. 19, no. 2, pp. 195–204, 1952, ISSN: 0021-8936. DOI: [10.1115/1.4010446](https://doi.org/10.1115/1.4010446).
- [22] M. A. Souza and L. M. Assaid, “A new technique for the prediction of buckling loads from nondestructive vibration tests”, *Experimental Mechanics*, vol. 31, no. 2, pp. 93–97, 1991, ISSN: 00144851. DOI: [10.1007/BF02327558](https://doi.org/10.1007/BF02327558).
- [23] J. Singer, J. Arbocz, and T. Weller, *Buckling Experiments: Experimental Methods in Buckling of Thin-Walled Structures*. Hoboken, NJ, USA: John Wiley & Sons, Inc., 2002, vol. 2, ISBN: 9780470172995. DOI: [10.1002/9780470172995](https://doi.org/10.1002/9780470172995). [Online]. Available: <http://doi.wiley.com/10.1002/9780470172995>.
- [24] D. Hui, “Effects of geometric imperfections on frequency-load interaction of biaxially compressed antisymmetric angle ply rectangular plates”, *Journal of Applied Mechanics, Transactions ASME*, vol. 52, no. 1, pp. 155–162, 1985, ISSN: 15289036. DOI: [10.1115/1.3168987](https://doi.org/10.1115/1.3168987).
- [25] J. Gutiérrez Álvarez and C. Bisagni, “A study on thermal buckling and mode jumping of metallic and composite plates”, *Aerospace*, vol. 8, no. 2, p. 56, Feb. 2021, ISSN: 2226-4310. DOI: [10.3390/aerospace8020056](https://doi.org/10.3390/aerospace8020056). [Online]. Available: <https://www.mdpi.com/2226-4310/8/2/56>.
- [26] Hexcel Corporation, *HexPly 8552*, 2016. [Online]. Available: <https://www.hexcel.com/Resources/DataSheets/Prepreg> (visited on 10/15/2020).
- [27] Re-Steel, *Invar 36 for Composite Tooling (commercial catalog)*, 2021. [Online]. Available: <https://re-steel.com/invar-plate/invar-36/>.
- [28] J. L. Sanders, “Nonlinear theories for thin shells”, *Quarterly of Applied Mathematics*, vol. 21, no. 1, pp. 21–36, 1963, ISSN: 0033569X, 15524485. [Online]. Available: <http://www.jstor.org/stable/43634948> (visited on 08/15/2022).

6

FINAL CONCLUSION AND RECOMMENDATIONS

During this Thesis, diverse aspects of thermomechanical buckling in composite plates have been investigated. It is now expedient to have a look at the objectives set at the beginning of this research before making a balance of what has been achieved. The main goal of this research was gaining understanding on buckling and post-buckling behavior in composite plates subjected to thermomechanical loads. This rather general research objective was reformulated into four different research questions, reproduced below for convenience:

1. What is the relation between thermal and external mechanical loads in the onset of thermomechanical buckling on flat composite plates?
2. Is it possible to predict whether or not a composite plate will experience mode jumps during a thermal buckling experiment? If yes, can the mode jumping temperature be predicted accurately?
3. During an experiment in thermal buckling, would the occurrence of an hypothetical mode jump be in any way affected by the introduction of additional, external mechanical load? If yes, are there any relation between these two factors?
4. Can the Vibration Correlation Technique (VCT) be successfully applied to heated composite plates to determine thermal buckling? And also, does the occurrence of a mode jump during a thermal buckling experiment leave identifiable traces in the frequency signature of the tested plate?

Prior to deepening into how this dissertation attempted to answer these questions, a brief summary of the main conclusions reached in the four performed investigations is presented below.

- In the first investigation, the relation between mechanical and thermal loads in flat, symmetric and balanced composite plates was studied. For this, a closed-form solution for the buckling of orthotropic composite plates subjected to thermal and mechanical loads was derived. For a given plate configuration, the obtained formula establishes a relation between critical temperature and applied plate size variation, i.e. plate stretching or shortening. Analytical results show that plate stretching causes the critical buckling temperature to increase, and conversely, plate compression sinks the buckling temperature down. Due to this, a mechanically loaded plate can be stabilized or destabilized by applying cooling or heating. Moreover, the amount of mechanical preload has an effect over the buckling shape of the plate.
- The second investigation dealt with the prediction of buckling and mode jumping subjected to thermal loads. This study was approached by performing a combined numerical-experimental study in which plates with mode jumps were intentionally sought for. A numerical parametric study was performed, in order to find plates showing mode jumps when heated. As a result, two composite plate configurations were selected for experimentation. Based on the plate design and dimensions, a test setup for thermal buckling of plates was developed, and the selected plates were subsequently tested. Test results showed that both buckling and mode jumping in thermally loaded composite plates could be successfully reproduced, and hence the followed numerical strategy appears to have worked successfully for the two tested plates. Numerical simulations correctly predicted general trends in plate deflections but they overpredicted the mode jumping temperature for both tested composite plates, with differences up to 13%.
- During the third investigation, the impact of combined thermomechanical loads over the post-buckling and mode jumping behavior of composite plates was studied. This was done by performing a combined numerical-experimental study. A numerical parametric study was performed, in which the plates tested during the previous investigation were subjected to load combinations of either “compression + heating” or “heating + compression”. Numerical results showed that for increasing values of plate compression, both buckling and mode jumping temperatures experienced a linear decrease, and for initially applied heating load, both buckling and mode jumping critical plate shortening reflected that a similar linear decrease. Based on these results, a novel experimental setup for combined thermomechanical testing was developed. A linear decrease for the mode jumping decrease was captured. A linear decrease in the buckling temperature could not be successfully captured, but the results appear to be encouraging about the existence of such tendency.
- The fourth investigation dealt with the study of vibrations of composite plates during thermal buckling and post-buckling in heated composite plates. For this, two different tests in two different experimental setups were performed. The Vibration Correlation Method (VCT) was applied, and the vibration changes in the proximities of the mode jump were tracked. The VCT method successfully predicted

the occurrence of buckling, however, in both experiments, the buckling temperature were slightly overpredicted. Several changes in the vibration mode shapes could be tracked after the mode jump, although no relation between these vibration changes and the jumps could be definitely established.

6.1. DETAILED CONCLUSIONS

The first laid out research question was:

- *What is the relation between thermal and external mechanical loads in the onset of thermomechanical buckling on flat composite plates?*

Chapter 2 of this dissertation was devoted to answering the aforementioned research question. A closed-form solution for the buckling of orthotropic composite plates subjected to thermal and mechanical loads was derived. For this, a Duhamel-Neumann approach was assumed, in combination with laminate theory and plate theory. The mechanical load was introduced in the form of plate size variation Δ_x , and the thermal load as homogeneous temperature increment ΔT over the whole plate. Plate edge rotations were allowed in the four plate edges, as per classical simply supported boundary conditions. The obtained formula establishes a relation between critical temperature and applied plate size variation. For a case in which the plate does not experience size variation, i.e. thermal buckling case, the buckling temperature depends on laminate bending stiffness, membrane stiffness, and laminate Coefficients of Thermal Expansion (CTE's), being the latter the most important of these factors. Orthotropic plates typically have two laminate CTE's, corresponding to X and Y directions.

For plates with two positive CTE's, and when the plate is subjected to plate stretching, the buckling temperature increases, and conversely the buckling temperature decreases when compression is applied. Due to this, plate stretching could be used to stabilize a heated plate against buckling, while in the same fashion, cooling could be used to stabilize a compressed plate. When the plate has at least a negative CTE, a case-to-case study is necessary. All combinations of heating and in-plane loading were represented in a buckling chart representing ΔT vs. Δ_x divided into four quadrants, corresponding to combinations of heating-cooling and plate stretching-shortening. For a given plate, the buckling temperatures are located in a curve that divides the space into buckled and unbuckled states. This curve is formed by rectilinear segments along which the plate adopts a different buckling shape. It was also shown that for certain combinations of material and stacking orientation, laminates could be found that could buckle under both heating and cooling.

The second laid out research question was:

- *Is it possible to predict whether or not a composite plate will experience mode jumps during a thermal buckling experiment? If yes, can the mode jumping temperature be predicted accurately?*

Chapter 3 of this dissertation was dedicated to answering the above-mentioned research question. The approach was to identify composite plates that would experience buckling and mode jumps when heated. In order to do this, a combined numerical-experimental approach was followed. The numerical part consisted in two parametric studies where two suitable plates were identified for experimentation. In order to limit the design space, and also to suit the testing equipment, these two parametric analysis were limited to a plate size of $300 \times 200 \text{ mm}^2$ and to plates made of AS4/8552 composite material. Two laminate families were analyzed: the first family was the $[\theta, -\theta]_{2s}$, with θ angles ranging from 0° to 90° , and the second laminate family was the $[\theta, -\theta, \varphi, -\varphi]_{2s}$, with θ angles ranging from 0° to 90° and $\varphi = \theta - 25^\circ$. The experimental part consisted on the implementation of a test setup for thermal buckling, and the subsequent testing of the two plates.

During the first numerical parametric study, the analyzed composite plates were examined for their two first thermal buckling eigenvalues. For a given plate, its two first eigenvalue temperatures represent two contiguous equilibrium shapes. Three relevant cases were identified. (i) Eigenvalues are very close, so a small perturbation may cause the plate to change from one shape into the other. This kind of plates are very likely to have low bending stiffness and/or high thermal expansion along a given direction, and as a consequence, to be unstable in post-buckling. For instance, this would be the case for the $[\theta, -\theta]_{2s}$ family with θ values close to either 0° or 90° . (ii) Eigenvalues are far apart, so the initial buckling shape will likely be very stable in post-buckling and a mode jump may not be possible. Such laminates are likely to have suitable combinations of high bending stiffness and/or very low thermal expansion, such as $[\theta, -\theta]_{2s}$ laminates with θ values close to 45° (iii) Eigenvalues are far apart, yet at a reachable distance plate can achieve stable post-buckling behaviour and yet display mode jumps when heated beyond certain temperature. From these three options, the last one was the most desirable of the three. This kind of plate is likely to have a combination of bending stiffness and CTE's that allows for initially stable post-buckling behaviour, but also likely to experience a snap-through event during deep post-buckling, an event that could be clearly identifiable during an experiment.

During the second numerical parametric study, the post-buckling behaviour was examined to confirm the existence of mode jumps as well as the possible influence of geometrical imperfections, which was conducted with the help of dynamic explicit analysis.

The outcome of the first numerical parametric study showed that, for the $[\theta, -\theta]_{2s}$ family, laminates with values of θ close to either 0° to 90° , the two first eigenvalues were very close and thus the plate may buckle indistinctly under any of the two. Conversely, plates with angles close to 45° would have high bending stiffness and low CTE's along both X and Y directions, their two first eigenvalues would be too far apart, and thus achieving mode jumps is likely to be unreachable in practice. Between these two cases, $[\theta, -\theta]_{2s}$ plates with θ within $[25^\circ, 40^\circ]$ could show stable thermal post-buckling behaviour and eventually reach mode jumps, since the two eigenvalues are relatively far apart, yet at a reachable distance during a hypothetical experiment. The results showed that, in order for plates to be able to hold thermally post-buckled states, they must have the appropriate balance of bending stiffness and thermal expansion properties, a balance that is different for each combination of plate geometry, material and

boundary conditions. Laminates belonging to the $[\theta, -\theta]_{2s}$ laminate family always have a fibre-dominated direction and a matrix dominated direction, along which, bending stiffness and thermal expansion are maximal, respectively. This has therefore the consequence of having to choose between having either large CTE or large bending stiffness along a given plate direction. Large bending stiffness is required for post-buckling stability, and large CTE are required for the plate to buckle thermally, because in thermal post-buckling, mode jumps happen in the direction of maximal thermal expansion. Additionally, $[\theta, -\theta]_{2s}$ plates ended up having mode jumping temperatures which were too high for experimentation with AS4/8552 material. Conversely, the laminate family $[\theta, -\theta, \varphi, -\varphi]_s$, where $\varphi = \theta - 25^\circ$, can achieve both high bending stiffness and high thermal expansion along the Y direction, and plates within the $[25^\circ, 40^\circ]$ range can both show stable post-buckling behaviour and achieve mode jumps within material service temperature.

A second parametric analysis was performed over both $[\theta, -\theta]_{2s}$ and $[\theta, -\theta, \varphi, -\varphi]_s$, laminate families. During this study, the behavior of the laminates in post-buckling was simulated using a dynamic explicit procedure. Laminates were subjected to uniform, monotonically increasing temperature distributions, under which the studied laminates either display mode jumps or remain stable at their initial post-buckling configuration. The results showed a very high influence of the shape and amplitude of the initial geometric imperfection in the occurrence of the mode jump. Imperfection shapes with the form of one half-wave in both X and Y directions, i.e. (1, 1) appeared to make the mode jumping temperature increase slightly, while unfavorable imperfection shapes with sufficient amplitude such as i.e. (1, 2), may destroy the mode jumping effect altogether, since the plate directly would enter a (1, 2) shape directly.

The outcome of the two numerical parametric analysis was the identification of two laminate configurations, $[30, -30, 5, -5]_s$ and $[35, -35, 10, -10]_s$, which were to be used in experimentation. A third plate made in aluminium alloy 2024T23 was also tested for comparison. A test setup was designed, in order to test the aforementioned plates. The working principle of the test setup consisted on clamping the tested plate between the two halves of an Invar 36 frame, which would restrain plate in-plane thermal expansions when plate and frame were heated, and thus the plate would buckle due to arisen thermal stresses. For the experiments, an oven was used as a heating source. All tested plates buckled, and the two composite plates experienced also mode jumping. Dynamic numerical simulations successfully predicted the general trends in post-buckling behaviour, however the mode jumping temperature was overpredicted for both tested plates, showing a maximum difference of 13%. The sources for this difference may range from changes in material properties with temperature, irregular heating in the plate, initial imperfections etc. The large sensitivity to unfavorable geometrical imperfections that was observed in the numerical analysis did not manifest during experimentation. It is believed that, since heating came from just one side of the panel may have counteracted possible present geometrical imperfections.

The obtained numerical-experimental results could be understood as a validation of the strategy followed during this investigation, as well as confirmation that the existence of mode jumps in thermally buckled composite plates can, to some extent, be predicted. However, a significant amount of experimental work is yet to be performed before these

predictions can be deemed reliable.

The third laid out research question was:

- During an experiment in thermal buckling, would the occurrence of an hypothetical mode jump be in any way affected by the introduction of additional, external mechanical load? if yes, are there any relation between these two factors?

Chapter 4 of this dissertation was dedicated to answering the above-mentioned research question. In order to do this, a combined numerical-experimental approach was followed.

The numerical part of this investigation consisted on a numerical parametric study in which the post-buckling regime of plates subjected to combinations of heat and compression was simulated by means of a dynamic explicit procedure. In these analysis, the plates were subjected to four different types of load cases, referred either as pure load cases, “pure compression” and “pure heating”, or combined: “heating + compression” and “compression + heating”, where load application in combined load steps were applied in a sequential manner. The composite plate used for these analysis had dimensions $300 \times 200 \text{ mm}^2$, was made of AS4/8552 material and had a $[35, -35, 10, -10]_s$ layup. This plate had been used in Chapter 3, and had a demonstrated capability of showing mode jumps when heated. By subjecting this plate to combined loading, the influence over mode jumping could be evaluated. The numerical analysis revealed that, in combined load cases, both buckling and mode jumping showed a linear decrease for increasing initial values of preload. It was also found that the type of initial preload and the order of load application, i.e. “heating + compression” versus “compression + heating”, appeared not to be relevant in this linear behavior. While the obtained linear relation for buckling is in line with the findings reported for Chapter 2, a linear relation the occurrence of mode jumping is somewhat unexpected, since load superposition is not expected to hold in non-linear plate post-buckling regime.

The results of the numerical analysis were used also to design a test setup in which the trends identified during the numerical analysis could be verified. The result was a test setup capable of applying compression and heat simultaneously. The restriction of thermal expansion in the plates was ensured by bolting the plates to a frame made of Invar 36 material, which had a very low CTE. The introduction of mechanical shortening in the plate was performed indirectly, by applying displacements to the Invar 36 frame with a compression machine. Heating loads were introduced using an Infrared (IR) array lamp. During the tests, the load application for the combined load cases was performed in sequentially, as previously done for the numerical analysis.

During the experiments it was found that the shape and amplitude of the initial imperfection had a significant effect over the post-buckling shape, and subsequently over mode jumping behaviour. An initial, geometric imperfection in the plate caused that, for both “pure compression” and “pure heating” experiments, the buckling shape was visibly shifted downwards. However, this influence was not the same for either of the two test types. For “pure compression” tests the imperfections played a critical role. The initial buckling deflections had an asymmetrical (1,2) shape, i.e. a buckling shape with one and two half-waves in X and Y directions. At buckling, the out-of-plane deflections

would, however, started much sooner at one of the crests of the buckling shape, and the mode jump effect was a gradual transition rather than a sudden event. Conversely, for “pure thermal” tests, the impact of imperfection was much less significant: the plate buckled under a (1, 1) mode, even though the buckling shape was slightly shifted downwards. For any performed combined test, increasing the contribution of the external mechanical load also increased the influence of the initial geometrical imperfection.

Answering the research question, the final results of the experiments confirmed the existence of a linear decrease for increasing levels of preload in the occurrence of the mode jump, as well as the independence on the order of load application. However, the same could not be confirmed for the occurrence of buckling, even though the results appeared to be encouraging of the existence of such linear tendency. The difficulties found in the implementation of the combined loading setup drastically reduced the amount of experiments that could be performed: all results presented correspond to only one plate specimen. This limits in great manner the validity and reach of the conclusions, since the reached observations can hardly be generalized. Due to this, the results of this experimental campaign cannot have other character than being preliminary, and these results should only be taken as an encouragement towards more investigation in this direction.

There are several aspects of the complete testing procedure and analysis that need further refinement. The most acute issue is, probably, the irregularity in load application. Temperature distributions were only relatively uniform at low temperature levels. Compression was also slightly non-uniformly applied, although it is believed this had much less impact in the results. This testing concept could greatly benefit from improvements in the design of the low CTE fittings, and in the introduction of mechanical and heating loads. A big difference found between the results of this setup and the one in Chapter 3 is that the test set-up frame reached a ΔT of approximately 90°C , while in this combined test setup, ΔT reached 30°C . Even if Invar 36 has a very low CTE, large temperature increments can still add up if the ΔT is large, and can produce a noticeable stretching in the plate, varying the buckling temperature and also likely the mode jumping behavior. This would explain, at least in part, why the mode jumping temperatures for the $[35, -35, 10, -10]_S$ plate are higher in Chapter 3 than in Chapter 4. Additionally, the procedure used for the detection of buckling under combined load cases, which was based on the use of regression lines, needs further refinement, as often there are not enough data points to perform a reliable linear regression.

The fourth laid out research question was:

- *Can the Vibration Correlation Technique (VCT) be successfully applied to heated composite plates to determine thermal buckling? And also, does the occurrence of a mode jump during a thermal buckling experiment leave identifiable traces in the frequency signature of the tested plate?*

The Chapter 5 of this dissertation was dedicated to answering the above-mentioned research questions. In this chapter, two different experiments on vibration of plates were performed.

The composite plates used for these experiments had dimensions $300 \times 200 \text{ mm}^2$, were made of AS4/8552 material and had $[30, -30, 5, -5]_s$ and $[35, -35, 10, -10]_s$ stacking orientations. These plates were previously used in Chapter 3 and had demonstrated capability to buckle and show mode jumps when heated. During this investigation, these plates were tested in two different experimental setups, which were modified versions of the experimental setups used in Chapter 3 and Chapter 4. Both experimental setups used the same Invar 36 frame to induce thermal buckling. The main difference between the two test setups was the source used for the heating loads: the Test Setup No. 1 used an oven to study the post-buckling of plates, and was a modification of the test setup used in Chapter 3; conversely, the Test Setup No. 2 used infrared lamps to heat the plate and frame, and was a modification of the test setup used in Chapter 4. The most remarkable modification of Test Setup No. 2 was the use of metallic chains to emulate free-free boundary conditions in the frame.

The testing procedure for both plates was very similar: the temperature was gradually increased in steps, stabilized, and then the frequencies were measured through a modal test performed with a laser vibrometer, which used a loudspeaker as an excitation source. At every temperature, frequency spectra and information about the individual vibration modes were extracted.

During both experiments, decreases in the vibration shape more similar to the buckling mode could be captured for both plates, and thus, for the two tests, a linear extrapolation on the square of the frequencies was performed, obtaining in this way predictions for the buckling temperatures. VCT provided reasonable predictions for thermal buckling in composite plates. However, for both performed experiments, the predictions for the buckling temperature were non-conservative. Conversely, modal tests were able to track some occurrences in the frequency signatures of the plates, however, no conclusive evidence about possible changes in the frequency signature of the plates pointing towards the mode jump could be found. The combination of low CTE frame and free-free boundary conditions seems to be a good implementation of mechanical boundary conditions for vibration testing of heated composite plates, since it avoided all the additional noise caused by the oven setup.

6.2. RECOMMENDATIONS FOR FUTURE RESEARCH

Even if this research works presents several approaches and methodologies for the study of thermal and thermomechanical post-buckling, there are still plenty of relevant features of this phenomenon that are of big relevance. In this section, some recommendations of potentially interesting topics or research directions are given.

- The buckling case studied analytically in Chapter 2 deals with simply supported boundary conditions, while the three experiments in Chapters 3, 4 and 5 deal with clamped boundary conditions. A further development of the formulation to include clamped boundary conditions could be beneficial.
- Semi-analytical formulations to predict the post-buckling behavior of compressed-heated stiffened panels could greatly contribute to the understanding and design

of these kind of heated composite structures. Special attention should be paid to the CTE and stiffness of the panel stringers

- The capabilities of the developed combined thermomechanical setup could be greatly increased by incorporating “stretching” and “cooling” loading conditions. This would considerably expand the range of the ΔT vs. Δx loading diagrams proposed in this thesis since up to now, obtained points are only located in the “shortening/heating” loading quadrant.
- The proposed experimental methodology could, with some effort, be extended to perform thermal buckling test on shallow curved composite panels and also mid-size stiffened panels.
- Understanding vibration variations after mode jumps during thermal post-buckling happened to be a difficult task, since it is difficult to regulate the amount of temperature that it is applied to the plate, temperature distributions were non uniform. It is recommended to study mode jumps and their related frequency changes under purely mechanical loading conditions, and gradually implement heating loads in the setup.
- Studying the dynamic post-buckling behavior of steered, composite panels under combined thermomechanical loads could be important to improve the performance of these structures. Steered panels tend to have highly directional laminates, which will locally have large CTE's. This can cause the panel to either buckle locally, and/or experience other vibration phenomena.
- The linear trends observed in mode jumping phenomena indicate that, eventually, this mode jumping under thermomechanical loads could be reliably predicted and harnessed for application. A potentially interesting research direction would be structural morphing, since mode jumps could be used to alter the shape of a structure without the need of external actuation, using thermomechanical buckling as a source for shape change.

ACKNOWLEDGEMENTS

On the way to Santiago de Compostela, every pilgrim walking the Way of St. James has to climb a particularly long and steep mountain pass. Once the top is reached, the pilgrim is rewarded with a breathtaking view of the landscape. Even if it is easy to get distracted by such an amazing view, no traveler will forget to stop before a big steel cross that emerges from a large elevation on the ground. Such mound was not created by an earth movement, but rather created overtime by thousands of pilgrims who, one by one, placed a small stone while making a wish. Today, this Ph.D. phase has been finished, and just like the pilgrim after the climb, it is only fair to sit and look back at what was achieved. However, it is clear to me that I did not get here alone. And even more, what does this "I, me, mine" mean? I am the result of the contributions from everyone that tough me anything, or helped me in any way: family, teachers, students, colleagues and friends. Just like the pilgrims shaped the large stone heap, we are all shaped by a multitude of people who left on us their small contribution. I can also see today that the person that finishes a long travel is never the same person that started it. And that, if you ask me, may be in itself the reason and the meaning of the travel.

Just like a pilgrimage, doing a Ph.D. can at times be a solitary experience. However, I was lucky to share many parts of it with excellent travel companions. I would like to express my deepest gratitude to my promotor/daily supervisor, Prof. dr. Chiara Bisagni, between many other things, for her guidance and mentorship during all these years, for showing me the importance of focusing only on the things that really matter and to keep going, especially in dire times. Without her, this thesis would have not been possible. I would like to thank Dr. Haim Abramovich, for his co-supervision during a brief period of time of this Ph.D., and for all what I learned from him through our work together. I am truly thankful to the late Prof. dr. Pim Groen and to Dr. Roeland deBreuker, as they effectively provided this Ph.D. project with an extra bottle of oxygen that contributed to its completion. An special mention goes to Laura Chant, thank you for all the battles you fight for all Ph.D.'s without us even noticing. Also, this thesis contains a considerable amount of experimental work and the help of the lab technicians was invaluable. I want to thank Alexander Uithol, Dave Ruijtenbeek, Fred Bosch, Johan Boender, Misja Huizinga and Viktor Horbowiec for their outstanding support during the experimental phase of this thesis. Also, thanks to the DEMO technicians Ed Roessen and Rob van der List, for their support in manufacturing.

During all the time in Delft I got the opportunity to spend time and learn from all the senior research staff in the Aerospace Structures and Computational Mechanics (ASCM) group. My gratitude goes to Prof. dr. Chiara Bisagni and Prof. dr. Christos Kassapoglou, to the associate professors Dr. Irene Villegas, Dr. Roeland deBreuker and Dr. Sergio Turteltaub, to the assistant professors, Dr. Bianca Giovanardi, Dr. Boyang Chen, Dr. Daniël Peeters, Dr. Julien van Campen, Dr. Jurij Sodja, Dr. Saullo G. P. Castro and Dr. Xuerui Wang, and to the CAD specialists Eddy van der Vos and George Dom. Thank you

for all the multiple conversations, lectures, presentations, etc. that I got to experience during these years, as well as the advice, support and encouragement that I received from all of you. Having the chance to work within a section of such remarkable technical proficiency was simply fantastic.

I would like to thank all my fellow Ph.D. students, PostDocs, Ms.C. students and other colleagues that I got to interact with during my time in Delft. In the buckling research group: Arne, Antonio, Bas, Edgars, Javier, Jens, Kevin, Luc, Meryem, Michelle, Nythia, but very especially to my brilliant office mates, Inés, Marta and Yuqian (Tutu), and to my master thesis student, Helena. In the Aeroelasticity research group, many thanks to Andres, Darwin, Kristofer, Marco Tito, Mario, Natalia, Noud, Paul, Tigran, Vega and Yasir, with an special mention to Eric, host of the Counter-Strike events. Many thanks as well to Fardin and Niels, and to Sathiskumar, Jayaprakash and Zhi. A special mention goes to the Coding Initiative team, Bianca, Heather, Giorgio and Sai Kubair, it was fantastic to watch the whole project grow! From structural integrity, I want to thank Agnes, Eva, Hongwei, Janos, Luigi, Megan, Nakash, Nicolas, Nikos, Niels, Panos, and Xi. Thanks to the *Café español*/Spanish connection in the Aerospace Faculty: Fabricio, Johan, Roberto, Sebastián, Thiago and Víctor. My gratitude goes to Jaco, the patient man, and Bruce Leblanc, master in the Zen and the Art of wind turbine development.

During my phase working in the German aeronautical industry I had the chance to work next to highly competent individuals from which I got to learn the trade. From my time in the space section of Airbus Defence and Space (previously Astrium GmbH), many thanks to John, José, Gabriel, Giuseppe and to the rest of the Mechanical Engineering department. My gratitude goes to the late Jesús García Gómez, an example of courage and perserverance. From my time at the Airbus high lift department, many thanks to Byron and Christoph. From Premium Aerotec GmbH, many thanks go to all the colleagues in the design, stress and fatigue teams that I met during all those years. A big "Thank you!" goes to Alex, Cyril, Matthias, Esther, Otto, Volker and Valery, but especially to Altay, Claudio and Susanne. From Bertrandt, many thanks to Lukas and Stephan. Many thanks to Carlos and Vicente for all the nice discussions and great times together.

I am indebted to the Section of "Continuum Mechanics and Theory of Structures" of the University of León, Spain, especially to Dr. José Vallepuga Espinosa and Gonzalo Baladrón Gaitero, and to my high school teachers in math and physics, Antonio Mallo and J.A. Balerdi. Thank you for providing the foundations necessary for what would come after.

There are many people from all the corners of the world, especially León, Bremen, Hamburg and Delft, good old friends that I have to leave out due to lack of space. To all of you, I am grateful. Last, but certainly not least, I have to thank my family: my nephew Adrián, my sister-in-law Sonia, my siblings Andrés and Samuel, but especially my parents, Ana and Salvador. This thesis is dedicated to them.

CURRICULUM VITÆ

PERSONAL INFORMATION

Name Javier Gutiérrez Álvarez
Date of birth 19-12-1982
Nationality: Spanish
E-mail: javier.g.alvarez@gmail.com



PROFESSIONAL EXPERIENCE

03/2016 Airbus Defence and Space GmbH, stress engineer
08/2014

07/2014 Premium Aerotec GmbH (external), stress engineer
05/2011

03/2011 Bertrandt IngenieurBüro GmbH, 3D CAD/design engineer
06/2008

04/2008 Indra Sistemas, 3D CAD/design engineer
09/2007

EDUCATION

06/2007 Ms.C. Industrial Engineering (structural mechanics)
07/2004

07/2004 Bs.C. Industrial Engineering (structural mechanics)
09/2000

LIST OF PUBLICATIONS

JOURNAL PUBLICATIONS

4. **J.G. Álvarez, H. Abramovich and C. Bisagni**, *Vibration-buckling tests on heated composite plates*, [Journal of Sound and Vibration](#) **536**, 117145 (2022).
3. **J.G. Álvarez and C. Bisagni**, *Investigation on buckling and mode jumping of composite plates under thermomechanical loads*, [International Journal of Non-Linear Mechanics](#) **138**, 103837 (2022).
2. **J.G. Álvarez and C. Bisagni**, *A Study on Thermal Buckling and Mode Jumping of Metallic and Composite Plates*, [Aerospace](#) **8**, 56 (2021).
1. **J.G. Álvarez and C. Bisagni**, *Closed-form solutions for thermomechanical buckling of orthotropic composite plates*, [Composite Structures](#) **233**, 111622 (2020).

CONFERENCE PUBLICATIONS

1. **J.G. Álvarez and C. Bisagni**, *Thermal-mechanical buckling of composite plates for aerospace applications*, [ECCM 2018 - 18th European Conference on Composite Materials](#) (2018).